0-315-01255-2

National Library of Canada
Bibliothèque nationale du Canada

Canadian Theses Division
Division des thèses canadiennes

Ottawa, Canada
K1A 0N4

49113

PERMISSION TO MICROFILM — AUTORISATION DE MICROFILMER

- Please print or type — Écrire en lettres moulées ou dactylographier

Full Name of Author — Nom complet de l'auteur

RANA NARVINJIT SINGH SODHI

Date of Birth — Date de naissance 25 AUGUST 1954	Country of Birth — Lieu de naissance ENGLAND

Permanent Address — Résidence fixe

c/o 74 SELWYN ROAD
BIRMINGHAM B16 0SW

Title of Thesis — Titre de la thèse

A COMPARISON OF THE AUGER ELECTRON AND THE CORE ELECTRON SHIFTS IN A SERIES OF PHOSPHORUS AND SULPHUR COMPOUNDS

University — Université

UNIVERSITY OF ALBERTA

Degree for which thesis was presented — Grade pour lequel cette thèse fut présentée

M.Sc.

Year this degree conferred — Année d'obtention de ce grade 1980	Name of Supervisor — Nom du directeur de thèse Dr. R.G. CAVELL

Permission is hereby granted to the NATIONAL LIBRARY OF CANADA to microfilm this thesis and to lend or sell copies of the film.

The author reserves other publication rights, and neither the thesis nor extensive extracts from it may be printed or otherwise reproduced without the author's written permission.

L'autorisation est, par la présente, accordée à la BIBLIOTHÈQUE NATIONALE DU CANADA de microfilmer cette thèse et de prêter ou de vendre des exemplaires du film.

L'auteur se réserve les autres droits de publication; ni la thèse ni de longs extraits de celle-ci ne doivent être imprimés ou autrement reproduits sans l'autorisation écrite de l'auteur.

Date 29 August 1980	Signature R. Sodhi

NL-91 (4/77)

National Library of Canada
Collections Development Branch

Canadian Theses on
Microfiche Service

Bibliothèque nationale du Canada
Direction du développement des collections

Service des thèses canadiennes
sur microfiche

NOTICE

The quality of this microfiche is heavily dependent upon the quality of the original thesis submitted for microfilming. Every effort has been made to ensure the highest quality of reproduction possible.

If pages are missing, contact the university which granted the degree.

Some pages may have indistinct print especially if the original pages were typed with a poor typewriter ribbon or if the university sent us a poor photocopy.

Previously copyrighted materials (journal articles, published tests, etc.) are not filmed.

Reproduction in full or in part of this film is governed by the Canadian Copyright Act, R.S.C. 1970, c. C-30. Please read the authorization forms which accompany this thesis.

THIS DISSERTATION
HAS BEEN MICROFILMED
EXACTLY AS RECEIVED

AVIS

La qualité de cette microfiche dépend grandement de la qualité de la thèse soumise au microfilmage. Nous avons tout fait pour assurer une qualité supérieure de reproduction.

S'il manque des pages, veuillez communiquer avec l'université qui a conféré le grade.

La qualité d'impression de certaines pages peut laisser à désirer, surtout si les pages originales ont été dactylographiées à l'aide d'un ruban usé ou si l'université nous a fait parvenir une photocopie de mauvaise qualité.

Les documents qui font déjà l'objet d'un droit d'auteur (articles de revue, examens publiés, etc.) ne sont pas microfilmés.

La reproduction, même partielle, de ce microfilm est soumise à la Loi canadienne sur le droit d'auteur, SRC 1970, c. C-30. Veuillez prendre connaissance des formules d'autorisation qui accompagnent cette thèse.

LA THÈSE A ÉTÉ
MICROFILMÉE TELLE QUE
NOUS L'AVONS REÇUE

Ottawa, Canada
K1A 0N4

NL-339 (Rev. 8/80)

THE UNIVERSITY OF ALBERTA

A COMPARISON OF THE AUGER ELECTRON AND THE CORE ELECTRON SHIFTS IN A SERIES OF PHOSPHORUS AND SULPHUR COMPOUNDS

by

© RANA SODHI

A THESIS

SUBMITTED TO THE FACULTY OF GRADUATE STUDIES AND RESEARCH
IN PARTIAL FULFILMENT OF THE REQUIREMENTS FOR THE DEGREE
OF MASTER'S IN CHEMISTRY

DEPARTMENT OF CHEMISTRY

EDMONTON, ALBERTA

FALL, 1980

THE UNIVERSITY OF ALBERTA

FACULTY OF GRADUATE STUDIES AND RESEARCH

The undersigned certify that they have read, and recommend to the Faculty of Graduate Studies and Research, for acceptance, a thesis entitled A COMPARISON OF THE AUGER ELECTRON AND THE CORE ELECTRON SHIFTS IN A SERIES OF PHOSPHORUS AND SULPHUR COMPOUNDS submitted by RANA SODHI in partial fulfilment of the requirements for the degree of Master of Science.

Ronald Cavell
Supervisor

Otto P. Strausz

Martin Cowie

Date August 29, 1980

To My Parents

ABSTRACT

The KL_2L_3 ($^1D_2$) Auger, 1s and 2p photoelectron energies were measured for a series of phosphorus and sulphur compounds and a comparison of the Auger and photoelectron shifts was made. The potential model, utilising charges from both CNDO/2 and extended Hückel calculations, was used to attempt to explain the shifts.

On comparing the 1s and 2p photoelectron shifts a good linear correlation was obtained with the 1s electron showing the larger shift. This reflects the more core-like nature of the 1s electron as compared to the 2p electron. No such correlation was obtained on comparison of the Auger electron shifts with the photoelectron shifts. The Auger parameter, when defined properly, related the Auger electron shift to the photoelectron shift in a convenient way. The variations in shift could be rationalised by consideration of the relaxation accompanying the loss of the two electrons in the final two hole state. It was found that relaxation depended upon the ability of a group attached to the central atom to release electrons. Many factors can contribute to this and reversals of the expected relaxation trends based upon electronegativity arguments were noted.

The group shift concept was also applied to the experimental data. Inherent in the group shift concept is the assumption that shifts incurred by each group are independent

of each other. It was found that this assumption was only valid within a very limited series of compounds at best.

The ground, relaxation and transition potential models were tested with the aid of two semi-empirical methods. The CNDO/2 calculation gave reasonable correlation when using fitted parameters though the parameters obtained did not match the expected theoretical trends too well. The EWMO (Hückel) calculation was found to partition charge differently depending upon the number of lone pairs on the central atom and hence the general applicability of this method was severely limited.

ACKNOWLEDGEMENTS

The author wishes to express his sincere thanks to his research supervisor, Dr. R.G. Cavell. His support, direction and assistance will always be greatly appreciated.

Thanks go to the various members of Dr. Cavell's research group, especially to Dr. D.A. Allison for his help in the early days, Dr. L. Vande Griend for help in preparing and purifying some of the compounds and to Dr. Nonita Yap for some interesting discussions.

Dr. Norman Gee is to be thanked for much advice and for help in the preparation of this thesis.

Larry Coulson of the Radiation Lab is to be thanked for supplying a plotting package which produced some of the diagrams and to Faye Nagle who drafted the others.

Appreciation is due to Annabelle Wiseman for the typing of this thesis.

Thanks are also due to the capable assistance of the staff in the departmental workshops.

Finally, the author wishes to thank all his friends too numerous to list for making life worthwhile.

Table of Contents

Page

Chapter 1. Introduction 1

A. General Introduction 1

B. Description of the Various Processes 2

(i) Photoionisation 2

(ii) "Shake-up and Shake-off" 6

(iii) X-ray Fluorescence and the Auger Process 7

C. Models for Chemical Shift 18

(i) Koopman's Theorem versus ΔE_{SCF}. The Concept of Relaxation 19

(ii) Correlation of Potential with Binding Energy Shifts 22

(iii) Models Involving Transition Operator Formalism 30

(iv) Extension of Potential Models to Auger Spectroscopy 32

Chapter 2. Experimental 42

Chapter 3. Calculations 46

A. Semi-empirical Problems 46

B. Models for Chemical Shift 48

Page

Chapter 4. Results and Discussion 53

A. Experimental Results 53

B. Application of the Experimental Results to the Group Shift Concept 64

C. Results of Calculations - Charges and Potentials 68

(i) CNDO/2 Results 76

(ii) EWMO (Hückel) Results 81

D. Results of Calculations - Application of the Various Models and Comparison With Experiment 87

(i) CNDO/2 Calculations 93

(ii) EWMO (Hückel) Calculations 114

E. Relationship of the Auger Electron Shift to the Core Electron Binding Energy Shift 143

Chapter 5. Summary and Conclusions 159

References 161

Appendix 1. Molecular geometries used in the calculations 167

Appendix 2. Reparameterisation of the EWMO (Hückel) program 172

Appendix 3. Corrected values for the calculated Auger shifts in reference 8 181

LIST OF TABLES

Table	Description	Page
1.1	States arising from the L-S coupling scheme.	14
4.1	Experimental chemical shifts relative to PH_3.	54
4.2	Experimental chemical shifts relative to H_2S.	56
4.3	Experimental group shifts.	66
4.4	Central atom charge and off-atom potential from CNDO/2 calculations - P series.	70
4.5	Central atom charge and off-atom potential from CNDO/2 calculations - S series.	72
4.6	Central atom charge and off-atom potential from EWMO calculations (original parameterisation) - P series.	74
4.7	Central atom charge and off-atom potential from EWMO calculations (original parameterisation) - S series.	75
4.8	Phosphorus valence population on $P(CH_3)_3$ and PCl_3 from CNDO/2 calculations with d-orbitals included.	82
4.9	Central atom charges and off-atom potentials from EWMO calculations (new P parameterisation).	88
4.10	Theoretical k's from Slater's exponents.	92
4.11	Parameters from least-squares fit for the atom charge model (CNDO/2 charges and potentials).	94

Table	Description	Page
4.12	Calculated atom charge model shifts obtained from CNDO/2 charges and potentials - P series.	95
4.13	Calculated atom charge model shifts obtained from CNDO/2 charges and potentials - S series.	97
4.14	Correlation obtained from least-squares fit on calculated and experimental shifts (CNDO/2 calculation: atom charge model).	99
4.15	Calculated potential model shifts obtained from CNDO/2 calculation.	105
4.16	Correlation obtained from least squares fit on calculated and experimental shifts (CNDO/2 calculation: potential model).	107
4.17	Calculated atom charge model shifts obtained from CNDO/2 charges and potentials with d-orbitals included in basis set.	115
4.18	k values obtained from least-squares fit using CNDO/2 charges and potentials - d-orbitals included in basis set.	117
4.19	Parameters from least-squares fit for atom charge model (EWMO charges and potentials).	119
4.20	Calculated atom charge model shifts obtained from EWMO (original parameterisation) charges and potentials - P series.	121

Table	Description	Page
4.21	Calculated atom charge model shifts obtained from EWMO (new P parameterisation): charges and potentials - P series.	122
4.22	Calculated atom charge model shifts obtained from EWMO (original parameterisation): charges and potentials - S series.	123
4.23	Calculated atom charge model shifts obtained from EWMO (new P parameterisation) charges and potentials - S series.	125
4.24	Correlation obtained from least-squares fit on calculated and experimental shifts (EWMO calculation).	126
4.25	Fits on limited P and S series where there are no lone pairs on the central atom (EWMO calculation).	140
4.26	Relaxation and the Auger parameter - P series.	148
4.27	Relaxation and the Auger parameter - S series.	150
4.28	Experimental and calculated relaxation energy shifts - P series.	155
4.29	Experimental and calculated relaxation energy shifts - S series.	156
Al.1	References from which experimental geometries were obtained.	168
Al.2	Basis for assumed geometries of compounds.	170

Table	Description	Page
A2.1	New parameters for P.	179

LIST OF FIGURES

Figure	Description	Page
1.1	Processes involved in electron spectroscopy.	3
1.2	KLL Auger spectra of Ar, PH_3 and PF_3.	12
1.3	KLL line positions as a function of atomic number.	16
4.1	Experimental P2p binding energy shifts versus P1s binding energy shifts.	59
4.2	Experimental (-) P KL_2L_3 Auger energy shifts versus P1s binding energy shifts.	60
4.3	Experimental S2p binding energy shifts versus S1s binding energy shifts.	61
4.4	Experimental (-) S KL_2L_3 Auger energy shifts versus S1s binding energy shifts.	62
4.5	Comparison of the P valence population (from CNDO/2 calculation) with the state of core ionisation for some phosphorus compounds.	77
4.6	Comparison of the P valence population (from EWMO calculation) with the state of core ionisation for some phosphorus compounds.	78
4.7	Comparison of the S valence population (from CNDO/2 calculation) with the state of core ionisation for some sulphur compounds.	79

Figure	Description	Page
4.8	Comparison of the S valence population (from EWMO calculation) with the state of core ionisation for some sulphur compounds.	80
4.9	Comparison of the P valence population (from CNDO/2 calculation) with the state of core ionisation for $P(CH_3)_3$ and PCl_3 with and without d orbitals included in the basis set.	83
4.10	Comparison of the P valence population (from EWMO calculation) with the state of core ionisation for some phosphorus compounds going from the Si^- equivalent core state to the Cl^{++} equivalent core state.	85
4.11	Comparison of the central atom valence population (from EWMO calculation) with the state of core ionisation for $SiCl_4$, PCl_3 and SCl_2.	86
4.12	Comparison of the P valence population (from EWMO calculation with new P parameterisation) with the state of core ionisation for some phosphorus compounds.	89
4.13	Correlation of ΔE (RPM) versus ΔE (expt.) P2p binding energy shifts - atom charge model, CNDO/2 calculation.	100

Figure	Description	Page
4.14	Correlation of ΔE(RPM) versus ΔE(expt) S2p binding energy shifts - atom charge model, CNDO/2 calculation.	101
4.15	Correlation of ΔE(RPM) versus ΔE(expt) P KL_2L_3 Auger energy shifts - atom charge model, CNDO/2 calculation.	102
4.16	Correlation of ΔE(RPM) versus ΔE(expt) S KL_2L_3 Auger energy shifts - atom charge model, CNDO/2 calculation.	103
4.17	Correlation of ΔE(RPM) versus ΔE(expt) P1s binding energy shifts - potential model, CNDO/2 calculation.	108
4.18	Correlation of ΔE(RPM) versus ΔE(expt) S1s binding energy shifts - potential model, CNDO/2 calculation.	109
4.19	Correlation of ΔE(RPM) versus ΔE(expt) P2p binding energy shifts - potential model, CNDO/2 calculation.	110
4.20	Correlation of ΔE(RPM) versus ΔE(expt) S2p binding energy shifts - potential model, CNDO/2 calculation.	111
4.21	Correlation of ΔE(RPM) versus ΔE(expt) P KL_2L_3 Auger energy shifts - potential model, CNDO/2 calculation.	112

Figure	Description	Page
4.22	Correlation of ΔE(RPM) versus ΔE(expt) S KL_2L_3 Auger energy shifts - potential model, CNDO/2 calculation.	113
4.23	Correlation of ΔE(RPM) versus ΔE(expt) P2p binding energy shifts - EWMO calculation.	127
4.24	Correlation of ΔE(RPM) versus ΔE(expt) S2p binding energy shifts - EWMO calculation.	128
4.25	Correlation of ΔE(RPM) versus ΔE(expt) P2p binding energy shifts - EWMO calculation with new P parameterisation.	129
4.26	Correlation of ΔE(RPM) versus ΔE(expt) S2p binding energy shifts - EWMO calculation with new P parameterisation.	130
4.27	Correlation of ΔE(TPM) versus ΔE(expt) P2p binding energy shifts - EWMO calculation with new P parameterisation.	131
4.28	Correlation of ΔE(TPM) versus ΔE(expt) S2p binding energy shifts - EWMO calculation with new P parameterisation.	132
4.29	Correlation of ΔE(RPM) versus ΔE(expt) P KL_2L_3 Auger energy shifts - EWMO calculation.	133
4.30	Correlation of E(RPM) versus E(expt) S KL_2L_3 Auger energy shifts - EWMO calculation with new P parameterisation.	134

Figure	Description	Page
4.30	Correlation of $\Delta E(RPM)$ versus $\Delta E(expt)$ S KL_2L_3 Auger energy shifts - EWMO calculation with new P parameterisation.	134
4.31	Correlation of $(\Delta E_{2p*}-V)$ with $(kq+\ell)$ using EWMO RPM charges and potentials- P series.	137
4.32	Correlation of $(\Delta E_{2p*}-V)$ with $(kq+\ell)$ using EWMO RPM charges and potentials- S series.	138
4.33	Correlation of $(\Delta E_{1s}-V)$ with $(kq+\ell)$ using EWMO RPM charges and potentials- P series.	139
4.34	Correlation of $(\Delta E_{2p*}-V)$ with $(kq+\ell)$ using CNDO/2 RPM charges and potentials- P series.	142
4.35	Relationship of the Auger energy shift to the photoelectron binding energy shift- P series.	146
4.36	Relationship of the Auger energy shift to the photoelectron binding energy shift- S series.	147
4.37	Correlation of the Auger parameters and the sum of the calculated relaxation energy shifts and K_α X-ray shift- P series.	152
4.38	Correlation of the Auger parameters and the sum of the calculated relaxation energy shifts and K_α X-ray shift- S series.	153

Figure	Description	Page
A2.1	Core integrals (from Sichel and Whitehead)[49] versus the second row elements.	173
A2.2	Core integrals (from Oleari et al.)[57] versus the second row elements.	174
A2.3	One centre electron repulsion integrals versus the Slater exponent.	176
A2.4	Core integrals from Oleari et al.[57] versus core integrals from Sichel and Whitehead.[49]	178
A2.5	Core integrals (from Sichel and Whitehead[49] but with new P parameterisation) versus the second row elements.	180

Chapter 1. Introduction

A. General Introduction

In 1964, Hägstrom, Nordling and Siegbahn[1] demonstrated that high resolution β-ray spectrometers could be used to determine the binding energies of inner shell electrons in elements of low atomic number and that the binding energy of an inner shell electron from a particular element in different chemical environments could vary significantly. Since then the field of photoelectron spectroscopy has been shown to have many applications.[2] Photoelectron spectroscopy is in essence the application of the Einstein Photoelectric Law:

$$E_K = h\nu - I \tag{1.1}$$

which relates the energy of the incident photon ($h\nu$) to the ionisation potential (I) and the kinetic energy of the ejected photoelectron (E_K), to chemical systems.

Following initial photoionisation the system can undergo secondary processes to achieve a lower energy state. An electron from a higher energy level can fill the vacancy releasing the excess energy either as:

(a) a photon (X-ray fluorescence) or

(b) an electron (the Auger process).

The Auger process[3] is an internal rearrangement of electrons with the ejection of one electron carrying the excess energy. The energy of the ejected electron depends upon the energies of the levels involved. As is the case with primary photoionisation the Auger electron energy can also vary significantly with the chemical environment. Understanding how these shifts arise and how they relate to each other is of fundamental importance.

B. Description of the Various Processes

The various types of processes which can occur are illustrated in figure 1.1. Note that both X-ray (K, L, M,..) and orbital (1s, 2s, 2p, 3s, 3p,..) notation for the electron energy levels are used in the figure to demonstrate the relationship.

(i) Photoionisation

When the initial state of a molecule or atom is bombarded with photons of a characteristic energy, $h\nu$, a transition occurs in which the final state is an ion plus a free electron. Conservation of energy requires that

$$h\nu = E_K + E_i$$

where E_K is the kinetic energy of the free electron and E_i is the energy of formation of the ion. This is the ionisation energy for removal of an electron from the molecule. The ion is several thousand times heavier than the electron and conservation of momentum dictates that for all practical

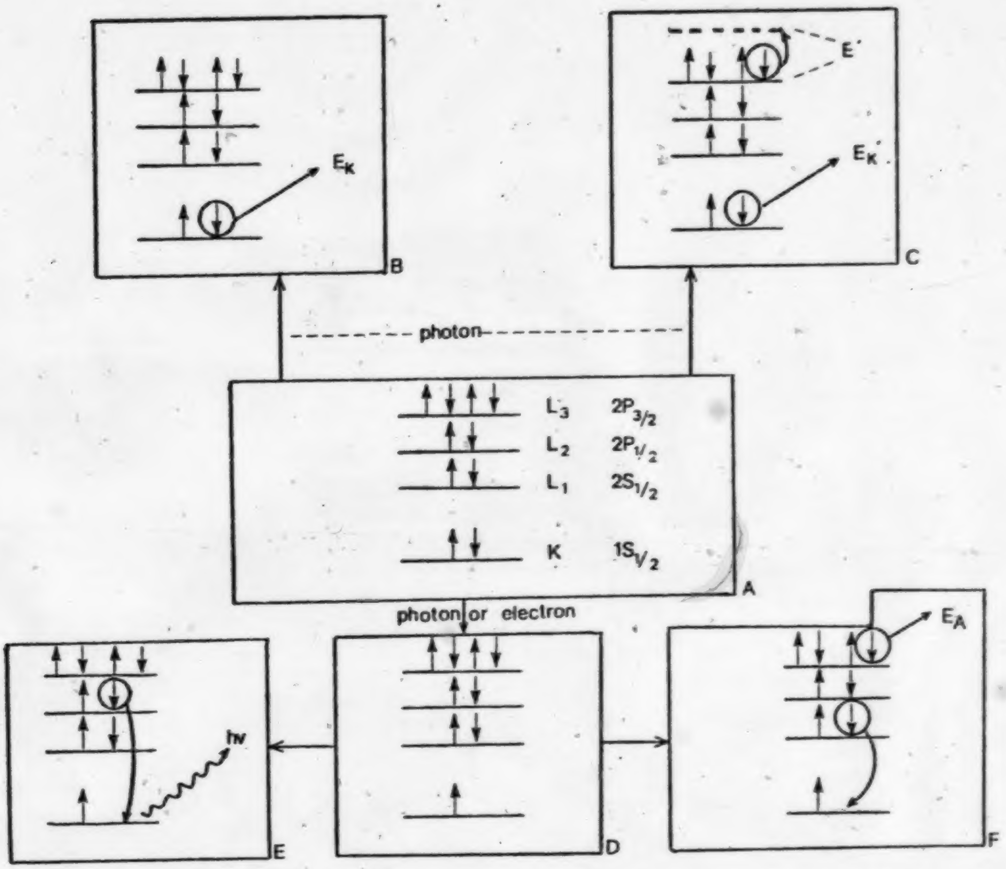

Figure 1.1 Processes involved in electron spectroscopy.

A. Initial state, e.g. Ne.

B. Photo ionisation.

C. "Shake-up" - "Shake-off" produces satellite structures.

D. Core vacancy produced by any means allows E and F.

E. X-ray fluorescence, core vacancy filled by an electron from a higher level and a photon of energy released.

F. Auger process, core vacancy filled by an electron from a higher level and a secondary electron is released.

purposes the free electron takes up all the kinetic energy.

The ionisation energy can be equated to the difference in the total energy of the ion state and that of the ground state of the molecule or atom:

$$E_I^{s} = E_f^{s}(N-1) - E_o(N) \qquad (1.2)$$

where E_I^{s} = ionisation energy of electron s

$E_o(N)$ = total energy of the ground state (the initial state of the system)

$E_f^{s}(N-1)$ = total energy of the ion which is formed when electron s is removed.

Rigorous calculation of the appropriate total energies yields the ionisation energy.

Quantum mechanically the probability of a transition from the initial ground state (Ψ'') to the final state (Ψ' - ion + free electron) is given by the square of the transition moment integral[4]

$$M = \langle \Psi'' \mid \Sigma p \mid \Psi' \rangle \qquad (1.3)$$

where p is the dipole moment operator. Application of the Born-Oppenheimer approximation separates the wave functions into a product of electronic and nuclear functions. Equation 1.3 then becomes

$$M = \int \Psi_v^{*}{}''(R)\ \Psi_v{}'(R)\ dR.\ \int \Psi_e^{*}{}''(r;R)\ \left|\sum_i p_e\right| \Psi_e{}'(r;R)\,dr \qquad (1.4)$$

The nuclear function has been further split into rotational and vibrational parts and since, in the majority of cases rotational structure cannot be resolved, the former is ignored.

For a photoelectron transition to be allowed the integrals in equation 1.4 must be non-zero. The final state includes a free electron as well as the ion and hence there is always a non-zero value for equation 1.4. As a consequence all one-electron transitions are allowed.

In the past photoelectron spectroscopy has been divided (somewhat artificially) into two sections depending on the photon source being used. One major branch is Photoelectron Spectroscopy (PES) or Ultraviolet Photoelectron Spectroscopy (UPS). In this case ultraviolet radiation provides the photon source and hence this spectroscopy only deals with the valence region. The other major branch is Electron Spectroscopy for Chemical Analysis (ESCA) or X-ray Photoelectron Spectroscopy (XPS). The photon source in this case is an X-ray. Depending on the X-ray being used and the molecule being studied, the deeper core levels of the atom can be probed as well as the valence shell levels. In this thesis only the techniques appropriate to XPS will be discussed.[5]

Because the core electrons do not take part in bonding, it was originally thought that they would be of little practical interest to the chemist. It is now known that the core electron binding energy values are affected by the valence electron distribution and yield chemical information upon core level ionisation. The interaction of the core electron with the valence shell gives rise to a potential energy contribution to the total ground state energy of the molecule. Electron withdrawing substituents would reduce this contribution whereas electron donating groups would increase the contribution and hence the *chemical shift* from a suitable reference gives an indication of the chemical environment.

(ii) "Shake-up and Shake-off"

In addition to the major peak, the photoelectron spectra of the core-levels can also exhibit many satellite structures. Energy-loss peaks occur on the low kinetic energy side of the main peak. They arise when the ejected electron collides with molecules in the chamber thereby losing some kinetic energy. The latter contributions are pressure dependent and are not part of the photoionisation process.

Upon photoionisation an excited ion state may be formed in which the photoelectron has been emitted along with the simultaneous excitation of an outer electron either to an excited bound state or to the continuum. The former is termed "shake-up" while the latter is termed "shake-off". Upon ionisation the resultant ion can be in one of a number of states with the ionisation energy of the photoelectron being given by a modified form of equation (1.2)

$$E_I^{s,k} = E_f^{s,k}(N-1) - E_o(N) \qquad (1.5)$$

When k = 0 the ion is in its ground state and this gives rise to the major peak. The satellite lines are defined by k = 1, 2, etc. and since they denote excited ion states the satellites will appear on the low *kinetic* energy side of the major peak.

Photoionisation follows dipole selection rules (see equation 1.3), that is $\Delta L = 1$ and $\Delta S = 0$, thus the allowed excited ion states must have the same symmetry as the ion in its ground state.

Satellites also appear in the spectrum due to the fact that the photon source is not monochromatic. The principal satellites are observed on the high kinetic energy side of the main peaks. By knowing the "diagram lines" of the characteristic X-ray these satellites can be easily identified and removed mathematically.

(iii) X-ray Fluorescence and the Auger Process

Following creation of the core-hole state of the ion, secondary processes can occur to allow the system to achieve a lower energy state. The two major decay modes are X-ray fluorescence and the Auger process. In the case of X-ray fluorescence the excess energy is released in the form of a photon whereas in the Auger process the excess energy is given to an emitted electron.

For the lighter elements the Auger process dominates.[6] The respective yields for K-shell fluorescence and Auger yields are given by

$$w_K = \frac{P_f}{P_f+P_A} \text{ and } a_K = \frac{P_A}{P_f+P_A} \qquad (1.6)$$

w_K = K-shell fluorescence yield
a_K = Auger yield
P_f = transition probability for X-ray Fluorescence
P_A = transition probability for the Auger process.

For P(Z = 15) $w_K = 0.061$ and $a_K = 0.939$. Since X-ray fluorescence is not the most important decay mode for light elements and is not directly measurable with our equipment it will only be discussed briefly to illustrate the differences between it and the Auger process.

The selection rules governing X-ray transitions are given by

$$\Delta L = \pm 1,\ \Delta j = 0,\ \pm 1 \text{ with } j = 0 \nleftrightarrow j = 0 \qquad (1.7)$$

Thus in transitions from the L shell to a K-hole the $L_2(K_{\alpha 2})$ and $L_3(K_{\alpha 1})$ transitions are allowed whereas that from L_1 shell is forbidden.

The X-ray line emitted corresponds to the energy difference between the two levels involved in the X-ray transition, and to the first approximation the shifts for the core levels of a molecule are very similar.[7] Thus *shifts* in the X-ray line in a series of molecules should be very similar. This limits the use of X-ray emission for the study of the chemical environment however, as will be seen later, there is a measurable difference in core electron chemical shifts between the 1s and 2p levels (1.3 eV for PF_5 compared to PH_3).[8]

The energy of the Auger electron is given by the difference between the total energy of the initial hole state and that of the two hole state:

$$E_{AU}(XYZ) = E_{M^+(X)} - E_{M^{++}(YZ)} \qquad (1.8)$$

$E_{AU}(XYZ)$ is the kinetic energy of the emitted XYZ Auger electron, $E_{M^+(X)}$ is the total energy of the initial hole state, a singly ionised species with a hole in level X, $E_{M^{++}(YZ)}$ is the total energy of the final two-hole state, a doubly ionised species with holes in levels Y and Z. Thus in figure 1F the emitted Auger electron would be designated KL_1L_3. The nomenclature follows the j-j coupling scheme which will be described later.

The Auger energy can also be expressed in terms of the binding energies of the levels involved:[9]

$$E_{AU}(XYZ) = E_B(X) - E_B(Y) - E_B(Z) - R \qquad (1.9)$$

R includes terms which further reduce the Auger energy due to differences in orbital energy values once an electron is removed. This form allows the Auger energy to be put in terms of measurable quantities and provides a basis upon which semi-empirical methods of calculation can be applied. The indistinguishability of electrons does not permit distinction of whether electron Y or Z is emitted as the Auger electron.

Unlike X-ray fluorescence, the Auger process can involve the L_1 shell. The selection rules are:[10]

$$\Delta L = \Delta S = \Delta J = 0 \text{ , parity unchanged}$$

and the transition probability is given by:

$$P = \frac{2\pi}{h} \left| \langle \phi_f(r_1)\ \Psi_f(r_2) \left| \frac{e^2}{|r_1 - r_2|} \right| \phi_i(r_1)\ \Psi_i(r_2) \rangle \right|^2 \qquad (1.10)$$

The Auger transition arises from a coulombic rearrangement due to the interaction of the two electrons involved.[10] ϕ_i and ψ_i are the single electron wavefunctions describing the initial hole state and ϕ_f and Ψ_f are the wavefunctions describing the final state, which includes the continuum electron. The wavefunctions must be correctly anti-symmetrised. The continuum electron can be treated as a plane wave and hence its orbital angular momentum is unrestricted thus allowing many transitions.

The second row (Si-Ar) KLL Auger spectra provides a suitable system for the study of Auger electron chemical shifts. Figure 1.2 shows the Auger KLL spectra of Ar, PH_3 and PF_3. The spectra are atomic in nature and show very similar features. Auger spectra which involve the valence-

Figure 1.2 KLL Auger spectra of Ar, PH_3 and PF_3. The initial hole state was created with the Ti K_α X-ray (4510.84 eV). The major peaks on the Argon spectrum are labelled in both the j-j and L-S coupling schemes. The '1' denotes satellites thought to be associated with M electron "shake-off".

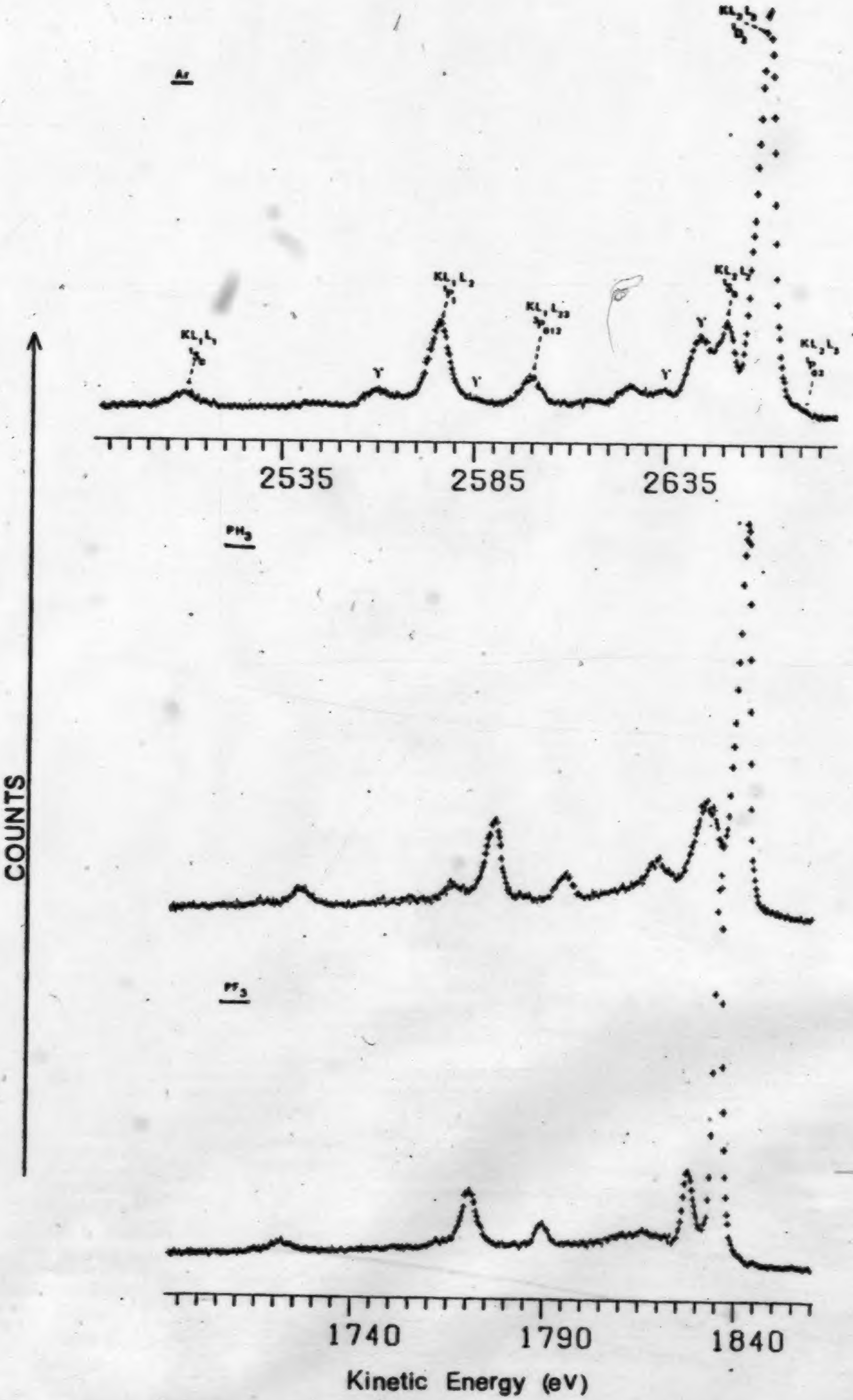
Ar
KL2L3 1D2
KL1L1 1S0
Y
KL1L2 1P1
Y
KL1L23 3P012
Y
Y
KL2L2 1S0
KL2L3 3P02
2535
2585
2635
PH3
COUNTS
PF3
1740
1790
1840
Kinetic Energy (eV)

shell, the KLL Auger spectra of the first row for example,[11] are more complex because the L shell atomic orbitals involved are now shared with other atoms. Hence KLL Auger spectra of these elements are unsuitable for the study of chemical shift, however, complimentary information to UPS can be derived therefrom.

The number of lines in the low Z region of the periodic table can be described by L-S coupling. In this case the spin angular momenta, s, of each of the electrons involved couple to give the total spin orbital momentum, S, of the system and similarly the orbital angular momenta, ℓ, of each electron couple separately to give the total orbital angular momentum, L, of the system. The total spin and orbital momenta couple to give the total angular momentum, J, of the system. The resultant state is designated as $^{2S+1}L_J$ where 2S+1 is called the multiplicity, J is the total angular momentum and L, the angular momentum is designated by the letters S, P, D, F, etc., for L=0, 1, 2, 3 respectively. Six final states are possible and these are shown in table 1.1.

The KLL Auger spectrum shows only five major lines in the low Z region since the ^3P state from the $2s^22p^4$ configuration is forbidden because parity is not conserved. The initial K-hole state ($^1S_{1/2}$) in the KLL Auger process has even parity. The final state consists of a doubly-ionised core hole, which in this case is the $2s^22p^4$ (^3P)

TABLE 1.1

CONFIGURATION	STATES
$2s^0 2p^6$	$^1S_0$
$2s^1 2p^5$	$^3P_{0,1,2}$; $^1P_1$
$2s^2 2p^4$	$^1D_2$; $^3P_{0,1,2}$; $^1S_0$

configuration having even parity and an emitted electron. The electron, a continuum wave, must be in the P state (i.e. of angular momentum L = 1) in order to conserve the total angular momentum of the system. Hence the final state of the total system will have odd parity thereby making the ^3P state forbidden.

In the high Z region j-j coupling dominates. In this scheme the s and ℓ momenta of each electron couple to form a total angular momentum, j, for each electron. Thus each electron is described by a definite j value which must be specified before electron-electron coupling is invoked. This gives the $2s_{1/2}(L_1)$, $2p_{1/2}(L_2)$ and $2p_{3/2}(L_3)$ electrons, and along with the initial hole state, $^1S_{1/2}(K)$, gives rise to six possible Auger lines, namely; KL_1L_1, KL_1L_2, KL_2L_2, KL_1L_3, KL_2L_3 and KL_3L_3.

By following the total J values, the j-j coupling scheme can be correlated with the L-S scheme. This is illustrated in figure 1.3.[10] In the intermediate coupling scheme nine Auger lines are now possible. The $^3P_0$ and $^3P_2$ lines of the $2s^22p^4$ configuration are able to mix with the $^1S_0$ and $^1D_2$ lines of the same configuration respectively *via* the same J quantum number and parity is no longer violated. The $^3P_1$ state of the $2s^22p^4$ configuration is still forbidden since there is no state of $2s^22p^4$ configuration with the same J quantum number for it to mix with.

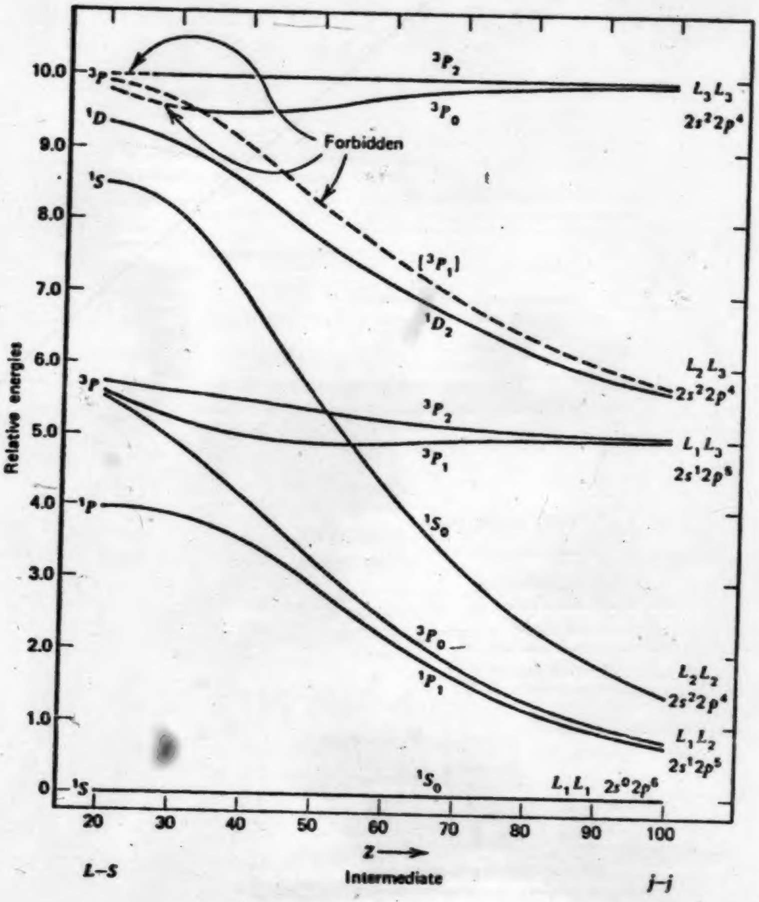

Figure 1.3 KLL line positions as a function of atomic number. (Reproduced with permission from Reference 10.)

The major lines are marked on the Ar spectrum (Figure 1.2) using both coupling schemes. In this region of Z, the L-S coupling still dominates and only the five major lines are observed. Other peaks are also present, the majority of these peaks arise from the emission of an Auger electron associated with a more highly excited initial K hole state. Thus Auger electrons emitted by such excited states will have a lower kinetic energy.

The excited initial K-hole state can be produced by "shake-up" or "shake-off" accompanying the initial photoionisation. For the second-row elements the probability of outer shell excitation accompanying K ionisation is approximately 4% from the L shell and 20% from the M shell.[12] Peaks associated with concomitant M shell excitation should appear on the low kinetic energy side of each peak and should possess similar relative energies and intensities as the major Auger lines,[13,14] since the M shell electrons are not involved in the KLL Auger process and should not interact strongly with the L shell electrons. The lines marked '1' in Figure 1.2 are thought to be satellite lines which are associated with M electron "shake-off" and can therefore be designated as KM-LLM lines. It can be seen that they are equidistant from their respective ground state Auger peaks. Comparing the spectra of PH_3 and PF_3 reveals that the energies of these features are chemically dependent.[12,14] Peaks arising from states in which the L shell is excited are less intense than those in which the M shell is excited. These satellites should be irregular both in position and intensity since the excited electron arises from the same shell as that partaking in the Auger process, and strong interactions would be expected.[14] Excitation of a bound electron upon ejection of the Auger electron can also contribute to the satellite structure. This is known as the double-Auger process and should be difficult to see because the energy is divided between two electrons.[12]

Excitation of the Auger spectrum can be effected by different means; the only essential feature is the creation of an ion with an inner shell hole. X-ray excitation used herein generally yields a simpler spectrum because production of highly excited ions is limited. Electron beam excitation frequently produces highly excited hole-state ions, hence satellite features are frequently more prominent.

C. Models for Chemical Shift

It is not feasible or practical to calculate initial and final state energies for all molecules studied in order to describe the chemical shift in both photoelectron or Auger spectroscopy. Simple models can greatly extend the utility of the data obtained and we discuss here the basis for the models and the concepts involved.

(i) Koopman's Theorem versus ΔE_{SCF}. The Concept of Relaxation

The binding (or ionisation) energy is properly defined by the difference in the total energy of the ground state and that of the final state (equation 1.2). The total energy of the ground state can be obtained by use of a full self consistent field calculation within the Hartree-Fock scheme,[15] as can that of the final state with the appropriate core hole. The difference in the total energies will give the binding energy of the electron. This is known as the ΔE_{SCF} method.[16] The method can prove expensive and within itself be subject to various levels of approximation and sophistication such as the extent and type of basis set and the inclusion of configuration interaction.

The most drastic simplification that can be made to the scheme is to use the same wave functions for the passive orbitals in the ionised state as in the ground-state. This is the "frozen orbital approximation".

The Hamiltonian, in the Hartree-Fock scheme, for an N-electron system with spin-orbitals Ψ_i which are solutions of the Hartree-Fock equation $\hat{H}\hat{\Psi}_i = \varepsilon_i\hat{\Psi}_i$ is given by

$$\hat{H} = h + \sum_{j=1}^{N} (J_j - K_j) \tag{1.11}$$

where h is the one-electron operator $(-\frac{1}{2}\nabla^2 - \sum_{\alpha} \frac{Z_\alpha}{r_{1\alpha}})$ and J_j

K_j are the coulomb and exchange operators.

The total energy for the N-electron system is

$$E(N) = \sum_{i=1}^{N} \langle\Psi_i|h|\Psi_i\rangle + \frac{1}{2}\sum_{i=1}^{N} \langle\Psi_i|\sum_{j=1}^{N}(J_j-K_j)|\Psi_i\rangle$$

$$= \sum_{i=1}^{N} h_i + \frac{1}{2}\sum_{i=1}\sum_{j=1}^{N}(J_{ij}-K_{ij}) \qquad (1.12)$$

where $J_{ij} = \langle\Psi_i(1)\ \Psi_j(2)|1/r_{12}|\Psi_i(1)\ \Psi_j(2)\rangle$

$K_{ij} = \langle\Psi_i(1)\ \Psi_j(2)|1/r_{12}|\Psi_j(1)\ \Psi_i(2)\rangle$

and for the N-1 system, with electron ℓ missing

$$E(N-1,\ell) = \sum_{i\neq\ell}^{N} h_i + \frac{1}{2}\sum_{i,j\neq\ell}^{N}\sum (J_{ij}-K_{ij}) \qquad (1.13)$$

The difference is simply

$$E(N) - E(N-1,\ell) = h_\ell + \frac{1}{2}\sum_{j}^{N}(J_{\ell j}-K_{\ell j}) \qquad (1.14)$$

but this is simply the eigenvalue for electron $\ell(\varepsilon_\ell)$ in the original Hartree-Fock equation

$$E(N) - E(N-1,\ell) = \varepsilon_\ell \qquad (1.15)$$

This result is known as Koopman's theorem[15,17] which states that the binding energy is taken to be the negative of the eigenvalue of the Hartree-Fock equation. Only one calculation is required.

The major flaw in the Koopman's Theorem approach is that it is a frozen orbital approach and takes no account of electronic reorganisation which accompanies photoionisation. This would not be a problem if reorganisation energies were constant for each element, however it is apparent that the contributions vary significantly with structure and valence. A method of correcting the Koopman's Theorem value to the full ab initio ΔE_{SCF} standard would provide a cost and time advantage, avoid problems that can possibly occur with hole-state calculations[16] as well as providing a deeper conceptual understanding of the nature of the processes involved. Such an approach was described by Hedin and Johannson.[18]

The Hamiltonian for the ground state was written as:

$$\hat{H} = h + \sum_{k} V_k = h + V \qquad (1.16)$$

h is the one-electron operator, $V_k = J_k - K_k$, the two-electron coulomb and exchange operators from orbital k. For the hole state the Hamiltonian was written as:

$$\hat{H}^* = h + V^* \qquad (1.17)$$

where $V^* = V - V_k + V_p$, the * indicating a hole state. The potential describing the hole state is the original potential minus that due to the removed electron from orbital k plus a polarisation potential due to the polarisation of the orbitals upon removal of electron ℓ.

$$V_p = \sum_{k \neq \ell} (V_k^* - V_k) \tag{1.18}$$

This is the sum of the differences in the potential of the passive orbitals before and after ionisation.

Hedin and Johannson[18] showed that

$$E_\ell = \varepsilon_\ell + \frac{1}{2} \langle \ell | V_p | \ell \rangle + \frac{1}{2} \sum_{i \neq \ell} \langle \delta i | H^* - H - \delta\varepsilon_i | \delta i \rangle \tag{1.19}$$

the δ signifying the difference between the initial and final values. Expression (1.19) is exact, no approximations have been made. The final term on the right-hand is small compared to the polarisation (or relaxation) term and so the relaxed orbital energy becomes

$$E_\ell = \varepsilon_\ell + \frac{1}{2} \langle \ell | V_p | \ell \rangle \tag{1.20}$$

This result provides a good basis for further studies, especially in the formulation of semi-empirical potential models.

(ii) Correlation of Potential with Binding-Energy Shifts

Basch[19] and Schwartz[20] showed, almost simultaneously, that the change in orbital energy paralleled the change in potential at the nucleus on which the core orbital resided.

The potential at nucleus A arising from *doubly-occupied* orbitals k and other nuclei, Z_B, is given by

$$\Phi_A = -2\sum_{k} <k|1/r_{1A}|k> + \sum_{B\neq A} Z_B/R_{AB} \qquad (1.21)$$

In the Hartree-Fock-SCF theory the orbital energy is given by

$$\varepsilon_k = <k|-\tfrac{1}{2}\nabla_1^2|k> + <k|\sum_{B} - Z_B/r_{1B}|k> +$$

$$\sum_{\ell\neq k} (2J_{k\ell} - K_{k\ell}) + J_{kk} \qquad (1.22)$$

This is the same as equation (1.14) except that the summations are performed over doubly-occupied orbitals.

Basch collapsed orbital k onto nucleus A for all terms except those giving zero or indeterminate results. Thus $<k|-\frac{1}{2}\nabla_1^2|k>$, J_{kk} and $\sum_{\ell\neq k} K_{k\ell}$ were kept,

$$<k|\sum_{B}-Z_B/r_{1B}|k> = <k|-Z_A/r_{1A}|k> + <k|\sum_{B\neq A}-Z_B/r_{1B}|k>$$

$$= <k|-Z_A/r_{1A}|k> + \sum -Z_B/R_{AB}$$

($r_{1B} = R_{AB}$, the internuclear distance since electron 1 is centered on A.)

$$\sum_{\ell\neq k} 2J_{\ell k} = 2\sum_{\ell\neq k} <k(2)\ \ell(1)|1/r_{1A}|k(2)\ \ell(1)>$$

$$= 2\sum_{\ell\neq k} <k|k><\ell|1/r_{1A}|\ell> = 2\sum_{\ell\neq k} <\ell|1/r_{1A}|\ell>$$

Hence equation (1.22) became

$$\varepsilon_k' = V_A + \langle k|-\tfrac{1}{2}\nabla_1^2|k\rangle + \langle k|-Z_A/r_{1A}|k\rangle + J_{kk} - \sum_{\ell\neq k} K_{k\ell} \qquad (1.23)$$

where $V_A = 2\sum_{\ell\neq k}\langle \ell|1/r_{1A}|\ell\rangle + \sum_{B\neq A} -Z_B/R_{AB}$

and finally $\varepsilon_k \sim \Delta V_A$

on the assumption that the change in the other terms in equation (1.23) can be taken to be negligible. Calculations[19] have indicated that this assumption is valid.

Comparison of V_A with Φ (equation 1.21) shows it to be basically an "external potential", with ΔV_A being the difference in potential "felt" by the atom.

Schwartz[20] analysed the system in a slightly different manner. The 1s orbital was separated from the others which had previously been transformed to localised molecular orbitals, L. The interaction of the 1s orbital with orbitals L in the two electron integrals was further split into a local contribution, L_i (molecular orbitals connected to atom A) and a distant contribution, L_j (those not connected to atom A). Equation 1.22 became

$$\varepsilon_{1s} = \langle 1s|-\tfrac{1}{2}\nabla_1^2 - Z_A/r_{1A}|1s\rangle + J_{1s1s} - \sum_{B\neq A}\langle 1s|Z_B/r_{1B}|1s\rangle +$$

$$\sum_{i=loc}(2J_{1si}-K_{1si}) + \sum_{j=dist}(2J_{1sj}-K_{1sj}) \qquad (1.24)$$

This form allows the following approximations to be made.

The 1s orbital is highly localised (becoming essentially a delta function) and so the distant exchange integrals (K_{1sj}) should be approximately zero. Furthermore, the distant coulomb integrals should have the same order as the electron-nuclear attraction integral of the distant L_j for nucleus A and the attraction of the 1s density to other nuclei can be approximated by a point charge:

$$<1s|Z_B/r_{1B}|1s> \simeq Z_B/R_{AB}$$

Finally, the localised internal energy of 1s

$$\varepsilon_{1s}^{int} = <1s|-\frac{1}{2}\nabla_1^2 - Z_A/r_{1A}|1s> + J_{1s1s}$$

should be insensitive to environment, leaving

$$\begin{aligned} -\varepsilon_{ext} &= -\varepsilon_{1s} + \varepsilon_{1s}^{int} \\ &= -2 \sum_{j=dist} <L_j|1/r_{1A}|L_j> + \sum_{B\neq A} Z_B/R_{AB} - \\ &\quad \sum_{i=loc} (2J_{1si} - K_{1si}) \qquad (1.25) \end{aligned}$$

comparing this with Φ_{ext}

$$\begin{aligned} \Phi_{ext} &= \Phi - \Phi_{int} \\ &= -2 \sum_{j=dist} <L_j|1/r_{1A}|L_j> + \sum_{B\neq A} Z_B/R_{AB} - \end{aligned}$$

$$- \quad 2 \sum_{i=\mathrm{loc}} \langle L_i | 1/r_{1A} | L_i \rangle \tag{1.26}$$

The final expressions on the right-hand side of equations (1.25) and (1.26) are not identical to each other but should be similar and their changes with the environment should be very nearly the same, thus:

$$\Delta(-\varepsilon_{1s}) \simeq \Delta(\Phi_{ext})$$

and by application of Koopman's Theorem

$$\Delta E_B \simeq \Delta(\Phi_{ext})$$

Furthermore, the core orbitals at the other nuclei are very localised and screen their respective nuclei and so only the valence orbitals need be considered:

$$\Delta E_B = \Delta(\Phi_{val}) \tag{1.27}$$

where $\Phi_{val} = -2 \sum_{\ell=val} \langle \ell | 1/r_{1A} | \ell \rangle + \sum_{B \neq A} Z_B^*/R_{AB}$ with Z_B^* being the effective reduced nuclear charge. This result allows semi-empirical models utilising such methods as the CNDO formalisation[21] to be used.

The potential model can also be expressed in the following manner for an N-electron system

$$E_B = k_i^N q_A^N + V_A^N + \ell \tag{1.28}$$

this expression, which will be termed the "atom-charge model", was originally based upon purely electrostatic considerations. It can also be shown to follow directly from the Hartree-Fock orbital energy[22] using arguments analogous to those of Schwartz and Basch.[19,20]

q_A^N = charge on atom A

$V_A^N = \sum_{B \neq A} q_B/R_{AB}$; q_B = charge on atom B

R_{AB} = internuclear distance between atoms A and B

Thus V_A^N is the potential on atom A due to the charges at all other atoms.

$k_i = \langle ij|1/r_{ij}|ij\rangle$; j = valence electron.

This is the coulomb repulsion integral between the core and the valence electron.

The value ℓ is simply a constant depending on the reference level.

By invoking the point-charge approximation the atom charge model reduces to the potential model of Schwartz or Basch. In this case

$$k_i = \langle j|1/r_i|j\rangle = \zeta/n$$

The nuclear attraction integral of the valence orbital at A for nucleus A, which in turn can be equated to the Slater orbital exponent for the valence shell (ζ) divided by the principal quantum number (n) of that shell provided Slater type orbitals are used. Both the calculated integral[23a] and the Slater exponent[24] have been employed in the evaluation of this model.

The value for k_i can also be determined empirically by a least-squares fit on experimental data in conjunction with the charges and potentials obtained from the semi-empirical calculation. A separate k_i can thus be obtained for each core-level.

The above models have assumed the validity of Koopman's Theorem. This is satisfactory for predicting shifts in *carefully* selected series of compounds where the relaxation is similar. This model is known as the Ground Potential Model (GPM). Further improvement would allow for variation in relaxation and is known as the Relaxation Potential Model (RPM).[23]

The relaxation potential model follows directly from equation (1.20).[18] Re-expanding this equation:

$$\begin{aligned} E_\ell &= \langle \ell | h+V | \ell \rangle + \frac{1}{2}\langle \ell | \sum_{k \neq \ell} (V_k^* - V_k) | \ell \rangle \\ &= \frac{1}{2}\langle \ell | h+V | \ell \rangle + \frac{1}{2}\langle \ell | H^* + V_\ell | \ell \rangle \\ &= \frac{1}{2}(\varepsilon_\ell + \varepsilon_\ell^*) \qquad (1.29) \end{aligned}$$

since by definition $\langle \ell | V_\ell | \ell \rangle = \langle \ell\ell | 1/r_{12} | \ell\ell \rangle = 0$; ε_ℓ^* is the hole state orbital energy. The result confirms an empirical rule proposed by Liberman.[25] Equating the change in orbital energies to changes in potential leads to

$$E_{\ell} = \frac{1}{2}(V_A + V_A^{*}) = - E_B \qquad (1.30)$$

where E_B is the shift in the binding energy of the core-electron. One further approximation must be made if semi-empirical approaches are to be used. To calculate V_A^{*} the concept of equivalent cores must be invoked. The idea was originally applied to the estimation of binding energy shifts by Jolly[26] using thermochemical data. However the concept had been well established for analogous systems.[27]

The 1s electrons effectively shield the other electrons from one unit of nuclear charge. In the (1s) hole state the valence electrons belonging to a nucleus of charge Q are subjected to (Q-1) units of charge. This behaviour can be mimicked by replacing the parameters of the ionised atom by those of the atom with one additional unit of atomic charge, ie Z+1. Increasing the net molecular charge by one unit equates the number of electrons in the two species and preserves the closed shell structure. Thus the $M(Z)X_n$ core hole ion is approximated by the $M(Z+1)X_n^{+}$ ion. The same number of valence electrons in the ion are subjected to a nucleus of total charge (Q+1) shielded by *two* 1s electrons and hence are under the influence of (Q-1) units of charge as in the case of the ion with a (1s) hole. The assumptions made in the equivalent-core approximation are on the same level as those leading to the potential model[23c] (compare equation 1.27) and so equation 1.30

finally becomes

$$\Delta E_B = -\frac{1}{2}\ (\Delta V_A(Z) + \Delta V_A(Z+1)) \qquad (1.31)$$

(iii) Models Involving Transition Operator Formalism

The RPM requires that two calculations be performed. The Transition Potential Model (TPM)[28] has been suggested as a method of avoiding the need for two calculations. The TPM follows from the Transition Operator Method (TOM)[29] and before discussing the specific application it is necessary to consider some of the formalism behind TOM.

TOM maintains the one-electron picture at ΔE_{SCF} accuracy by optimising the mean energy of the initial and final states with respect to a set of common spin orbitals. The shift in binding energy is obtained from the eigenvalue of the ionised spin orbital (i) using the transition Fock operator which is defined as

$$F_i^T(1) = h_1 + \sum_{j\neq i} <j^T(2)||j^T(2)> + \frac{1}{2} <i^T(2)||i^T(2)> \qquad (1.32)$$

(where $<a(2)||a(2)>\ q(1) = \int a^*(2)\ 1/r_{12}\ (1-P_{12})\ a(2)\ q(1)\ d\nu_2$) and associated with the following eigenvalue problem

$$F_i^T(1)\ q^T(1) = \varepsilon_i^T\ q^T(1) \qquad (1.33)$$

The coulomb-exchange term associated with the i-th spin orbital is multiplied by occupation number $\frac{1}{2}$ to simulate the mean initial and final state.

Second-order perturbation analysis has shown that the "transition" eigenvalue differs from the Koopman's Theorem value in the same way as does the ΔE_{SCF} ionisation energy:[29]

$$-\Delta E_{SCF}(i) = \varepsilon_i^T = \varepsilon_i + \sum_{j,a} |\langle ji||ai\rangle|^2/(\varepsilon_a - \varepsilon_j) \qquad (1.34)$$

where a is a virtual orbital. Further analysis has led to a variational argument to justify F^T and it has also been shown that the "transition" eigenvalue is equal to the ΔE_{SCF} energy through to third-order in perturbation analysis.[30]

With the justification of TOM it is now convenient to extend the transition concept to the potential model. The ionised atom in the molecule of interest is replaced by a pseudo-atom of effective charge, $Z_A^* = Z_A + \frac{1}{2}$. The parameters used for this atom in semi-empirical calculations are interpolated between those appropriate to the Z_A and $Z_A + 1$ values. Put in the form of the atom charge model (equation 1.28), the TPM can be expressed as

$$\Delta E_B = k^{N,N-1}\, q_A^{N,N-1} + V_A^{N,N-1} + \ell' \qquad (1.35)$$

The superscript (N,N-1) denotes (transition) values associated with a system of going from N to N-1 electrons. Comparison of the TPM with the GPM should yield an estimate of the relaxation energy.

(iv) Extension of Potential Models to Auger Spectroscopy

The Auger KLL' electron kinetic energy is given by the difference in the total energy of the initial state, a species with a K-shell hole, and the total energy of the final state which contains 2 L shell holes.

$$E_A(KLL') = E_K^{(N-2)} - E_{LL'}^{(N-2)} \qquad (1.36)$$

In terms of the binding energies of the levels involved, the Auger process can be expressed as:

$$E_A(KLL') = E_B(K) - E_B(L) - E_B(\bar{L}') \qquad (1.37)$$

The bar indicates that electron L' arises from a hole state. Equation 1.37 is equivalent to equation 1.9.

Both Liberman and transition operator approaches can be applied to these equations. Adams[31] applied the Liberman expression to the Auger process for some chlorine containing species. Equation 1.36 was modified to become a "two-step" process.

$$E_A(KLL') = (E_K^{N-1} - E_o^N) - (E_{LL'}^{N-1} - E_o^N)$$

$$= E_B(K) - E_B(LL') \qquad (1.38)$$

$E_B(LL')$ can be called a "two electron binding energy". Applying the Liberman expression to equation (1.38) gave:

$$E_A = -\tfrac{1}{2}[\varepsilon(K)^N + \bar{\varepsilon}(K)^{N-1}] + \tfrac{1}{2}[\varepsilon(L)^N + \bar{\varepsilon}(L)^{N-2}] +$$

$$\frac{1}{2}[\varepsilon(L')^{N} + \bar{\varepsilon}(L')^{N-2}] \qquad (1.39)$$

and to equation 1.37 ("three-step" process)

$$E_A = -\frac{1}{2}[\varepsilon(K)^{N} + \bar{\varepsilon}(K)^{N-1}] + \frac{1}{2}[\varepsilon(L)^{N} + \bar{\varepsilon}(L)^{N-1}] + \frac{1}{2}[\varepsilon(L')^{N-1} + \bar{\varepsilon}(L')^{N-2}] \qquad (1.40)$$

Both of these expressions were tested against ΔE_{SCF} calculations and it was found that the three-step process gave the better result. Adams[31] applied the "potential at the nucleus" approximation, the equivalent core approximation and made the further (dubious) approximation (which is inherent in the "potential at the nucleus" approach) that core-level shifts were the same, obtained the following RPM expressions:

$$\Delta E_A \simeq \frac{1}{2}[\Delta V_N(Z) - \Delta V_N(Z+1) + 2\Delta V_N(Z+2)] \qquad (1.41)$$

for the two-step process and

$$\Delta E_A \simeq \frac{1}{2}[\Delta V_N(Z+1) + \Delta V_N(Z+2)] \qquad (1.42)$$

for the three-step process. Equation 1.42 is also the negative of the RPM expression for the binding-energy shift of a core-electron leaving an ion with a single-core hole. Thus by utilizing equation 1.37 the Auger energy shift can be written as

$$\Delta E_A = \Delta E^{L\rightarrow K}_{X\text{-ray}} + \frac{1}{2}[\Delta V(Z+1) + \Delta V(Z+2)] \qquad (1.43)$$

where $\Delta E^{L \rightarrow K}_{X\text{-ray}} = \Delta E_B(K) - \Delta E_B(L)$

The 1s level and 2p level interact differently with the valence shell due to their different proximities. This manifests itself in a larger shift for the 1s electron than for the 2p.[8] The "potential at the nucleus" model should reflect the 1s shift better than the 2p, however the potential part of equation 1.43 refers to an electron from the 2p shell. A measure of the interaction of the core-levels with the valence shell can be made by comparing the two-electron electrostatic integrals $F_o(1s,3p)$ and $F_o(2p,3p)$ obtainable from Mann's tables[32] and this can be used to modify equation 1.43. As will be seen later $\Delta E_{1s} =$ (constant) × ΔE_{2p} to a very good degree and so equation 1.43 should still reflect the trend of the Auger shift even if the potential part is not modified, though the slope may not be unity.

The transition operator gave the following result for the two-step process

$$\Delta E_A(KLL') = -\Delta(\varepsilon^{N,N-1} - 2\varepsilon^{N,N-2}) \qquad (1.44)$$

and for the three-step process[24]

$$\Delta E_A(KLL') = \Delta E^{L \rightarrow K}_{X\text{-ray}} - \Delta\varepsilon^{N-1,N-2} \qquad (1.45)$$

Application of the "atom-charge model" to equation 1.45 gave

$$-E_A + \Delta E^{L \to K}_{X\text{-ray}} = -\Delta\varepsilon^{N-1,N-2}$$

$$= k^{N-1,N-2} q_A^{N-1,N-2} V_A^{N-1,N-2} + \ell \quad (1.46)$$

The charges and potentials are calculated using a pseudo atom with nuclear charge $Z + \frac{3}{2}$ in place of the original Z atom. The parameters being obtained from interpolation between those associated with the Z+1 atom and those with the Z+2 atom.

The three-step model is the easiest to handle and with the findings of Adams represents the more obvious application of the potential model. The meaning of $\varepsilon^{N,N-2}$ within the TPM formalism, as would be required in the two-step model, leads to possible ambiguities with the equivalent core expression for the singly-ionised state (ε^{N-1}) in that the same parameters for the central atom are being used but two different states are being described. It was noted[33] that

$$\varepsilon_i^{N,N-1} \equiv \frac{1}{2}(\varepsilon_i^N + \varepsilon_i^{N-1})$$

when full calculations are used to determine the *orbital* energies. The ambiguities arise when the potential model is applied. These can be removed by imposing the following relationships[33]

$$\Delta\omega^{N,N-1} = \frac{1}{2}\,\Delta(\omega^N + \omega^{N-1})$$

$$\Delta\omega^{N,N-2} = \frac{1}{2}\Delta(\omega^{N,N-1} + \omega^{N-1,N-2})$$

where ω represents the "true" potential. By assuming a similar linearity for the charges, q, potentials, V, and K, namely

$$x^{N,N-1} = \frac{1}{2}(x^{N} + x^{N-1}) \ , \ x^{N-1} = \frac{1}{2}(x^{N,N-1} + x^{N-1,N-2})$$

expressions were obtained for the "correct" equivalent core potential[33] ($\tilde{\omega}$)

$$\begin{aligned} \tilde{\omega}^{N-1} &= \omega^{N-1} - 2(k^{N,N-1} - k^{N})Q \\ \tilde{\omega}^{N,N-2} &= \omega^{N-1} + (k^{N,N-1} - k^{N})Q \end{aligned} \qquad (1.47)$$

where $Q = q^{N,N-1} - q^{N}$.

The Auger parameter, α, was originally defined by Wagner[34] as

$$\alpha = (\Delta E_A + \Delta E_B) = 2\Delta R_{EA}$$

with ΔE_B being a core-binding energy shift and ΔR_{EA} the difference in extra atomic relaxation of the initial photoionisation. Application of equation (1.47) led to[33]

$$\Delta(E_A(KLL') + E_B(L")) = 2\Delta R^{N,N-1} - 6\Delta Q$$

$\Delta R^{N,N-1} = \Delta(\tilde{\omega}^{N} - \tilde{\omega}^{N,N-1})$, the molecular relaxation energy. This expression relates the shifts to the ground state and transition potential of the initial ionisation. The charge flow term ($6\Delta Q$) takes account of the differing initial states in the loss of the first electron to that of the second. The replacement of two-electron term by terms associated with the initial photoionisation removes the ambiguities however it is necessary to infer that the relaxation of the second step follows from the first.

In the original analysis[33] it was assumed that $\Delta E^{L\rightarrow K}_{X\text{-ray}}$ was close to zero. This assumption can lead to substantial errors. The ambiguity can be avoided by using the three-step process in which $\tilde{\omega}^{N-1,N-2}$ is used in conjunction with $\Delta E^{L\rightarrow K}_{X\text{-ray}}$.

A more accurate expression can be derived for the Auger parameter.

$$\begin{aligned}\Delta E_A(KLL) + \Delta E_L &= (\Delta E_K - \Delta E_L - \Delta E_{L'}) + \Delta E_L + (\Delta E_L - \Delta E_L)\\ &= \Delta E^{L\rightarrow K}_{X\text{-ray}} + 2\Delta E_L - \Delta E_L - \Delta E_{L'}\\ &= \Delta E^{L\rightarrow K}_{X\text{-ray}} - \Delta(\varepsilon^{N} + \varepsilon^{N-1}) + \Delta\varepsilon^{N,N-1} +\\ &\qquad \Delta\varepsilon^{N-1,N-2}\\ &= \Delta E^{L\rightarrow K}_{X\text{-ray}} + \Delta(\varepsilon^{N,N-1} - \varepsilon^{N}) + \Delta(\varepsilon^{N-1,N-2} - \varepsilon^{N-1})\\ &= \Delta E^{L\rightarrow K}_{X\text{-ray}} + \Delta R_L + \Delta R_{L'} \qquad (1.48)\end{aligned}$$

$$\begin{aligned}\Delta E_A(KLL) + \Delta E_K &= (\Delta E^{L\rightarrow K}_{X\text{-ray}} - \Delta E_{L'}) + \Delta E_K + (\Delta E_L - \Delta E_L)\\ &= (\Delta E^{L\rightarrow K}_{X\text{-ray}} - \Delta E_{L'}) + (\Delta E_L + \Delta E_{X\text{-ray}}) + (\Delta E_L - \Delta E_L)\\ &= 2\Delta E^{L\rightarrow K}_{X\text{-ray}} + \Delta R_L + \Delta R_{L'} \qquad (1.49)\end{aligned}$$

where the orbital approximations for the binding energy have been made using both the Liberman and transition operator approaches. The final expressions indicate that the shifts are dependant on the relaxation accompanying the loss of an initial L shell electron (the relaxation accompanying the loss of the initial K electron is altered upon the level being filled by an L electron) and that to the loss of an L electron leaving an ion with a L-shell hole. Applying the kq + V + ℓ model to ε^{N}, $\varepsilon^{N,N-1}$, ε^{N-1} and $\varepsilon^{N-1,N-2}$ will give estimates of $R_{L'}$ and R_{L} as long as the appropriate values for k are known.

The Auger parameter formalism provides a convenient way of relating the Auger shift to the binding energy shift. Rewriting equation 1.48 gives

$$\Delta E_{AUG} = (\Delta R_{L} + \Delta R_{L'}) - (\Delta E_{L} - \Delta E^{L\to K}_{X\text{-}ray}) \qquad (1.50)$$

This is nothing more than a rephrasing of equation 1.9. It can be seen that the Auger chemical shift depends on a reference level ($\Delta E_{L} - \Delta E^{L\to K}_{X\text{-}ray}$) which is modified by the relaxation contribution arising from the loss of the initial electron and that of the second.

D. The Purpose of This Study

As with core electrons, Auger electrons in a series of molecules also show a chemical shift. Core electron binding shifts have been studied extensively, however, until recently, there has been very little systematic study of the Auger electron shifts. It was of interest to study these shifts and to compare them to the photoelectron shifts.

To have readily comparable values only Auger transitions involving inner core electrons can be considered. The simplest system to study is the KLL spectra of the second row elements. The complete KLL Auger spectra for SF_6, SO_2 and H_2S have been studied quite extensively.[12,14]

For comparison of Auger shifts with those of core electron binding energies, only the KL_2L_3 ($^1D_2$) line need be considered. Keski-Rahkonen and Krause[35] compared the KL_2L_3 shift with the 1s electron shift in SF_6, H_2S and SO_2. Asplund et al.[36] compared the $2p_{3/2}$ shift with the Auger shift in SF_6, SO_2, H_2S, COS and CS_2. In this latter paper a formalism based upon the TPM[28] was presented, however no comparison of theory with experimental data was made.

An ab initio study of the Auger KL_1L_1 shift compared with the binding energy shifts in some chlorine-containing[31] and silicon-containing[37] species was conducted by Adams. He extended the Liberman expression[18,25] for binding energies to the Auger process and also outlined a relaxation potential expression.

The RPM was applied by Cavell and Sodhi[8] to a series of phosphorus compounds (PX_3, SPX_3, OPX_3 (X=F,Cl); PH_3 and PF_5) for both the core electron shifts and the Auger KL_2L_3

shifts using a CNDO/2 program.[38] The approach predicted the 1s shifts fairly well (and to a lesser extent the 2p shift). Its prediction of the Auger shifts was not as satisfactory. This was attributed as much to a possible failure of the CNDO formalism as to possible limitations in the potential model. (Note, after publication of this paper a looping error in the part of the program calculating the potential at the nucleus for the (Z+2) equivalent core state was discovered. Thus the calculated Auger shifts, as presented in the paper, are in error. Corrected shifts, as appropriate to the paper, are shown in appendix 3. The conclusions as stated above, however, are still valid.) The major feature of interest was the lack of correlation between the Auger shift and the P1s binding energy shift, not only were the magnitudes different but in some cases there was a reversal in trend. This was also observed by Asplund et al.[36] for some of the sulphur compounds.

Kelfve et al.[24] have performed the most extensive previous analysis of the relationship between the Auger shift and the 2p electron shift for a series of silicon compounds. They applied the TPM[28] using a modified extended Hückel program, EWMO.[39] The results showed satisfactory predictions for both the Auger and binding energy shifts. The shifts were also analysed by means of a "group shift" approach and in the limited geometry of the silicon compounds gave good correlation.

In this work the 1s and 2p core electron shifts are compared to the KL_2L_3 ($^1D_2$) Auger electron shifts in an extensive series of phosphorus and sulphur compounds. Unlike the silicon compounds in which the constant geometry limits general conclusions, compounds of sulphur and phosphorus show various coordination environments. It was of interest therefore, to see how the Auger and core electron shifts compared and hence how the relaxation effects differed with these various geometries. By studying two different series of compounds it is possible to see how the effects of one substituent transfer from one centre to another. We have therefore tested various phosphorus and sulphur compounds and analysed the results in terms of the various models available.

Chapter 2. Experimental

The 1s and 2p core levels and the KL_2L_3 Auger line were recorded using a McPherson ESCA 36 photoelectron spectrometer.

The 2p line was produced by irradiation with the Al K_α (1486.65 eV) X-ray or the Mg K_α (1253.64 eV) X-ray and referenced to the Kr $3p_{3/2}$ and Kr $3d_{5/2}$ lines (214.55 (15) eV and 93.80 (10) eV binding energies[40] respectively).

The 1s line was produced by irradiation with the Ag $L_{\alpha 1}$ (2984.34 (2) eV)[35] X-ray except for oxygen containing sulphur compounds, in which case the Ag $L_{\beta 1}$ (3150.97 (3) eV)[35] X-ray was used. The KL_2L_3 line was collected in the same scan as the 1s line and both lines were referenced to the Ne $KL_{2,3}K_{2,3}$ Auger line (804.56 (2) eV kinetic energy)[41] and the Ne 1s photoelectron line (870.37 (9) eV binding energy)[40] produced by the Ag $L_{\alpha 1}$ X-ray.

In all cases the X-ray sources were operated at a power of 400 watts (10 kV × 40 mA).

The reference gas supply was controlled with a Granville-Phillips series 203 variable leak valve. Liquid samples were contained in an evacuated glass vial equipped with a Teflon valve. The vapour was introduced via a Nupro SS-4BMW all metal bellows metering valve. Gaseous samples contained in cylinders were introduced via either the Granville-Phillips or the Nupro valve. In order to control the gas pressure accurately the cylinder pressure was reduced by a Matheson 3500 series regulator.

All lines were made of 1/4" stainless steel tubing and connections were made with 1/4" Swagelok fittings. The sample (and reference) supplies were mixed in the feed line prior to introduction into the sample cell. X-rays entered the sample cell through an aluminum window (0.0001" thickness).

The pressure of the mixture was monitored using a MKS Baratron Pressure meter. The sample and reference gases were of approximately equal pressures and typical (total) pressures ranged from 150-200 μ. The mixtures were successively scanned until adequate statistics ($1500 \geq$ c/s on highest peak) were achieved. Repeated rapid cycles were run to minimise any possible error between reference and sample peaks due to slight pressure drift.

The kinetic energy of the electron is calculated from the equation

$$\text{K.E.} = k\,\Delta V$$

where ΔV is the potential difference between the analyser plates and k is the experimentally determined machine constant. In order to compensate for any variations with time in the machine constant, k, which are noticable over the large kinetic energy differences involved in this work, all peak positions were normalised to give reference-line separations in agreement with those given in the literature, ie.

$$\frac{[\text{reference separation}]_{\text{expt}}}{[\text{reference separation}]_{\text{lit}}} = \frac{[x - \text{reference}]_{\text{expt}}}{[x_{\text{actual}} - \text{reference}]_{\text{lit}}}$$

hence the true kinetic energy of x, x_{actual}, was found. Subtracting the core electron kinetic energies from the energy of the exciting source gave the required binding energy.

At least three separate runs were performed for each data set and an average value was taken. The largest deviation from the average was 0.09 eV with the majority of cases deviating by 0.05 eV or less. It is concluded that the errors in the *shifts* are no more than ±0.1 eV.

Positions and areas of each peak were obtained by using a non-linear least squares program[42] which could fit either a Lorentzian or Gaussian curve. No attempt was made to deconvolute the spin orbital components of 2p peak as the resolution was insufficient. Some difficulty was experienced in deconvoluting the Kr 3d peak however constraining the Kr $3d_{5/2}$ and Kr $3d_{3/2}$ to equal FWHM gave a good fit with the required intensity ratios and separations. A sufficient portion of the low energy side of the KL_2L_3 Auger line was collected in order to ensure a good fit on the KL_2L_3 Auger peak, however this portion of the spectrum was not accurately fitted.

All the compounds were obtained commercially with the exception of SPF_3[43] and $P(CF_3)_3$[44] which were made by standard literature procedures in this laboratory, and $P(C_2H_5)_3$ which was supplied by Dr. John Malito of this department. Where necessary, the reagents were fractionated under vacuum to remove impurities, and the purity of the compound was verified by I.R. or N.M.R. spectroscopy or both. Chemical means had to be employed to purify SF_4[45], otherwise the compounds were run without further purification.

Chapter 3. Calculations

A. Semi-empirical Programs

Two types of semi-empirical calculations were employed. The first utilised the CNDO/2 formalisation[38] using the original parametrisation of Pople et al.[21] with the exception of Cl. The second was a modified iterative extended Hückel program (EWMO)[39] which was adapted for transition potential calculations. Calculations, in both cases, were performed with d-orbitals not included in the basis set. In the CNDO/2 case attempts were made to include d-orbitals, however difficulties occurred with convergence for many of the molecules.

Both programs had to be parametrised for Ar so that calculations could be performed to estimate the Auger electron chemical shift for the sulphur compounds.

In the CNDO/2 program the new Cl parameters[46] were

$$1/2(I + A)_s = -21.76 \text{ ev}$$

$$1/2(I + A)_p = - 9.56 \text{ eV}$$

The Ar parameters used for the CNDO calculations were those estimated by Støgard and Manne.[47]

The EWMO (Hückel) program has been used successfully by Kelfve et al.[24] on a series of silicon compounds. The main features of the program have been adequately described[24,48] and will not be dealt with here.

The Ar parameters for the EWMO (Hückel) program were obtained in the following manner. The expression for the electron-repulsion integrals, g_{ss}, within the CNDO formalisation reduces to

$$g_{ss} = [S_A S_A | S_A S_A]$$

where S_A represents the orbitals and are Slater-type s orbitals. This reduces to

$$g_{ss} = \text{const. } \zeta$$

where ζ is the Slater exponent. The ratio, $g_{ss}(\text{Ar})/g_{ss}(\text{Cl})$ then becomes the ratio of the Slater exponents:

$$\frac{g\ (\text{Ar})}{g\ (\text{Cl})} = \frac{\zeta_{\text{Ar}}}{\zeta_{\text{Cl}}} = \frac{2.25}{2.03} = 1.11$$

By using the values of the average one-centre electron repulsion integrals (g_{AA}) and the average two-centre electron repulsion integrals (g^*_{AA}) appropriate to the EWMO (Hückel) calculations for Cl[49], the following estimates for Ar were obtained:

$$g_{AA} = 11.42 \text{ eV} \qquad g^*_{AA} = 11.51 \text{ eV}$$

These values and the experimental ionisation potentials for Ar 3s and Ar 3p (29.24 eV and 15.82 eV respectively) give the core-matrix elements, U_{ss} and U_{pp}:

$$U_{ss} = -109.78 \text{ eV} \qquad U_{pp} = -96.36 \text{ eV}$$

by use of the relationship

$$-I_i = U_{ii} + (Z_A-1)g_{AA}$$

In all cases calculations were performed on each molecule for the ground state (Z) and the equivalent core states (Z+1) and (Z+2). The equivalent core states were obtained by replacing the atom of interest with the (Z+n) atom. A molecular charge of n throughout the series maintained a constant number of electrons. In this way the properties of the singly-ionised and doubly-ionised ions were mimicked.

Furthermore, in the Hückel case, calculations were performed on each molecule for the transition states (Z+1/2) and (Z+3/2). In this case the atom of interest was replaced by a pseudo-atom. For the (Z+1/2) case the pseudo-atom parameters were obtained by interpolation between those of the Z atom and those of the (Z+1) atom. In the (Z+3/2) case the parameters were interpolated between the (Z+1) atom and the (Z+2) atom.

B. Models for Chemical Shift

Semi-empirical calculations on ESCA shifts have proved useful in the context of the potential model. The original form of the potential model is

$$\Delta E_B = k_i q_A + V_A + \ell \qquad (3.1)$$

This will be termed the "atom charge model".

The terms in equation (3.1) are:

ΔE_B is the binding energy shift.

q_A is the charge on atom A, the atom of interest.

$V_A = \sum_{B \neq A} q_B/R_{AB}$, the potential on the ionised atom, A, due to the charges at all other atoms in the molecule.

$k_i = \langle ij|i/r_{ij}|ij\rangle$, the coulomb repulsion integral between the core electron (i) and the valence electron (j).

ℓ is a constant depending on the reference level.

In practice k_i and ℓ are obtained by a least-squares fit on experimental data. This allows a value of k for each core level to be estimated. However, in practice, it is found that the value of k varies according to the compounds selected for the least-squares fit.

By invoking the point-charge approximation, k_i becomes:

$$k_i = \langle j|i/r_i|j\rangle = \frac{\zeta}{n} \qquad (3.2)$$

that is the nuclear attraction integral of the valence orbital at A for nucleus A, which in turn is equal to the Slater orbital exponent (ζ) for the valence shell divided by the principal quantum number of the valence shell.

Equation (3.1) can be modified to form the potential model:

$$\Delta E_B = -\Delta V(Z) = -\Delta(KP_{AA} - \sum_{B\neq A} q_B/R_{AB}) \qquad (3.3)$$

where P_{AA} is the valence electron population on atom A and K is calculated for each case using the point charge approximation. This is the approach used by Davis et al.[23a]

Use of the ground state (i.e. parameters associated with the Z atom) in equation (3.1) or (3.3) allows an estimation of the chemical shift to be obtained. This approach ignores the relaxation occurring upon photoionisation and is known as the Ground Potential Model (GPM).

The Relaxation Potential Model (RPM) attempts to correct for relaxation by use of the equivalent core approach. Equation (3.1) is modified by using charges and the off-centre atom potentials given by

$$\begin{aligned} q_A &= 1/2(q_A(Z) + q_A(Z+1)) \\ V_A &= 1/2(V_A(Z) + V_A(Z+1)) \end{aligned} \qquad (3.4)$$

The appropriate k is obtained theoretically or by fitting.

The RPM as used by Davis et al.[23a] is obtained by taking the negative means of V(Z) and V(Z+1) found by use of equation (3.3). That is

$$\Delta E_B = -\frac{1}{2}\Delta(V(Z) + V(Z+1)) \qquad (3.5)$$

The use of the pseudo-atom (the Transition Potential Model - TPM) allows a direct estimate of the relaxed binding energies from equation (3.1). The appropriate charges and off-atom potentials, in this case, are given in one calculation.

An estimation for the relaxation energy can be obtained by subtracting the GPM value for the chemical shift from the RPM or TPM value.

The extension into Auger spectroscopy is obtained by using

$$\Delta E_{AUG} = \Delta(E_B(K) - E_B(L) - E_B(L^*)) = \Delta E_{XRAY} - \Delta E_B(L^*) \qquad (3.6)$$

where ΔE_{AUG} is the KLL Auger shift. The term $\Delta E_B(L^*)$ is the binding energy shift for an L-shell electron in a species already containing an L-shell hole.

The appropriate models, as described earlier, can be used by utilising a (Z+1) initial state and a (Z+2) final state or a (Z+3/2) transition state.

In the CNDO calculations ground and relaxation potential models were utilised for both the atom-charge and potential models. In the former case both fitted and theoretical k's were used. In the Hückel case the ground, relaxation and transition potential models were utilised for the atom-charge model.

All the geometries, where obtainable, were experimental.

Other geometries were assumed using bond lengths and angles from similar compounds of known geometry. Full details of the geometries used in the calculations can be found in Appendix 1.

Chapter 4. Results and Discussion

A. Experimental Results

All shifts were referenced to PH_3 in the phosphorus series and to H_2S in the sulphur series. Phosphorus 1s and 2p photoelectrons and KL_2L_3 Auger shifts are given in Table 4.1 and the corresponding data for the sulphur series in Table 4.2. The correlation between the 1s and 2p photoelectron shifts for phosphorus is shown in Figure 4.1 and the correlation between the 1s photoelectron and KL_2L_3 Auger shifts for phosphorus is shown in Figure 4.2. The corresponding correlations for sulphur are shown in Figures 4.3 and 4.4.

It was found that the oxygen KVV Auger region coincided with the S1s line under Ag $L_{\alpha 1}$ X-ray excitation. Accordingly S1s peaks were collected with Ag $L_{\beta 1}$ X-ray excitation for the oxygen-containing sulphur compounds. The S1s binding energies for H_2S differed when Ag $L_{\alpha 1}$ X-ray or Ag $L_{\beta 1}$ X-ray excitation were compared; the former gave a S1s value of 2478.87 eV whereas the latter gave a value of 2478.60 eV. Since the Ag $L_{\alpha 1}$ X-ray gave a more intense photoelectron line with a smaller FWHM than Ag $L_{\beta 1}$ X-ray the former value was considered to be more reliable. All S1s peaks obtained by means of Ag $L_{\beta 1}$ X-ray excitation were referenced to the S1s line of H_2S produced by the Ag $L_{\beta 1}$ X-ray in order to obviate binding-energy shift errors.

Table 4.1. Experimental chemical shifts[a] relative to PH_3[b]

	Compound #	$\Delta 1s$[c]	$\Delta 2p$[d]		$-\Delta KL_2L_3$[c]
PH_3	1	0.00	0.00		0.00
SPF_3	2	6.20	5.15		2.98
$P(CH_3)_3$	3	-0.98	-1.10	-1.08[e] -1.11[52]	-3.30
$SPCl_3$	4	4.21	3.57	3.58[52]	-0.47
OPF_3	5	6.96	5.91	6.03[52]	5.14
$OPCl_3$	6	4.70	4.01	4.01[52]	0.72
PF_5	7	8.55	7.33	8.83[52]	5.93
PCl_3	8	3.28	2.79	2.73[52]	-0.39
PF_3	9	5.48	4.72	4.70[e] 4.76[52]	4.62
$SP(CH_3O)_2Cl$	10	3.60	2.78		-0.95
$(CH_3O)_3PO$	11	3.34	2.54		-0.11
$(CH_3O)_3PS$	12	3.26	2.39		-0.95
$(CH_3O)_3P$	13	1.82	1.19		-1.03
$P(CH_3)Cl_2$	14	1.89	1.53		-1.33
$P(C_2H_5)_3$	15	-1.48	-1.53		-4.48
$OP(CH_2Cl)Cl_2$	16	3.77	3.18		-0.10
$SP(CH_3)Cl_2$	17	3.19	2.59		-1.44
$P(CF_3)_3$	18	1.74	1.70		-1.16

(a) All shifts taken as Δshift = compound - reference. Shifts are reliable to ±0.1 eV.

(Cont'd.)

Table 4.1. Cont'd.

(b) Reference lines for PH_3 (in eV)

	This work	Ref. 51	Ref. 52
1s	2150.88 (20)	-	-
2p	137.35 (20)	137.3	136.87
KL_2L_3	1841.46 (20)	1841.4	-

(c) The 1s lines were produced by AgL_α (2984.34 eV). The Auger line was collected in the same scan.

Calibration lines used were:

Ne $KL_{23}L_{23}$	804.56 (2) eV
AgL_α converted by Ne 1s	870.37 (9) eV

(d) The 2p lines were produced by AlK_α (1486.65 eV) or MgK_α (1253.64 eV).

Calibration lines used were:

Kr $3d_{5/2}$	93.80 (10) eV
Kr $3p_{3/2}$	214.55 (15) eV

(e) Values adjusted from Ref. 51.

Table 4.2. Experimental chemical shifts[a] relative to H_2S[b].

	Compound #	$\Delta 1s$[c]		$\Delta 2p$[d]		$-\Delta KL_2L_3$[c]	
H_2S	1	0.00		0.00		0.00	
$(CH_3)SH$	2	-0.74		-0.70		-1.97	
$(CH_3)_2S$	3	-1.25		-1.17	-1.18[51] -1.28[52]	-5.35	
$(CH_3)_2SO$	4	1.98		1.51	1.44[52]	-1.35	
$SOCl_2$	5	4.78		4.21		0.43	
SOF_2	6	6.83		5.88	6.00[52]	4.03	
SO_2	7	5.20	5.2[35]	4.43	4.40[36] 4.60[52]	3.10	3.02[36] 3.2[35]
SO_2ClF	8	7.82		6.48		3.01	
SO_2Cl_2	9	6.83		5.74		1.58	
SO_2F_2	10	8.91		7.56	7.30[52]	4.73	
SF_5Cl	11	10.38		8.94	9.00[52]	4.22	
SPF_3	12	-0.65		-0.55		-2.12	
$SPCl_3$	13	-1.49		-1.39		-4.28	
$(CH_3O)_2SO$	14	4.07		3.31		-0.17	
$(CH_3O)_3PS$	15	-2.67		-2.53		-5.20	

(Cont'd.)

Table 4.2. Cont'd.

SF_6	16	11.54	11.6[35]	9.86	9.84[36] 10.20[52]	5.94	5.90[36] 6.1[35]
CF_3SSCF_3	17	-.85		0.84		-2.32	
CH_3SSCH_3	18	-0.94		-0.88		-3.97	
$SP(CH_3O)_2Cl$	19	-2.02		-2.07		-4.78	
$(CH_3O)_2SO_2$	20	6.26		5.03		0.88	
SF_4	21	8.44		7.27		4.64	

(a) All shifts are taken as Δshift = compound - reference. Shifts are reliable to ±0.1 eV.

(b) Reference values for H_2S (in eV):

	This work	Ref. 35	Ref. 36	Ref. 52
1s	2478.87 (20)[i]	2478.5	-	-
2p	170.71 (20)	-	170.44[ii]	170.20
KL_2L_3	2098.46 (20)	2098.7	2098.46[iii]	-

(i) From AgL_α. The value obtained by using AgL_β was 2478.60 (30) eV and this was used as the reference value for all peaks collected with AgL_β.

(ii) $2p_{3/2}$ value. Assuming a separation of 1.3 eV between the spin-orbit components of the 2p peak a weighted average of 170.8 eV was obtained.

(Cont'd.)

Table 4.2. Cont'd.

(iii) Value after the calibration value of Ne $KL_{23}L_{23}$ was altered from 804.52 eV used in Ref. 36 to 804.56 eV used in this work.

(c) The 1s lines were produced by $AgL_{\alpha 1}$(2984.34 eV) with the exception of the compounds containing oxygen in which case $AgL_{\beta 1}$ (3150.97 eV) was the irradiating source.

The Auger line was collected in the same scan.

The calibration lines used were:

Ne $KL_{23}L_{23}$	804.56(2) eV
$AgL_{\alpha 1}$ converted by Ne 1s	870.37(9) eV

(d) The 2p lines were produced by AlK_{α} (1486.65 eV) or MgK_{α} (1253.64 eV).

The calibration lines used were

Kr $3d_{5/2}$	93.80 (10) ev
Kr $3p_{3/2}$	214.55 (15) eV

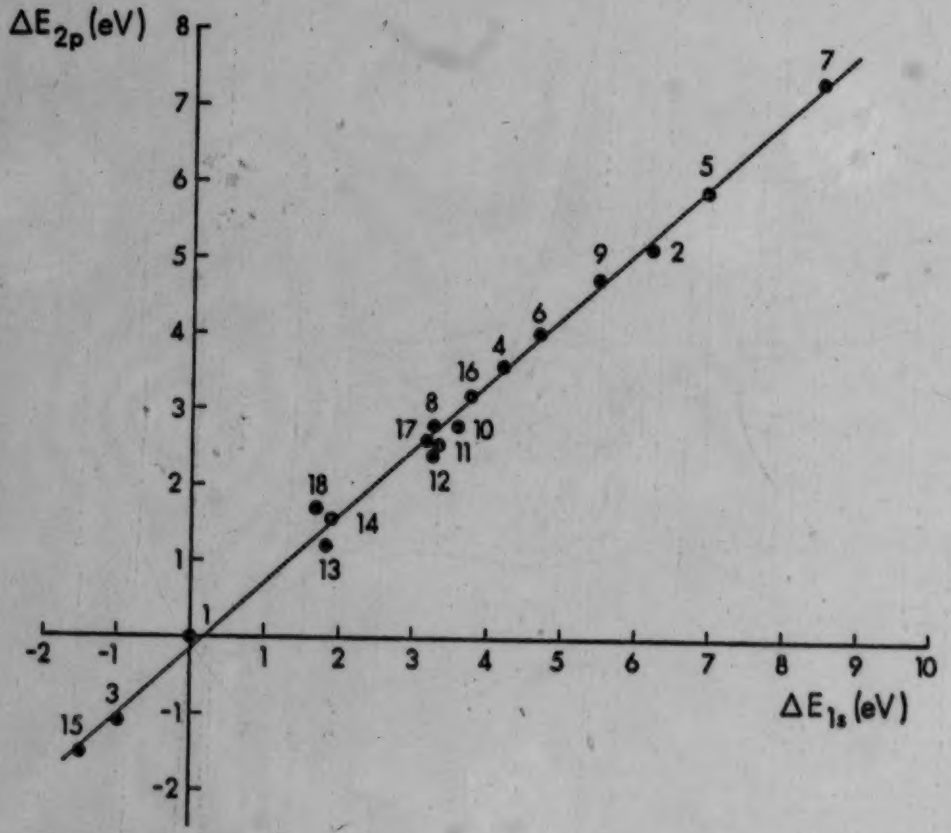

Figure 4.1 Experimental 2p binding energy shifts versus 1s binding shifts - phosphorus series. Compound numbers are presented in Table 4.1.

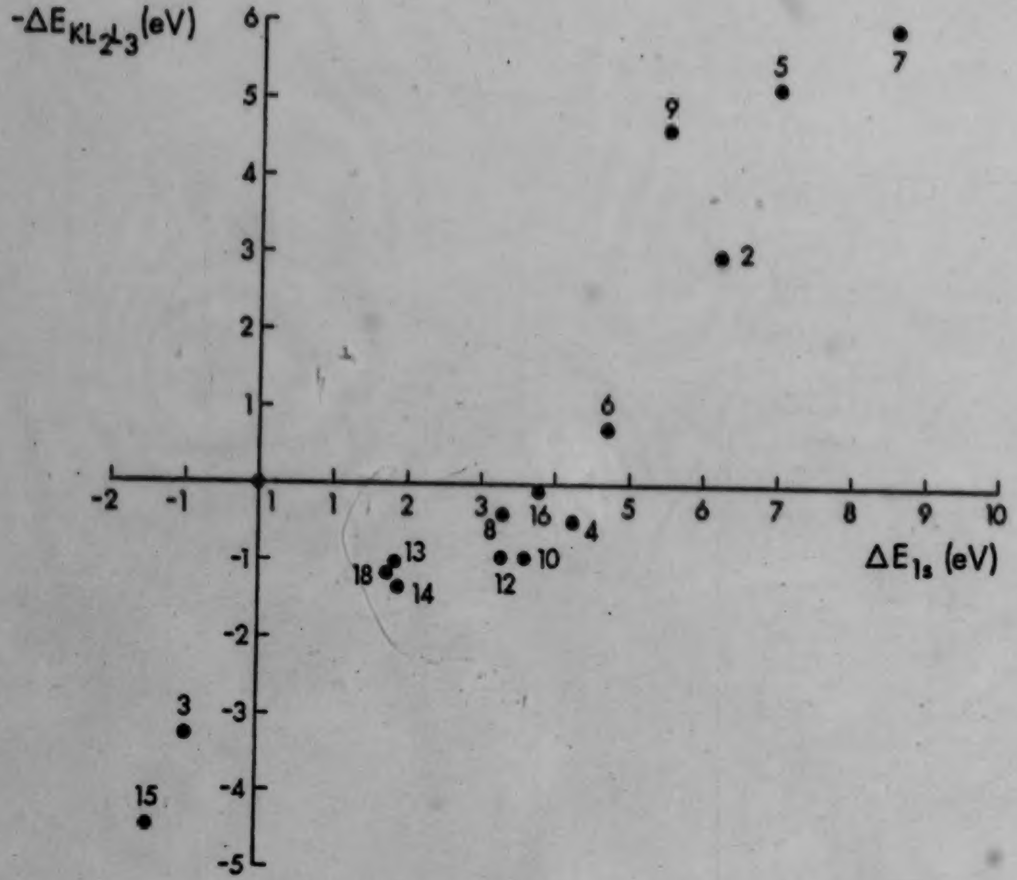

Figure 4.2 Experimental (-)KL_2L_3 Auger energy shifts versus 1s binding energy shifts - phosphorus series. Compound numbers are presented in Table 4.1.

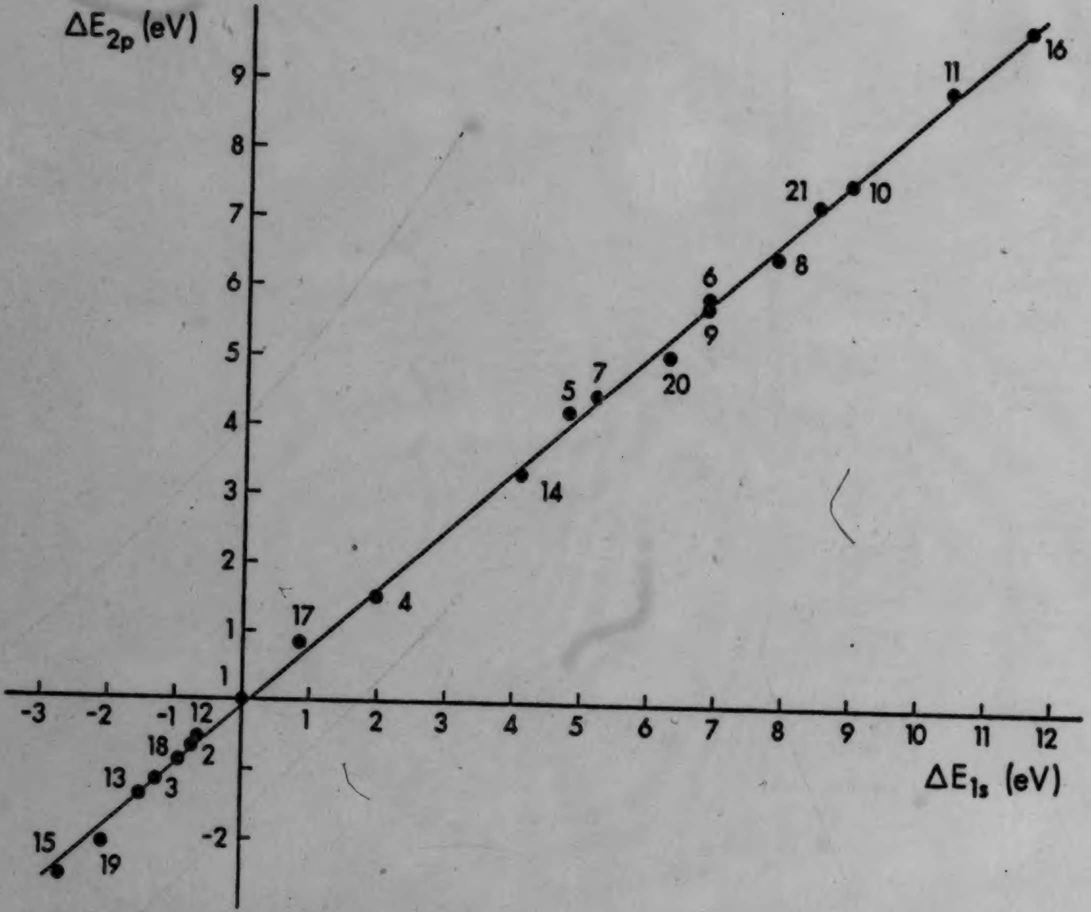

Figure 4.3 Experimental 2p binding energy shifts versus 1s binding energy shifts - sulphur series. Compound numbers are presented in Table 4.2.

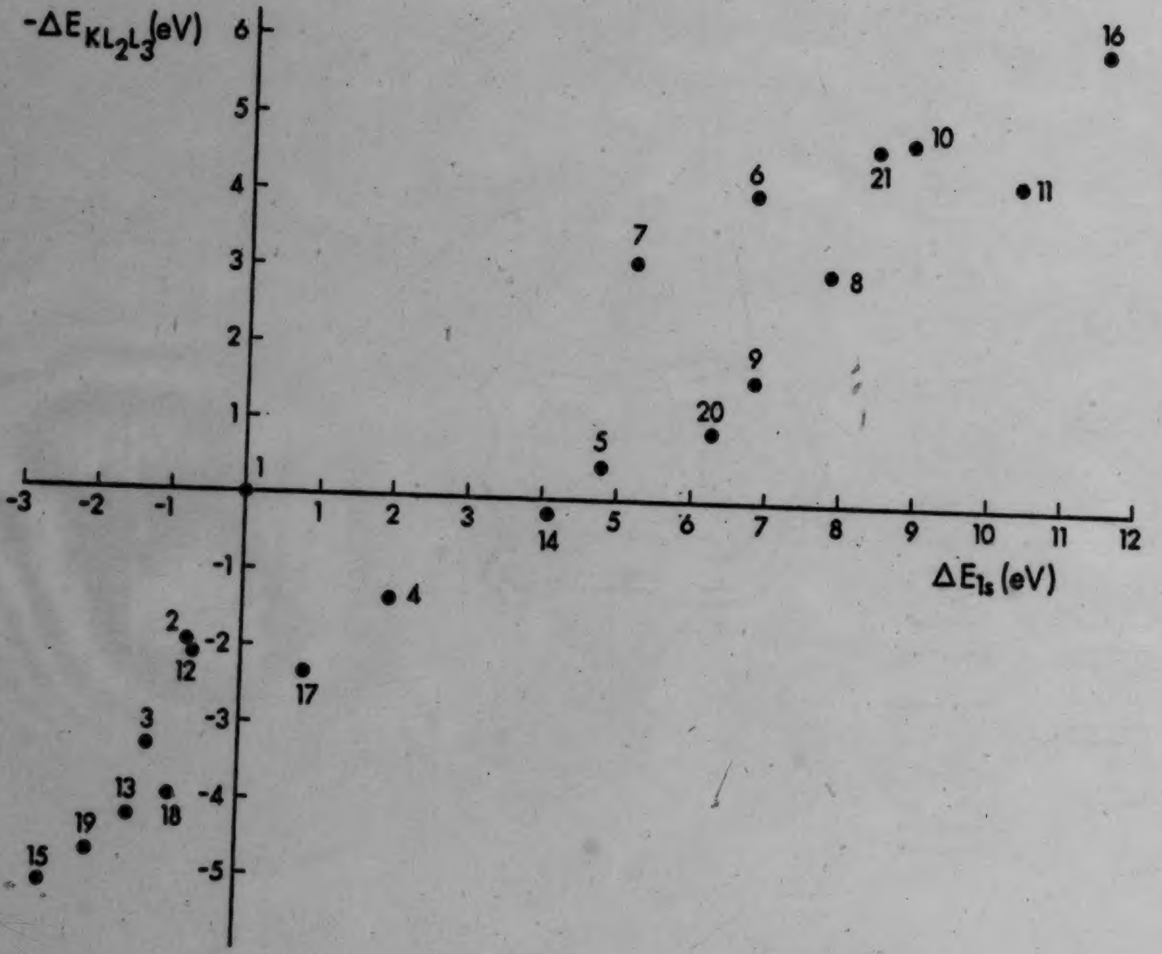

Figure 4.4 Experimental (-)KL_2L_3 Auger energy shifts versus 1s binding energy shifts - sulphur series. Compound numbers are presented in Table 4.2.

Agreement between the shifts reported here and those of other workers was found to be good with the exception of some of the 2p shifts shifts reported by Jolly et al.[52] The largest discrepancy was 1.5 eV for the P2p shift of PF_5. Our PF_5 2p spectrum was redetermined on different occasions and we are confident of the present value. Further support for the view that the value quoted by Jolly et al.[57] is in error is that their value gives a larger PH_3 to PF_5 shift for the 2p shift than that for our 1s shift which is inconsistent with the general 1s/2p shift relationship.

The absolute values of the photoelectron and Auger lines for the PH_3 reference are given in Table 4.1. The value of Ashe et al.[50] for the P2p line (137.3 eV) agrees well with the value of 137.35 eV found in this work, whereas the value quoted by Jolly et al.[52] (136.87 eV) is significantly lower. The KL_2L_3 auger value of Ashe et al.[50] (1841.4 eV) also agrees well with our value of 1841.46 eV.

The absolute values for the H_2S reference are given in Table 4.2. Agreement with the S KL_2L_3 Auger value of Asplund et al.[36] is excellent as is the agreement for the S2p photoelectron value, once the spin-orbit coupling is taken into account. A systematic calibration error (∿.4 eV) seems to be present in the S1s photoelectron energy between this work and that of Keski-Rahkonen and Krause,[35] however, the reported shifts agree well within the limits of experimental error.

As can be seen in Figures 4.1 and 4.3, the correlation between the 1s and 2p photoelectron shifts is good with the 1s shift being larger, however, when comparing the photoelectron with the Auger shifts (Figs. 4.2 and 4.4), there is poor correlation. The photoelectron and Auger shifts of an atom in a series of compounds of the same coordination state would be the most likely series to show any correlation of these values. Comparisons of compounds in which the coordination number of the central atom is altered is the least favourable case for correlation.

While the latter point is supported by the data (compare the relationship between SO_2F_2 and SF_5Cl or SPF_3 and PF_3) similar differences also occur in comparisons of the former type, the Auger shift between $SO(CH_3)_2$ and $SOCl_2$ is smaller than the corresponding S1s shift whereas the converse is true in the case of $SOCl_2$ and SOF_2. Another example is in the shifts of $P(CF_3)_3$ and PCl, from PH_3. The differences in trends must arise from the relaxation contribution associated with the initial photoionisation of the molecule and that associated with the removal of a second electron from the ion. It is this point that the various theoretical models must resolve.

B. Application of the Experimental Results to the Group Shift Concept

Group shift concepts might provide a useful means of predicting chemical shifts in Auger and photoelectron spectroscopy. It involves the partioning of the total shift into contributions made by each group. Inherent in the group shift idea is the assumption that shifts incurred by each group are independent of each other. This assumption ignores the fact that more electronegative substituents can induce a higher charge on the central atom which in turn can affect the other substituents.

A test of the group shift concept on a series of silicon compounds indicated that there was a very good correlation between group shift and total chemical shift.[24] In the silicon series however, all the molecules encountered were tetrahedral and only a limited range of groups, -Cl, OCH_2CH_3, -H, $-CH_3$, $-CH=CH_2$ and $-CH_2CH_3$ were evaluated. In the phosphorus and sulphur compounds presented here, additional factors such as the change of the coordination number, the effect of lone pairs, the inclusion of highly electronegative groups such as -F and $-CF_3$ and groups bonded to the central atom with a double bond were introduced which should provide a more thorough test upon the general applicability of the group shift model.

Experimental group shifts (group x - group y) are given in Table 4.3. It is apparent that in spite of occasional good agreement there exists serious discrepancies. For the P1s series the agreement is good with the exception of any compounds involving a terminal sulphur substituent.

Table 4.3. Relative Group Shifts (in eV).

Group Shift	Molecules Used	Δls	-ΔKL_2L_3	Group Shift	Molecules Used	Δls	-ΔKL_2L_3
F-Cl	$(PF_3-PCl_3)/3$	0.73	1.67	H-CH_3	$H_2S-(CH_3)SH$	0.74	1.97
	$(SPF_3-SPCl_3)/3$	0.66	1.15		$(CH_3)SH-(CH_3)_2S$	0.51	1.38
	$(OPF_3-OPCl_3)/3$	0.75	1.47				
				O-lone pair	$(CH_3)_2SO-(CH_3)_2S$	3.23	2.00
O-S	OPF_3-SPF_3	0.76	2.16		$(CH_3O)_2SO-(CH_3O)_2SO$	2.19	1.05
	$OPCl_3-SPCl_3$	0.49	1.19		$Cl_2SO_2-Cl_2SO$	2.05	1.15
	$OP(OCH_3)_3-SP(OCH_3)_3$	0.08	0.84		$F_2SO_2-F_2SO$	2.08	0.70
O-lone pair	OPF_3-PF_3	1.48	0.52	F-Cl	SF_6-SF_5Cl	1.16	1.72
	$OPCl_3-PCl_3$	1.42	1.11		$(SOF_2-SOCl_2)/2$	1.03	1.80
	$(OP(OCH_3)_3-P(OCH_3)_3$	1.52	0.92		$(SO_2F2-SO_2Cl_2)/2$	1.04	1.58
					$SO_2FCl-SO_2Cl_2$	0.99	1.43
S-lone pair	SPF_3-PF_3	0.72	-1.64				
	$SPCl_3-PCl_3$	0.93	-0.08				
	$SP(OCH_3)_3-P(CH_3)Cl_3$	1.44	0.08				
	$SP(CH_3)Cl_2-P(CH_3)Cl_2$	1.30	-0.11				

Cont'd.

Table 4.3. (Cont'd.)

Group Shift	Molecules Used	$\Delta 1s$	$-\Delta KL_2L_3$
$Cl-CH_3$	$(PCl_3-P(CH_3)_3)/3$	1.42	0.97
	$PCl_3-P(CH_3)Cl_2$	1.39	0.94
	$SPCl_3-SP(CH_3)Cl_2$	1.02	0.97
$F-CH_3O$	$(SPF_3-SP(OCH_3)_3)/3$	0.98	1.31
	$(OPF_3-OP(OCH_3)_3)/3$	0.21	1.75
	$(PF_3-P(OCH_3)_3/3$	1.22	1.88

For the P KL_2L_3 series there are many more exceptions and the validity of the concept appears to have vanished. This view is further supported by the values for the series of compounds with sulphur as the central atom. Comparison of group shifts obtained from compounds of differing coordination indicate the lack of general applicability readily revealed by comparing the shift obtained from the difference $((CH_3)_2SO-(CH_3)_2S)$ to that obtained from the difference $((CH_3O)_2SO_2-(CH_3O)_2SO)$. Furthermore the (CH_3-H) difference illustrates the lack of consistency in the group shift method even when compounds of the same coordination number are compared.

To summarise, the group shift concept appears to be valid only within very limited series of compounds at best and it must be used with caution, hence the concept is of little use.

C. Results of Calculations - Charges and Potentials

All of the calculations performed gave the net charge on the central atom, q_A, and the potential on the central atom due to the charges at all other atoms in the molecule, V_A. Charges and potentials were obtained for the neutral molecule (q_A^N, V_A^N), its singly-ionised core-hole state (q_A^{N-1}, V_A^{N-1}) and its doubly-ionised core-hole state (q_A^{N-2}, V_A^{N-2}). To obtain values for the ionised species within the context of the semi-empirical calculations used here the equivalent-core approximation was used. The central (Z) atom in the molecule was replaced by the isoelectronic $(Z+1)^{+}$ and $(Z+2)^{++}$ cations for the singly-ionised and doubly-ionised species respectively. Transition state charges and potentials for a N → (N-1) and a (N-1) → (N-2) transition ($q_A^{N,N-1}$, $V_A^{N,N-1}$; $q_A^{N-1,N-2}$, $V_A^{N-1,N-2}$) were also obtained, but only with the EWMO (Hückel) program. The central (Z) atom was replaced by a $(Z+1/2)^{+1/2}$ pseudo-atom for the N → (N-1) transition and by a $((Z+1)+1/2)^{+3/2}$ pseudo-atom for the (N-1) → (N-2) transition. Parameters for the pseudo-atom were obtained by interpolation between the Z, Z+1 and Z+2 atomic parameters.

Results of the CNDO/2 calculation are given in Tables 4.4 and 4.5 for the phosphorus and sulphur series respectively. The corresponding results of the EWMO (Hückel) calculations are given in Tables 4.6 and 4.7. Convergence problems occurred in the EWMO program in the case of $P(CF_3)_3$ and for the (N-2) state of $P(C_2H_5)_3$ thus these values are not available. In all other cases convergence was achieved.

The net charge on the atom being ionised (q_A) is related to its valence population (P_{AA}) by

$$q_A = Z_A^* - P_{AA} \tag{4.1}$$

Table 4.4. Central Atom Charge (q) and Off-atom Potential (V) From CNDO/2 Calculations - P series.

	q^N	$-V^N$	q^{N-1}	$-V^{N-1}$	q^{N-2}	$-V^{N-2}$
PH_3	0.1712	1.7378	0.3906	-6.1870	0.4437	-15.8010
SPF_3	1.5333	13.7418	1.4433	4.0723	1.2478	- 6.5360
$P(CH_3)_3$	0.1614	1.3394	0.3237	-4.0145	0.4173	- 9.8850
$SPCl_3$	1.0428	7.6449	0.8906	-0.7134	0.7173	- 9.1940
OPF_3	1.6623	15.9774	1.6184	5.9874	1.4464	- 5.1800
$OPCl_3$	1.1595	9.4866	1.0186	0.9298	0.8209	- 7.8800
PF_5	2.0802	19.3002	1.8517	7.8899	1.5247	- 4.4340
PCl_3	0.6690	4.7215	0.6808	-2.2533	0.5610	-10.1560
PF_3	1.0709	9.8209	1.2448	2.2446	1.1929	- 7.4010
$SP(CH_3O)_2Cl$	1.1756	10.3365	0.9795	1.7933	0.7803	- 6.7870
$(CH_3O)_3PO$	1.3477	13.5758	1.1505	4.7348	0.9294	- 4.2650
$(CH_3O)_3PS$	1.2653	11.9633	1.0500	3.2496	0.8515	- 5.3620
$(CH_3O)_3P$	0.8291	8.2947	0.8078	1.2001	0.6920	- 6.7230
$P(CH_3)Cl_2$	0.5089	3.7796	0.5779	-2.6183	0.5284	- 9.8820

(Cont'd.)

Table 4.4. Cont'd.

	$\underline{q^N}$	$\underline{-V^N}$	$\underline{q^{N-1}}$	$\underline{-V^{N-1}}$	$\underline{q^{N-2}}$	$\underline{-V^{N-2}}$
$P(C_2H_5)_3$	0.1164	0.8110	0.1873	-4.5988	0.2343	-10.0790
$OP(CH_2Cl)Cl_2$	1.0227	8.4129	0.9092	0.5237	0.7709	- 7.4760
$SP(CH_3)Cl_2$	0.9197	7.0777	0.8049	-0.8528	0.6829	- 8.8250
$P(CF_3)_3$	0.0448	-3.4819	0.1168	-9.1285	0.1785	-14.7120

Table 4.5. Central atom charge (q) and off-atom potential (V) from CNDO/2 Calculation - S series.

	q^N	$-V^N$	q^{N-1}	$-V^{N-1}$	q^{N-2}	$-V^{N-2}$
H_2S	-0.0796	- 0.8584	0.2877	-7.6777	0.5550	-15.5740
$(CH_3)SH$	-0.0703	- 0.5862	0.2467	-6.2190	0.5263	-12.4650
$(CH_3)_2S$	-0.0606	- 0.4134	0.2257	-5.0632	0.5105	- 9.7230
$(CH_3)_2SO$	0.4047	4.3125	0.5162	-2.0277	0.6678	- 8.0820
$SOCl_2$	0.7543	6.4121	0.7098	-1.2234	0.6573	- 8.7760
SOF_2	0.9941	9.4779	1.0997	1.1306	1.0434	- 8.6650
SO_2	0.7199	7.2392	1.0041	0.0411	1.0553	- 9.5000
SO_2ClF	1.3665	13.0893	1.2411	3.3525	1.0933	- 6.6220
SO_2Cl_2	1.2433	11.4953	1.0798	2.3361	0.9180	- 6.5730
SO_2F_2	1.5135	14.9642	1.4450	4.5638	1.2786	- 6.7030
SF_5Cl	1.9282	17.2774	1.5987	5.9409	1.2452	- 5.5270
SPF_3	-0.4021	- 6.2152	0.0474	-9.3587	0.4034	-13.0730
$SPCl_3$	-0.3756	- 5.0644	0.0151	-7.7228	0.3470	-10.7010
$(CH_3O)_2SO$	0.7062	7.2973	0.6608	-0.3561	0.6554	- 7.5920
$(CH_3O)_3PS$	-0.4557	- 5.1850	-0.0562	-7.5828	0.3184	-10.0150
SF_6	2.0774	19.0515	1.7412	6.7959	1.3570	- 5.8980

Cont'd.

Table 4.5. Cont'd.

	q^N	$-V^N$	q^{N-1}	$-V^{N-1}$	q^{N-2}	$-V^{N-2}$
CF_3SSCF_3	-0.0122	-1.8463	0.1447	-6.9124	0.3922	-11.2960
CH_3SSCH_3	-0.0281	-0.0913	0.1688	-5.0828	0.4335	- 9.6300
$SP(CH_3O)_2Cl$	-0.4261	-5.0656	-0.0348	-7.5688	0.3270	-10.1730
$(CH_3O)_2SO_2$	1.2146	12.8475	0.9959	3.4487	0.8631	- 5.2650
SF_4	1.3689	12.2304	1.2631	2.2439	1.0272	- 8.8400

Table 4.6. Central atom charge (q) and off-atom potential (V) from EHMO (original parameterisation)-P series.

	q^N	$-V^N$	q^{N-1}	$-V^{N-1}$	q^{N-2}	$-V^{N-2}$	$q^{N,N-1}$	$-V^{N,N-1}$	$q^{N-1,N-2}$	$-V^{N-1,N-2}$
PH_3	0.0273	0.2780	0.6932	-3.1150	1.2641	-7.4710	0.3165	-1.8630	0.9327	-5.7600
SPF_3	1.2642	11.6990	1.8059	7.5650	2.1099	1.4390	1.4941	9.2690	1.9949	4.6100
$P(CH_3)_3$	0.1131	1.3170	0.6648	-1.3830	1.1212	-5.1710	0.3459	-0.3050	0.8395	-3.6710
$SPCl_3$	0.7791	5.7640	1.3055	2.3340	1.6198	-2.6550	1.0048	3.7750	1.4786	0.0160
OPF_3	1.5345	14.8300	2.0908	10.5880	2.3985	3.9400	1.7712	12.3090	2.2136	6.9650
$OPCl_3$	1.0353	9.6010	1.5503	5.0690	1.8452	0.4140	1.2525	7.4080	1.6554	2.8000
PF_5	1.6671	15.4530	2.2064	11.1660	2.4789	4.4010	1.8982	12.9510	2.3144	7.5210
PCl_3	0.3540	2.4990	0.8515	-1.0480	1.2180	-5.5190	0.5600	0.4240	0.9794	-3.6730
PF_3	0.9865	9.0470	1.5103	4.6800	1.8718	-1.1760	1.2043	6.4590	1.6467	1.3460
$SP(CH_3O)_2Cl$	1.0559	11.0690	1.5618	7.2140	1.8491	1.5850	1.2669	8.8080	1.7274	4.5210
$(CH_3O)_3PO$	1.4313	17.0270	1.9406	12.9000	2.2166	6.5560	1.6411	14.5680	2.0442	9.4220
$(CH_3O)_3PS$	1.1991	13.8660	1.7082	9.8910	1.9989	4.0120	1.4095	11.5160	1.8798	7.0430
$(CH_3O)_3P$	0.8396	10.9120	1.3048	6.5380	1.6578	1.0410	1.0205	8.2900	1.4328	3.3630
$P(CH_3)Cl_2$	0.2891	2.2370	0.8031	-1.0640	1.1945	-5.3540	0.5035	0.2930	0.9443	-3.5980
$OP(CH_2Cl)Cl_2$	0.9983	9.3410	1.5090	5.8480	1.8016	0.6000	1.2136	7.2740	1.6130	2.8780
$SP(CH_3)Cl_2$	0.7512	5.8830	1.2843	2.6110	1.6107	-2.2880	0.9798	3.9770	1.4626	-0.3300
$P(C_2H_5)_3$	0.0697	0.7050	0.5535	-2.0800	-[a]	-[a]	0.2680	-0.9570	0.6874	-4.3930
$P(CF_3)_3$[a]	-	-	-	-	-	-	-	-	-	-

[a] No values obtained due to convergence problems in program.

Table 4.7. Central atom charge (q) and off-atom potential (V) from EWMO (original parameterisation) - S series.

	q^N	$-V^N$	q^{N-1}	$-V^{N-1}$	q^{N-2}	$-V^{N-2}$	$q^{N,N-1}$	$-V^{N,N-1}$	$q^{N-1,N-2}$	$-V^{N-1,N-2}$
H_2S	-0.0464	-0.5000	0.6398	-3.8820	1.3668	-6.8240	0.2422	-2.7780	0.9789	-5.6170
$(CH_3)SH$	-0.0402	-0.2610	0.5850	-3.3560	1.2643	-6.1200	0.2126	-2.3260	0.8959	-4.9880
$(CH_3)_2S$	-0.0300	-0.0820	0.5483	-2.8310	1.1905	5.3380	0.1963	-1.9030	0.8373	-4.3170
$(CH_3)_2SO$	0.8596	8.9710	1.2610	4.3380	1.7677	0.4330	0.9926	6.1080	1.4800	2.1090
$SOCl_2$	0.9844	9.1260	1.3114	3.9100	1.7413	-0.4060	1.0781	5.9450	1.5670	1.8130
SOF_2	1.3592	12.9640	1.6953	6.6800	2.1357	1.3890	1.4668	9.2450	1.8832	3.7290
SO_2	1.1116	11.1790	1.4771	4.7980	1.9757	-0.2450	1.2215	7.2560	1.6895	1.9060
SO_2ClF	1.8584	18.5800	2.1419	12.0210	2.5311	6.5030	1.9567	14.8930	2.3471	9.1540
SO_2Cl_2	1.7202	17.1800	1.9997	11.0420	2.3849	5.9630	1.8130	13.6880	2.2308	8.4890
SO_2F_2	2.0136	20.0150	2.3054	13.0410	2.7030	7.1130	2.1205	16.1420	2.4843	9.8810
SF_5Cl	2.0492	18.7330	2.2634	11.9070	2.5636	5.8810	2.1192	14.9920	2.4250	8.8140
SPF_3	-0.1157	-4.0570	0.3124	-7.2960	0.9326	-9.3830	0.0148	-6.1980	0.5813	-8.5960
$SPCl_3$	-0.3889	-4.2540	0.1144	-6.7240	0.7831	-8.2950	-0.2196	-5.9630	0.4419	-7.9090
$(CH_3O)_2SO$	1.2169	13.3360	1.5269	7.5130	1.9216	2.5860	1.3063	9.8560	1.6951	4.7350
$(CH_3O)_3PS$	-0.3328	-3.3960	0.1428	-6.1310	0.8075	-7.8530	-0.1821	-5.2680	0.4399	-7.2020
SF_6	2.2036	20.2090	2.4221	13.0420	2.7306	6.7000	2.2796	16.3210	2.5571	9.6950
CF_3SSCF_3	0.1181	-2.4800	0.5738	-5.4300	1.1184	-7.9000	0.3319	-3.8530	0.8091	-6.9110
CH_3SSCH_3	-0.0185	0.0040	0.4998	-3.0220	1.0944	-5.6460	0.2355	-1.3970	0.7607	-4.5880
$SP(CH_3O)_2Cl$	-0.3448	-3.6570	0.1348	-6.3330	0.8007	-8.0090	-0.1919	-5.4970	0.4424	-7.4450
$(CH_3O)_2SO_2$	1.9239	21.1970	2.1665	14.3310	2.5120	8.4840	2.0029	17.3860	2.3170	11.1860
SF_4	1.5355	13.7458	1.8184	7.2409	2.1974	1.6110	1.6202	9.9802	1.9755	4.1330

where Z_A^* is the effective reduced charge of atom A (the nuclear charge minus the number of core-electrons). Plots of the phosphorus valence population versus the state of core-ionisation derived from CNDO/2 calculations are shown in Figure 4.5 and from EWMO (Hückel) calculations in Figure 4.6. Similar plots for the sulphur series are shown in Figures 4.7 and 4.8. The change in valence population upon core-ionisation gives a measure of the electron flow towards the central atom due to the formation of a hole state.

(i) CNDO/2 Results

The CNDO/2 calculation gives an almost linear increase in the valence population of the core atom upon increasing core-ionisation. A larger increase in the valence population on the core-atom is perceivable upon second ionisation for some of the molecules, however for all practical purposes the trend is linear. A similar linear trend was observed by Kelfve et al.[24] for CNDO/2 calculations performed on the series $SiCl_n(CH_3)_{4-n}$, however the calculation predicted that $SiCl_4$ would have the highest silicon valence population in the series, contradicting the results expected on the basis of simple electronegativity arguments.[24] This behaviour was not observed in the present series of calculations for phosphorus or sulphur compounds. The

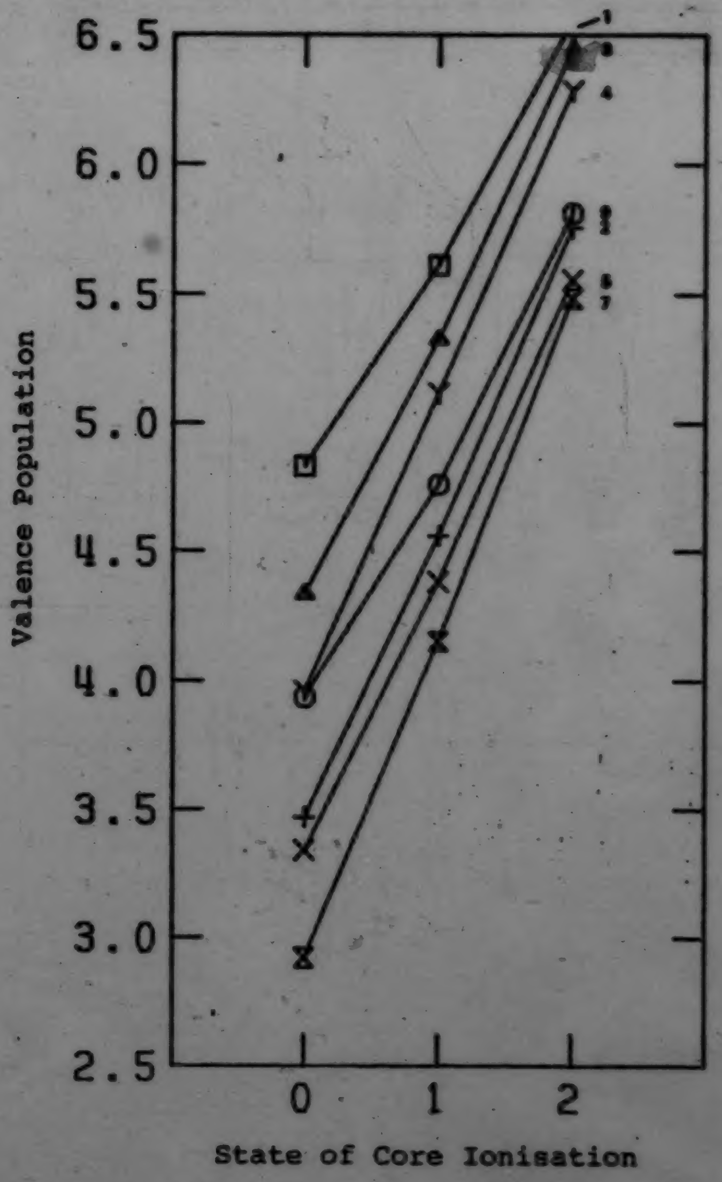

Figure 4.5 Comparison of the P valence population (from CNDO/2 calculation) with the state of core ionisation for some phosphorus compounds. Compound numbers are presented in Table 4.1.

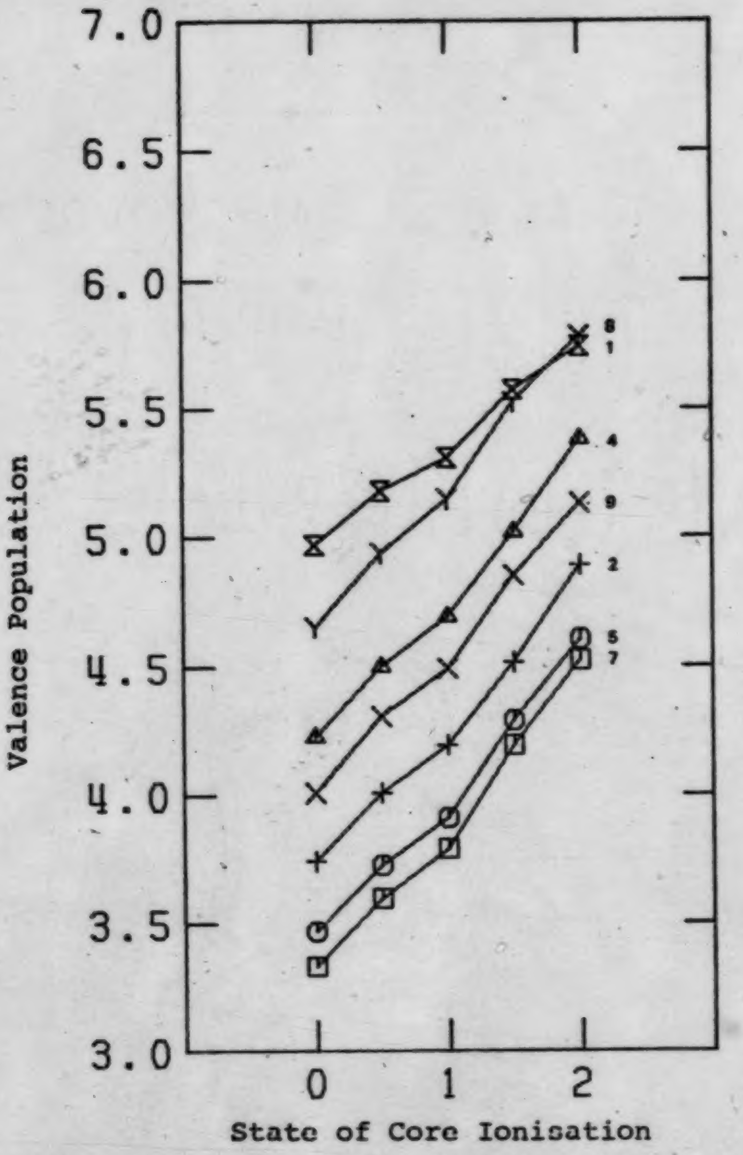

Figure 4.6 Comparison of the P valence population (from EWMO calculation) with the state of core ionisation for some Phosphorus compounds. Compound numbers are presented in Table 4.1.

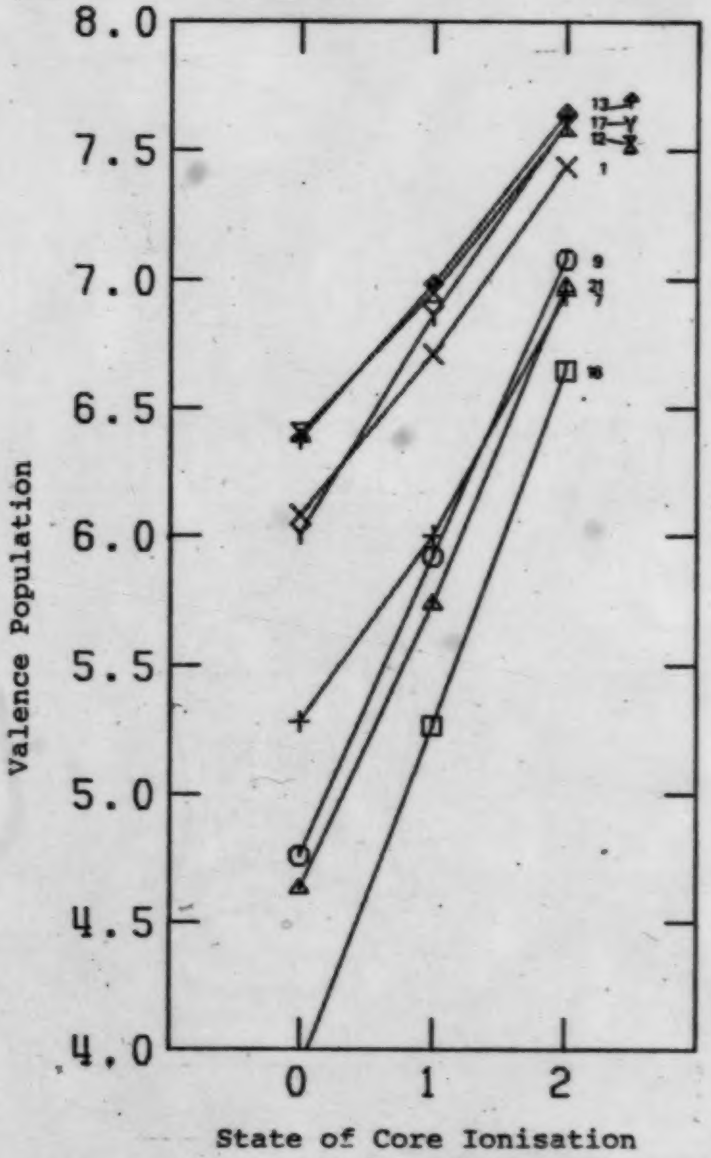

Figure 4.7 Comparison of the S valence population (from CNDO/2 calculation) with the state of core ionisation for some sulphur compounds. Compound numbers are presented in Table 4.2.

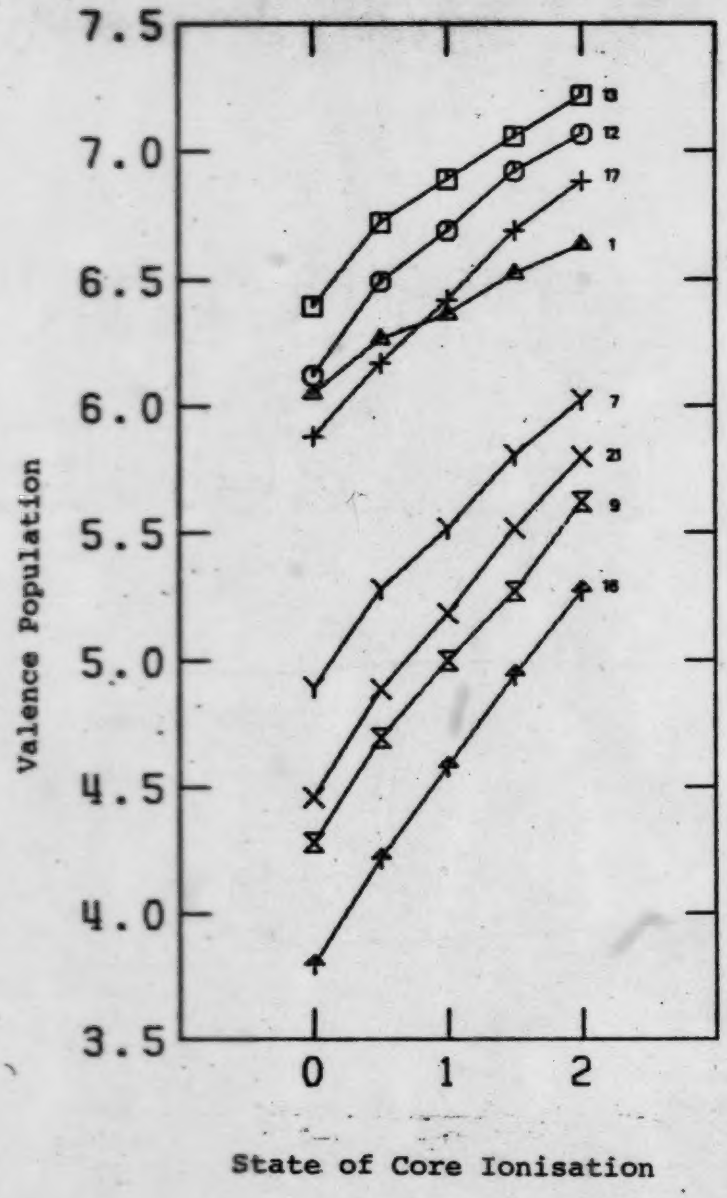

Figure 4.8 Comparison of the S valence population (from EWMO calculation) with the state of core ionisation for some sulphur compounds. Compound numbers are presented in Table 4.2.

valence population of the core atom in both cases follows the expected electronegativity trends.

The CNDO/2 calculations performed by Kelfve et al.[24] included d-orbitals whereas the calculations reported here did not. For comparison CNDO/2 calculations including d-orbitals were performed on PCl_3 and $P(CH_3)_3$. The results are presented in Table 4.8 and Figure 4.9. The expected trend in the phosphorus valence population is preserved when comparing the population in $P(CH_3)_3$ to PCl_3, however the calculation shows more of an increase in the valence population on the core atom upon second ionisation compared to the initial ionisation than in the case where d-orbitals were omitted from the basis set. These changes arising from a change in basis set illustrate the dangers of obtaining charges and potentials from semi-empirical methods involving a minimal basis set.

(ii) EWMO (Hückel) Results

The EWMO (Hückel) calculation shows different trends for the change in valence population of the core atom upon increasing core ionisation in the phosphorus and sulphur series. The sulphur series shows an almost linear relationship of population with possibly an indication of saturation. The phosphorus series shows a markedly larger increase in the valence population in going from the first

Table 4.8. Phosphorus valence population on $P(CH_3)_3$ and PCl_3 from CNDO/2 calculations with d-orbitals included.

	State of Core Ionisation		
	N	N-1	N-2
PCl_3	4.7338	5.4891	6.4732
$P(CH_3)_3$	4.9113	5.6569	6.5815

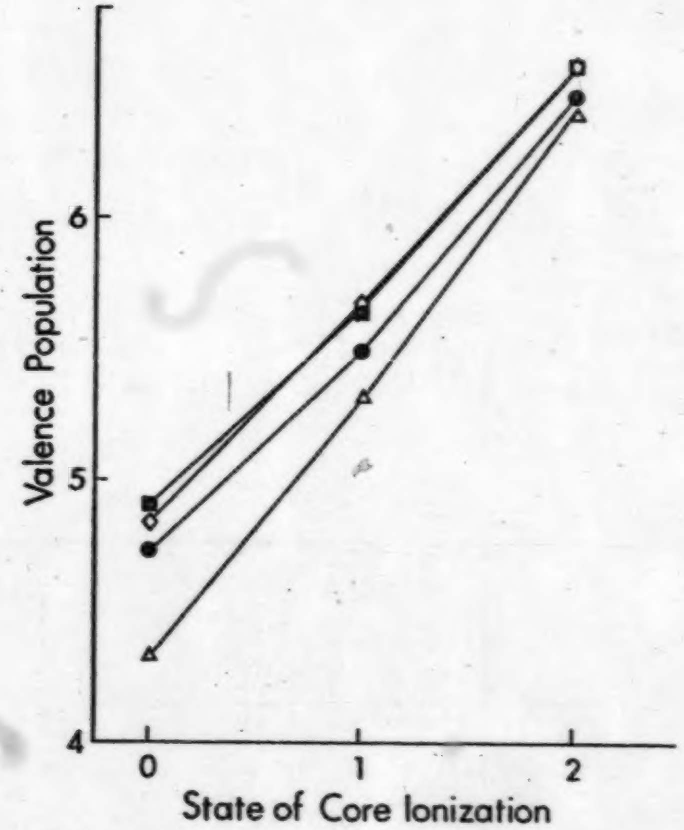

Figure 4.9 Comparison of the P valence population (from CNDO/2 calculation) with the state of core ionisation for $P(CH_3)_3$ and PCl_3 with and without d orbitals included in the basis set.

- ● PCl_3 with d orbitals in basis set
- △ PCl_3 without d orbitals in basis set
- ■ $P(CH_3)_3$ with d orbitals in basis set
- ◇ $P(CH_3)_3$ without d orbitals in basis set

ionisation to the second. Both of these trends contrast with that shown by Kelfve et al.[24] for silicon. Upon increasing core-ionisation, the silicon series showed a marked saturation in the increase of the valence population on the central atom.

This difference in trends between the three series of compounds for the same type of calculation is disturbing. A possible explanation for this occurrence might be in the parameterisation of the phosphorus atom in the EWMO (Hückel) program. As a test to see whether the behaviour of the phosphorus compounds is a quirk of the parameterisation or whether it is part of a general trend, a few of the phosphorus compounds were run with the silicon anion (Si^-) as an equivalent core. The results are shown in Figure 4.10. It can be seen that the values involving the use of the phosphorus parameters are too high and this implies that the trend in the phosphorus series is caused by the particular parameterisation chosen for phosphorus in the EWMO (Hückel) program.

In view of this result it was decided to change the parameters for phosphorus in the EWMO (Hückel) program. Full details of the methods used are given in Appendix 2. A plot of $SiCl_4$ valence population versus the state of core-ionisation obtained with both the original parameterisation[48] and for the new parameters is given in Figure 4.11. For comparison, similar data for PCl_3 and SCl_2 are

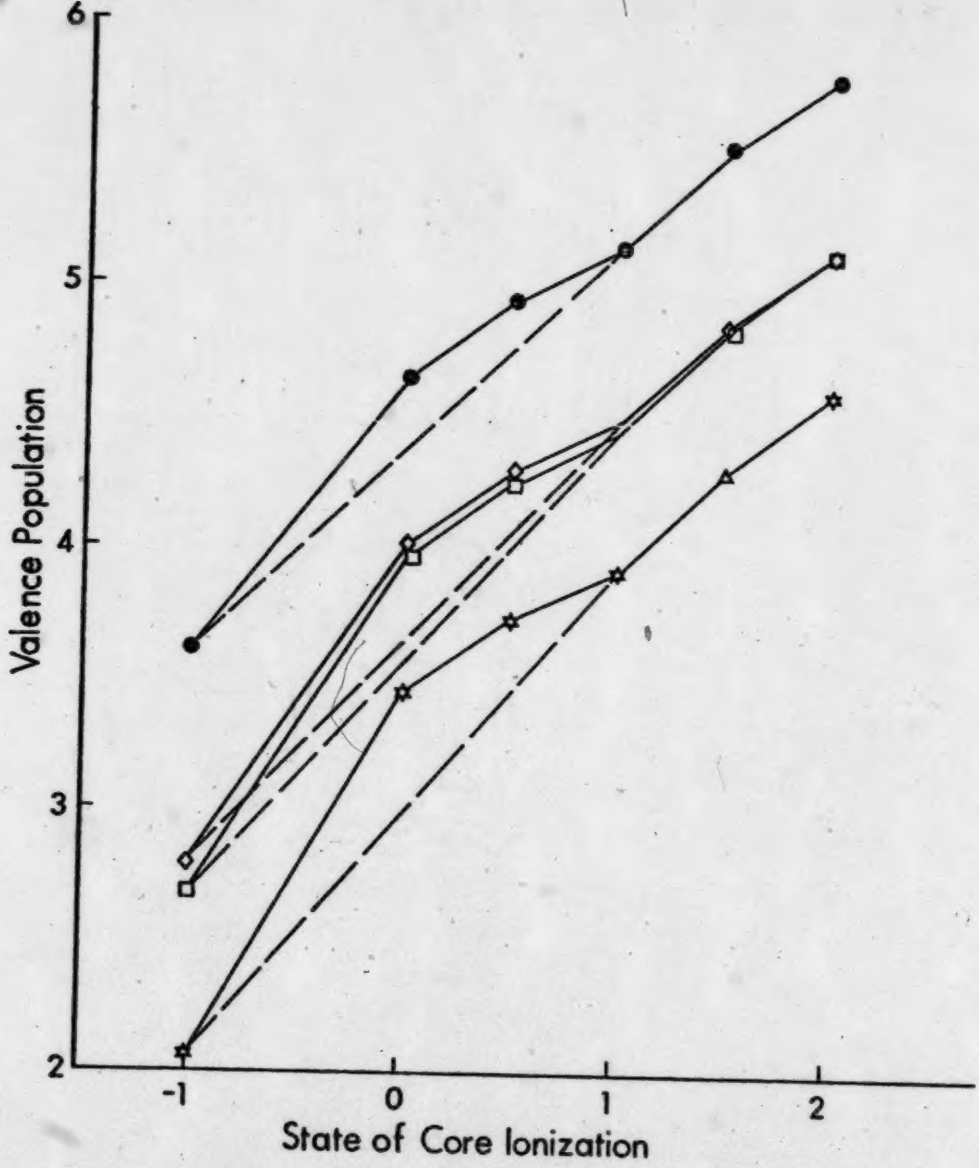

Figure 4.10 Comparison of the P valence population (from EWMO calculation) with the state of core ionisation for some phosphorus compounds going from the Si^- equivalent core state to the Cl^{++} equivalent core state.

✡ OPF_3 ◇ PF_3 □ $OPCl_3$ ● PCl_3

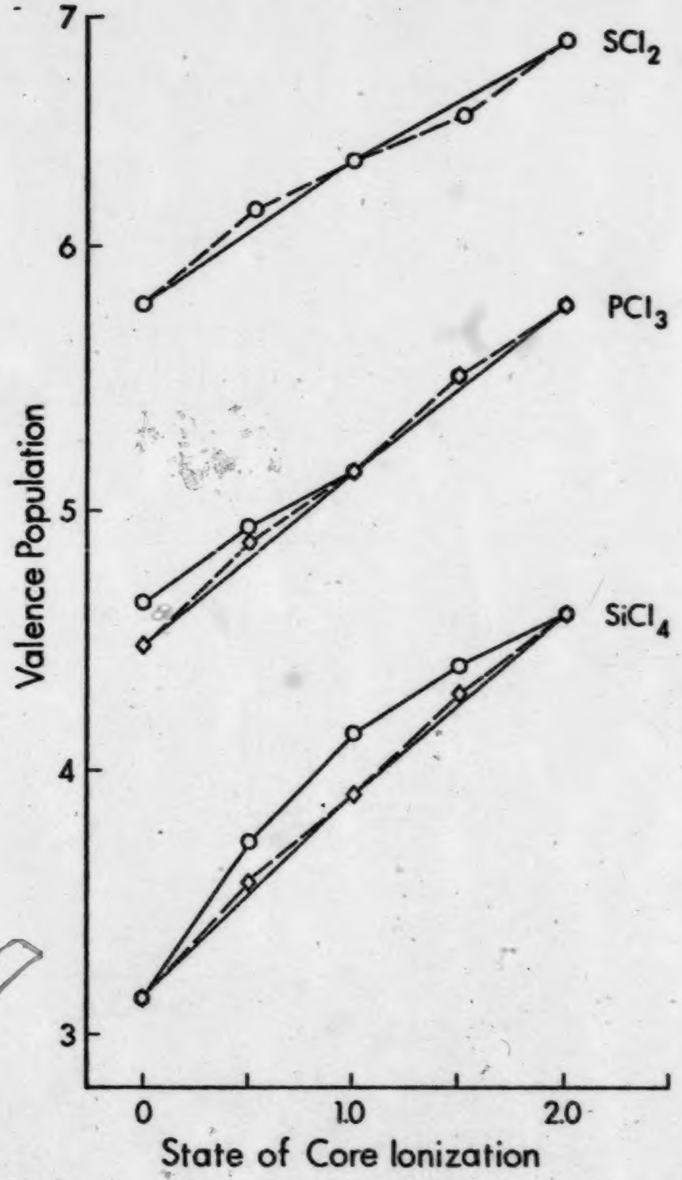

Figure 4.11 Comparison of the central atom valence population (from EWMO calculation) with the state of core ionisation for $SiCl_4$, PCl_3 and SCl_2.

○ original P parameterisation ◇ new P parameterisation also given.

It can be seen that all three series of compounds now proceed in a similar manner upon increasing core-ionisation. Also, the transition potential model values no longer lie in a smooth curve as originally indicated in the work on the silicon series.[24] Figure 4.12 summarises the results of the phosphorus series, the transition potential values are omitted for clarity. All the new values are presented in Table 4.9.

D. Results of Calculations - Application of the Various Models and Comparison with Experiment

The charges and potentials obtained by methods described in the previous section can be used in the "atom charge model" (Equation 3.1) to estimate the binding energy shifts of the core electrons emitted upon the initial photo-ionisation ($\Delta E(1s)$ or $\Delta E(2p)$), and the binding energy shifts of a 2p electron in a system already containing a 2p vacancy ($\Delta E(2p^*)$). The latter can be related to the Auger energy shifts ($\Delta E(KL_2L_3)$) by subtraction of the Auger shifts from the x-ray shifts as shown in Equation 3.6.

An estimation of the k and ℓ values required in Equation 3.1 may be obtained from a least squares fit of

$$\Delta E - V = kq + \ell \tag{4.2}$$

Table 4.9. Central atom changes (q) and off-atom potential from EWMO calculation (New P parameterisation).

	q^N	$-V^N$	$q^{N,N-1}$	$-V^{N,N-1}$
PH_3	0.1408	1.4300	0.3534	-1.4889
SPF_3	1.5711	14.3556	1.6481	10.6044
$P(CH_3)_3$	0.2344	2.2656	0.3854	0.0020
$SPCL_3$	1.0203	7.5312	1.1132	4.5691
OPF_3	1.8780	18.1503	1.9507	14.0444
$OPCl_3$	1.3143	11.8458	1.3861	8.4864
PF_5	2.0207	18.7377	2.0840	14.6774
PCl_3	0.5147	3.6329	0.6191	0.8408
PF_3	1.2254	11.2378	1.3161	7.4842
$SP(CH_3O)_2Cl$	1.3334	13.2892	1.4021	9.9061
$(CH_3O)_3PO$	1.7603	19.9901	1.8141	16.1657
$(CH_3O)_3PS$	1.4921	16.3118	1.5578	12.7833
$(CH_3O)_3P$	1.0580	12.8247	1.1194	9.1743
$P(CH_3)Cl_2$	0.4379	3.3191	0.5571	0.6842
$OP(CH_2Cl)Cl_2$	1.2700	11.5334	1.3431	8.3320
$SP(CH_3Cl_2$	0.9867	7.6398	1.0857	4.7713
$P(C_2H_5)_3$	0.1908	1.6142	0.3026	-0.7011

	q^N	$-V^N$	q^{N-1}	$-V^{N-1}$	q^{N-2}	$-V^{N-2}$	$q^{N,N-1}$	$-V^{N,N-1}$	$q^{N-1,N-2}$	$-V^{N-1,N-2}$
SPF_3	-0.2507	-5.5704	0.2158	-8.5869	0.8606	-10.5190	-0.0996	-7.6047	0.4990	-9.8020
$SPCl_3$	-0.4743	-5.4190	0.0555	-7.7404	0.7388	- 9.2170	-0.2885	-7.0489	0.3868	-8.9330
$(CH_3O)_3PS$	-0.4410	-4.7449	0.0665	-7.2801	0.7489	- 8.8750	-0.2712	-6.5120	0.3733	-8.2870
$SP(CH_3O)_2Cl$	-0.4453	-4.9479	0.0647	-7.4422	0.7470	- 9.0030	-0.2739	-6.6916	0.3798	-8.5140

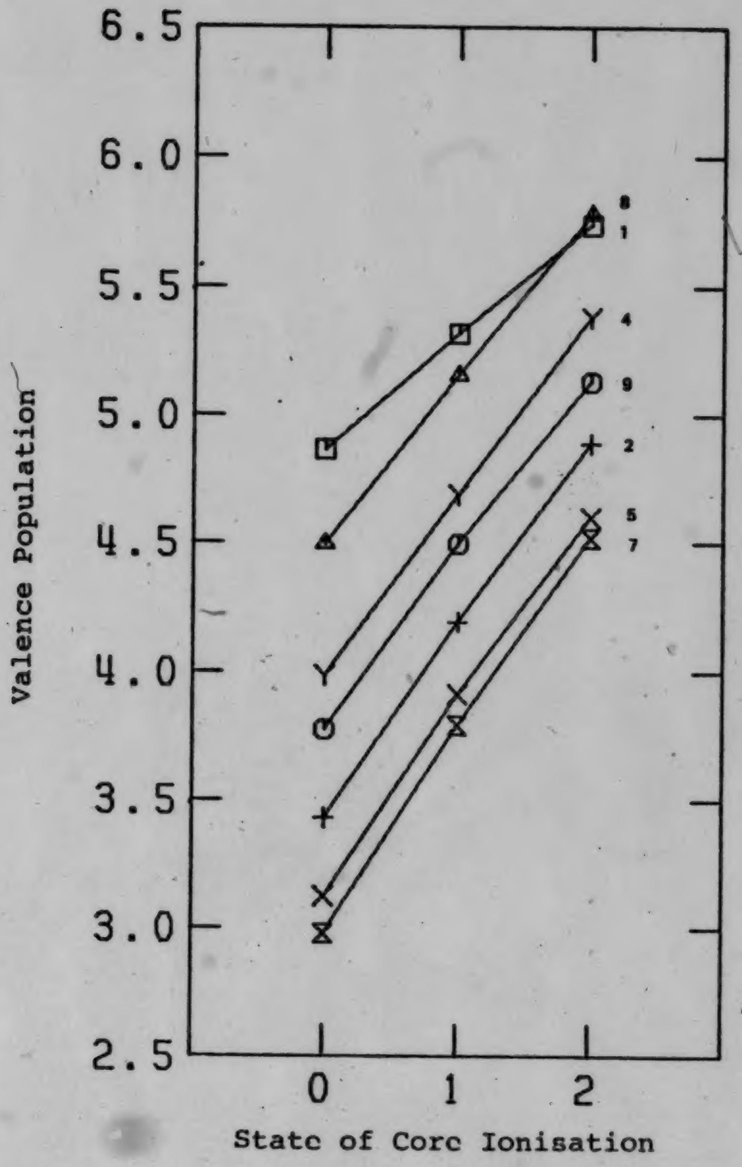

Figure 4.12 As Figure 4.6 but with new P parameterisation. The transition states have been omitted for clarity.

where ΔE is the appropriate experimental chemical shift, and q and V are the charges and potentials appropriate to the model under consideration.

The ground potential model (GPM) estimates $\Delta E(1s)$ and $\Delta E(2p)$ from ground-state charges and potentials (q^N, V^N). The charges and potentials of the singly-ionised core-hole state (q^{N-1}, V^{N-1}), obtained by using the $(Z+1)^+$ equivalent core for the Z atom, provided GPM estimates of $\Delta E(2p^*)$. The relaxation potential model (RPM) estimates $\Delta E(1s)$ and $\Delta E(2p)$ using $1/2(q^N+q^{N-1})$ and $1/2(V^N+V^{N-1})$ for the charges and the potentials and $\Delta E(2p^*)$ from $1/2(q^{N-1}+q^{N-2})$ and $1/2(V^{N-1}+V^{N-2})$. In the latter case q^{N-2} and V^{N-2} are the charges and potentials of the doubly-ionised core-hole states obtained by using the $(Z+2)^{++}$ equivalent core for the Z atom.

Both the GPM and RPM approaches have been used in conjunction with charges and potentials obtained from CNDO/2 and from EWMO (Hückel) calculations. The transition potential model (TPM), which uses the transition charges and potentials $(q^{N,N-1}, V^{N,N-1})$ obtained from equivalent core $(Z+1/2)^{+1/2}$ calculations was applied to estimate $\Delta E(1s)$ and $\Delta E(2p)$. $\Delta E(2p^*)$ was estimated using $(q^{N-1,N-2}, V^{N-1,N-2})$ as estimated with a $(Z+3/2)^{+3/2}$ equivalent core calculation. Only charges and potentials from the EWMO (Hückel) calculation were used for the TPM case.

A theoretical value for k can also be obtained within the context of the point-charge approximation

$$k_i = \langle j|1/r_i|j\rangle = \frac{\zeta}{n} \qquad (4\text{-}3)$$

where ζ is the Slater orbital exponent of the valence shell and n is the principal quantum number of that shell. The value for ζ is unambiguous within the CNDO/2 formalism, however, within the EWMO (Hückel) program a different ζ is used for the s and p valence orbitals. Table 4.10 lists the appropriate theoretical k's estimated from the Slater exponents. A weighted average is used for the EWMO (Hückel) exponents. The Z+1/2 values are the average of the exponents appropriate to Z (the atomic number) and Z+1 atoms.

The GPM approach assumes that the shifts in binding energy can be connected exclusively to the properties of the ground state of the molecule. In effect a constant relaxation contribution within a series of molecules is assumed. Furthermore, the use of a fitting technique to extract predictive parameters (k and ℓ) from experimental data tends to obscure differences arising from additional contributions which may be significant. Incorporation of relaxation, as in the use of the relaxation or transition potential models, should give a more correct estimation of k. The values for k obtained by fitting the 2p and $2p^*$

Table 4.10. Theoretical k's[a] from Slater's exponents.

Equivalent Core			
P	S	EWMO[b]	CNDO/2
P		15.3446	14.5124
		16.2938	15.4950
S^+	S	17.2430	16.4776
		18.2271	17.4601
Cl^{++}	Cl^+	19.2112	18.4425
		20.2061	19.4257
	Ar^{++}	21.2010	20.4080

(a) $k = \zeta/3 \times 27.2107$ ev.

(b) $\zeta = \frac{\zeta_s + 3\zeta_p}{4}$

experimental shifts with RPM (or TPM) charges and potentials should display a similar trend to the theoretical values. This relationship provides an indication of whether the charges and potentials obtained from the calculations truly reflect the differences between the photo-ionisation of the molecule and the loss of an electron from the singly-charged ion.

(i) CNDO/2 Calculations

The values obtained for k and ℓ from the least-squares fit are listed in Table 4.11. The GPM and RPM shifts for the phosphorus series are shown in Table 4.12 and those for sulphur in Table 4.13. The correlations obtained between the various calculated shifts and experiment are summarised in Table 4.14. The correlations obtained between the RPM calculated shifts and experiment for the 2p and ℓ Auger shifts are shown in Figures 4.13 to 4.16.

In general the models provide reasonable correlation with experiment. The RPM approach gives a slope with almost the ideal value of unity in all cases (a suitable choice of reference would give zero intercept). The phosphorus series shows clearly the improvement in correlation resulting from the RPM approach as compared to the GPM approach. The improvement is less pronounced for the sulphur series. The correlations obtained for the Auger data for both the phosphorus and sulphur series were not as good as those

Table 4.11. Parameters from least-squares fit[a] for the atom-charge model (CNDO/2 charges and potentials).

	k	ℓ	corr. coeff.
Phosphorus series			
1s (GPM)	14.2372	- 1.9357	0.9949
1s (RPM)	14.2604	- 5.6186	0.9988
2p (GPM)	13.6076	- 1.9476	0.9944
2p (RPM)	13.5715	- 5.5893	0.9988
2p* (GPM)	14.6411	-12.1232	0.9940
2p* (RPM)	14.3854	-15.3313	0.9914
Sulphur series			
1s (GPM)	15.3715	- 0.2772	0.9980
1s (RPM)	15.8820	- 4.8491	0.9977
2p (GPM)	14.6091	- 0.4162	0.9980
2p (RPM)	14.9901	- 4.8689	0.9978
2p* (GPM)	15.5111	-11.6618	0.9964
2p* (RPM)	16.1632	-16.2604	0.9890

(a) Data fitted to

$$\Delta E - V = kq + \ell$$

Table 4.12. Calculated atom charge model shifts (ev) obtained from CNDO/2 charges and potentials[a,b] - Phosphorus series.

MOLECULE	Δ_{1s}		Δ_{2p}		Δ_{2p^*}		$\Delta E_{X\text{-ray}}$ [c]	$-\Delta_{KL_2L_3}$	
	GPM	RPM	GPM	RPM	GPM	RPM		GPM	RPM[d]
PH_3	0.0	0.0	0.0	0.0	0.0	0.0	0.0	0.0	0.0
SPF_3	7.39	6.09	6.53	5.25	5.15	3.59	1.05	4.10	2.54
$P(CH_3)_3$	0.26	-1.43	0.27	-1.41	-3.15	-4.72	0.12	-3.27	-4.84
$SPCl_3$	6.50	4.09	5.95	3.62	1.85	-0.48	0.64	1.21	-1.12
OPF_3	6.99	6.18	6.05	5.24	5.80	4.65	1.05	4.75	3.60
$OPCl_3$	6.32	4.09	5.70	3.54	2.08	-0.29	0.69	1.39	-0.98
PF_5	9.62	8.21	8.41	7.05	7.32	5.56	1.22	6.10	4.34
PCl_3	4.10	2.16	3.79	1.89	0.32	-1.86	0.49	-0.17	-2.35
PF_3	4.73	4.25	4.16	3.64	4.07	3.12	0.76	3.31	2.36
$SP(CH_3O)_2Cl$	5.70	3.07	5.07	2.52	0.64	-1.84	0.82	-0.18	-2.66
$(CH_3O)_3PO$	4.91	2.43	4.17	1.76	0.20	-2.27	0.80	-0.60	-3.07
$(CH_3O)_3PS$	5.35	2.67	4.66	2.07	0.22	-2.26	0.87	-0.65	-3.13
$(CH_3O)_3P$	2.81	0.69	2.40	0.32	-1.28	-3.45	0.63	-1.91	-4.08
$P(CH_3)Cl_2$	2.77	0.94	2.55	0.76	-0.83	-2.79	0.36	-1.19	-3.15

(Cont'd.)

Table 4.12. (Cont'd.)

$P(C_2H_5)_3$	0.15	-2.17	0.18	-2.08	-4.56	-6.62	0.05	-4.61	-6.67
$OP(CH_2Cl)Cl_2$	5.45	3.08	4.91	2.60	0.88	-1.43	0.59	0.29	-2.02
$SP(CH_3)Cl_2$	5.32	2.95	4.85	2.55	0.73	-1.45	0.60	0.13	-2.05
$P(CF_3)_3$	3.42	1.23	3.50	1.36	-1.07	-2.95	0.04	-1.11	-2.99

(a) GPM = Ground Potential Model; RPM = Relaxation Potential Model

(b) Parameters obtained from least-squares fit on equation 4.2 are listed in Table 4.11.

(c) $\Delta E_{X\text{-}ray} = \Delta(E(1s)-E(2p))$; Experimental values have been used.

(d) $\Delta E(KL_2L_3) = \Delta E_{X\text{-}ray} - \Delta E(2p^*)$.

Table 4.13. Calculated atom charge model shifts (ev) obtained from CNDO/2 charges and potentials[a,b] - Sulphur series.

	Δ_{1s}		Δ_{2p}		Δ_{2p*}			$-\Delta_{KL_2L_3}$	
	GPM	RPM	GPM	RPM	GPM	RPM	$\Delta E_{X\text{-ray}}$[c]	GPM	RPM
H_2S	0.0	0.0	0.0	0.0	0.0	0.0	0.0	0.0	0.0
$(CH_3)SH$	-0.13	-1.12	-0.14	-1.10	-2.09	-2.85	-0.04	-2.05	-2.81
$(CH_3)_2S$	-0.15	-1.87	-0.17	-1.85	-3.58	-5.09	-0.08	-3.50	-5.01
$(CH_3)_2SO$	2.27	0.25	1.90	-0.07	-2.11	-3.81	0.47	-2.58	-4.28
$SOCl_2$	5.55	3.11	4.91	2.55	0.09	-2.39	0.57	-0.48	-2.96
SOF_2	6.17	5.40	5.35	4.56	3.79	2.65	0.95	2.84	1.70
SO_2	4.19	4.13	3.58	3.45	3.39	2.94	0.77	2.62	2.17
SO_2ClF	8.28	6.57	7.18	5.50	3.76	2.06	1.34	2.42	0.72
SO_2Cl_2	7.98	5.61	6.97	4.67	2.27	-0.17	1.09	1.18	-1.26
SO_2F_2	8.67	7.81	7.45	6.58	5.71	4.64	1.35	4.36	3.29
SF_5Cl	12.73	10.48	11.20	9.00	6.72	4.34	1.44	5.28	2.90
SPF_3	0.40	-0.95	0.65	-0.70	-2.05	-3.58	-0.10	-1.95	-3.48
$SPCl_3$	-0.34	-2.39	-0.12	-2.14	-4.18	-6.30	-0.10	-4.08	-6.20

(Cont'd.)

Table 4.13. (Cont'd.)

$(CH_3O)_2SO$	3.92	1.46	3.32	0.95	-1.53	-3.83	0.76	-2.29	-4.59
$(CH_3O)_3PS$	-1.45	-3.60	-1.17	-3.28	-5.43	-7.52	-0.14	-5.29	-7.38
SF_6	13.25	11.48	11.60	9.87	8.07	6.15	1.68	6.39	4.47
CF_3SSCF_3	2.02	-0.49	1.97	-0.46	-2.98	-4.99	0.01	-2.99	-5.00
CH_3SSCH_3	0.02	-2.22	-0.01	-2.19	-4.44	-6.21	-0.06	-4.38	-6.15
$SP(CH_3O)_2Cl$	-1.12	-3.26	-0.85	-2.97	-5.11	-7.20	0.05	-5.16	-7.25
$(CH_3O)_2SO_2$	6.19	3.48	5.20	2.59	-0.14	-2.50	1.23	-1.37	-3.73
SF_4	9.18	7.74	8.07	6.66	5.21	3.37	1.17	4.04	2.20

(a) GPM = Ground Potential Model; RPM = Relaxation Potential Model.

(b) Parameters obtained from least-squares fit on equation 4.2 are listed in Table 4.11.

(c) $\Delta E_{X\text{-ray}} = \Delta(E(1s)-E(2p))$; experimental values have been used.

(d) $\Delta E(KL_2L_3) = \Delta E_{X\text{-ray}} - \Delta E(2p^*)$.

Table 4.14. Correlation obtained from least-squares fit on calculated versus experimental shifts (CNDO/2 calculation:atom-charge model).

	slope	intcpt	corr. coeff.
Phosphorus series			
1s (GPM)	0.9522	1.3943	0.9504
1s (RPM)	1.0006	-0.6136	0.9903
2p (GPM)	0.9377	1.5246	0.9353
2p (RPM)	1.0003	-0.4484	0.9884
KL_2L_3 (GPM)	0.9466	0.2283	0.9615
KL_2L_3 (RPM)	1.0346	-1.6707	0.9629
Sulphur series			
1s (GPM)	0.9908	0.6749	0.9847
1s (RPM)	0.9972	-1.0617	0.9864
2p (GPM)	0.9911	0.7469	0.9818
2p (RPM)	0.9999	-0.9586	0.9848
KL_2L_3 (GPM)	0.9997	-0.4783	0.9765
KL_2L_3 (RPM)	1.0250	-2.1795	0.9555

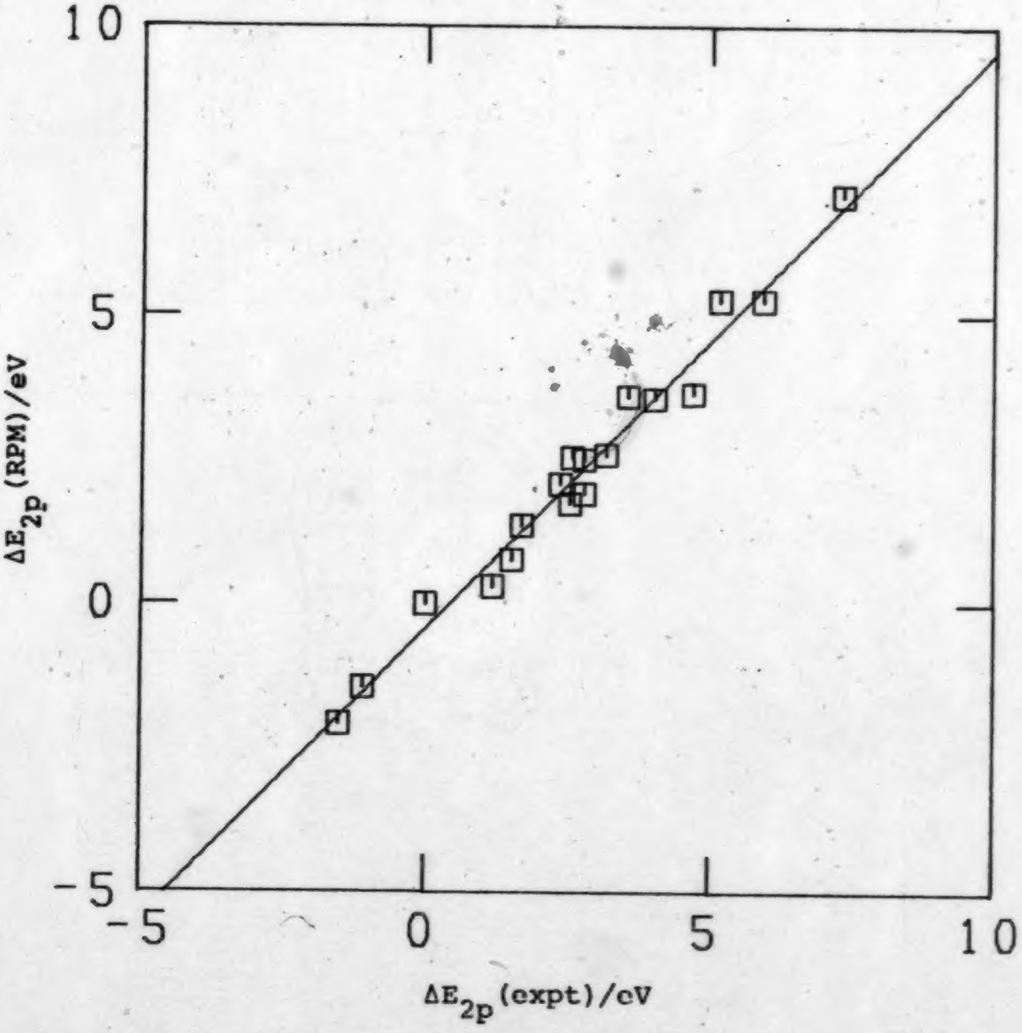

Figure 4.13 Correlation of calculated versus experimental P2p binding energy shifts. Calculated shifts are obtained from the atom charge model using CNDO/2 RPM charges and potentials.

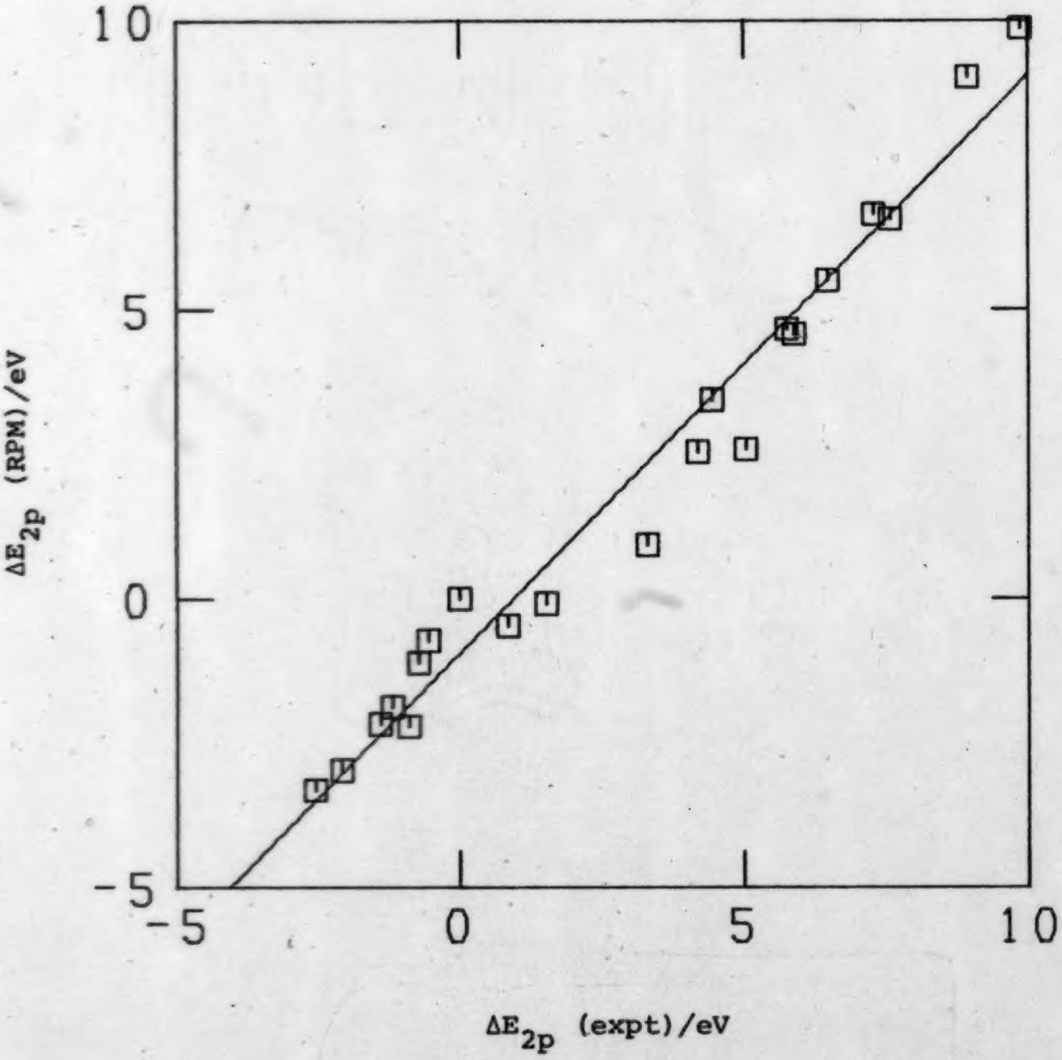

Figure 4.14 Correlation of calculated versus experimental S2p binding energy shifts. Calculated shifts are obtained from the atom charge model using CNDO/2 RPM charges and potentials.

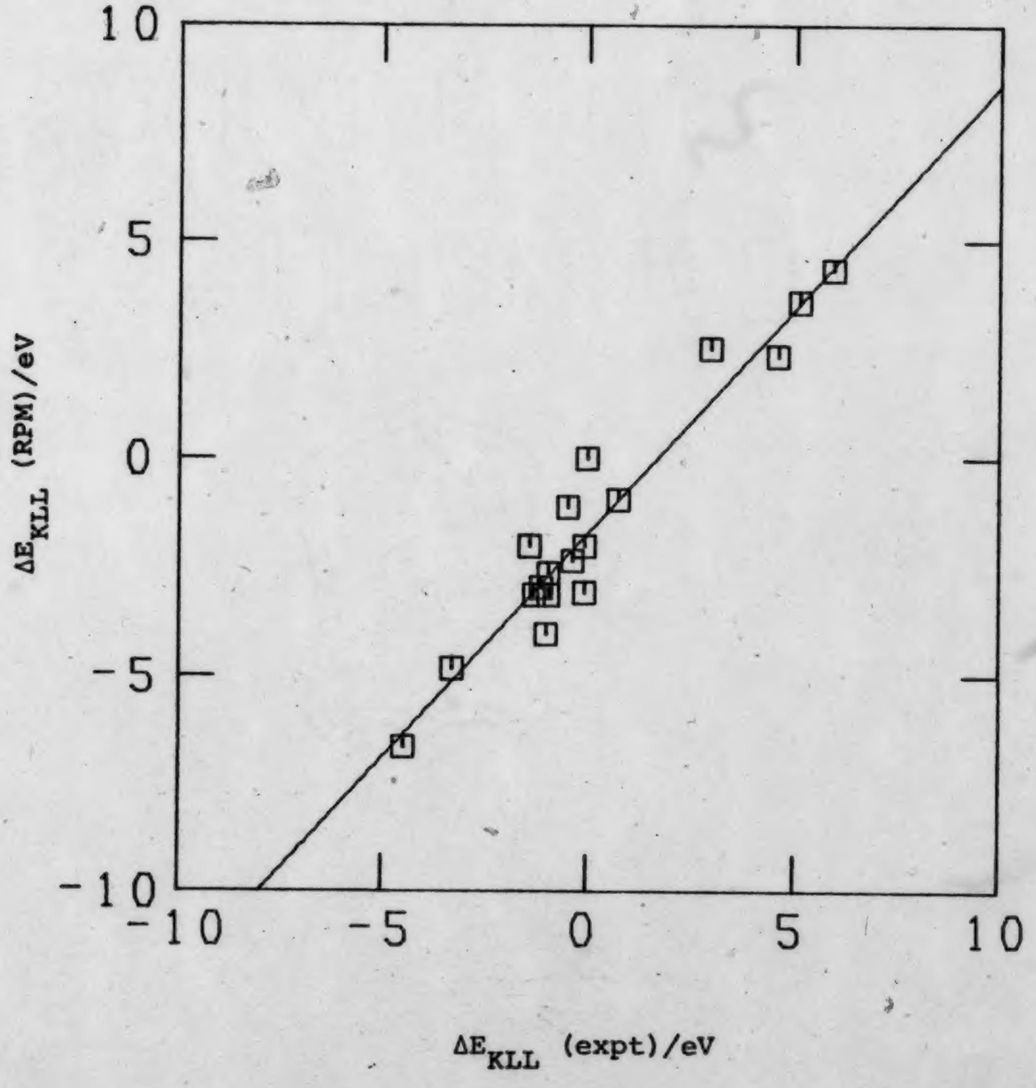

Figure 4.15 Correlation of calculated versus experimental P KL_2L_3 Auger energy shifts. Calculated shifts are obtained from the atom charge model using CNDO/2 RPM charges and potentials.

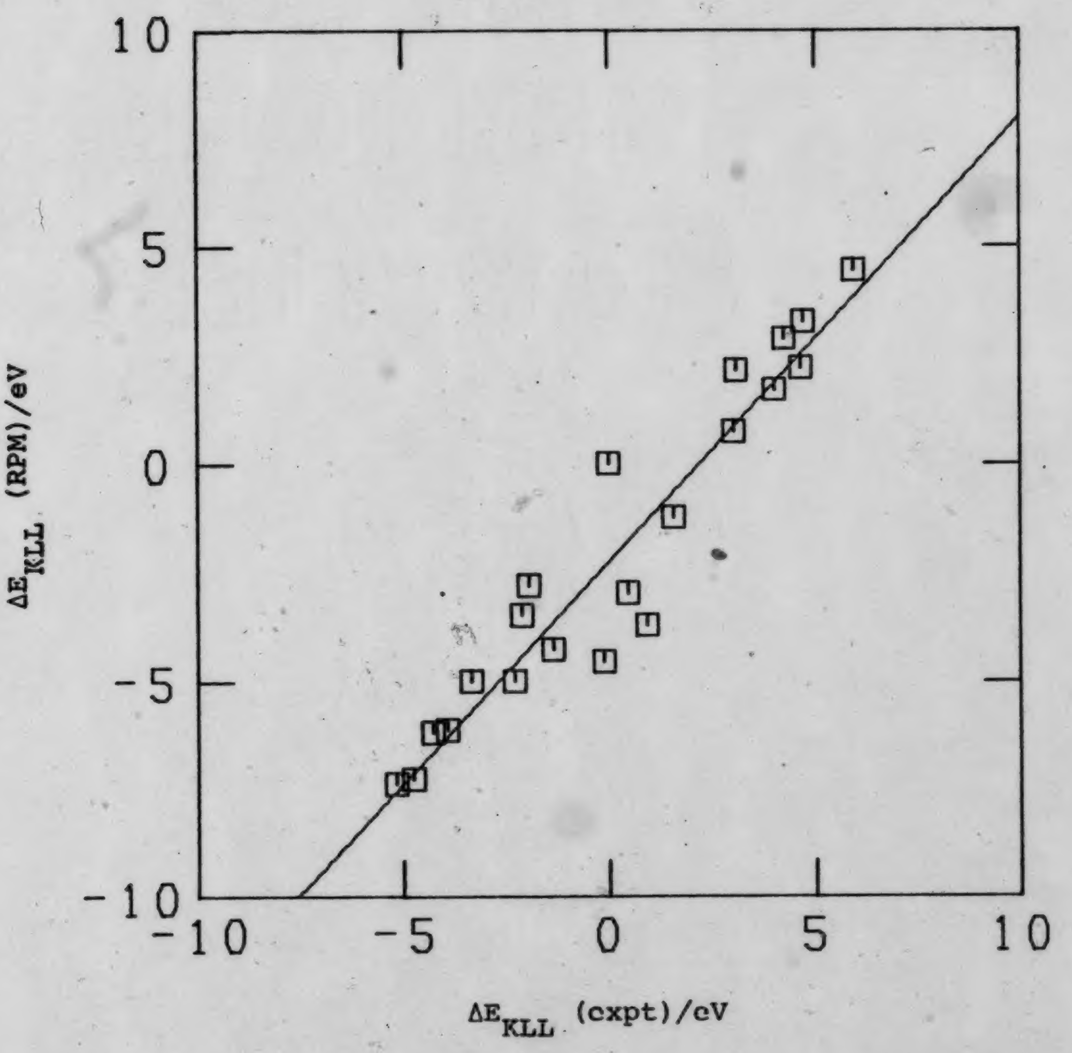

Figure 4.16 Correlation of calculated versus experimental S KL_2L_3 Auger energy shifts. Calculated shifts are obtained from the atom charge model using CNDO/2 RPM charges and potentials.

obtained for the core-electron shifts. This suggests limitations in the applicability of the equivalent core approximation for the doubly-charged ion, especially with charges and potentials obtained by the CNDO/2 methodology. The value obtained for k for the $2p^*$ (RPM) shift is larger than that for the 2p (RPM) shift, however, neither value is as large as the theoretical values. This suggests that the calculation is able to predict the general trend in a satisfactory manner although the charges and potentials may not be absolutely correct.

The shifts obtained by the potential model (equation 3.3) have also been evaluated and the results are presented in Table 4.15. The correlations between the calculated and experimental shifts are summarised in Table 4.16 and those from the relaxation potential model are shown in Figures 4.17 to 4.22. The correlations obtained between calculated and experimental shifts are as good or better than those obtained with the atom-charge model, however, the slope of the line is no longer unity. In this model a theoretical value for k is calculated each time using $k_i = \langle j|1/r_i|j\rangle$ (equation 3.2). This supports the point that the valence populations (and hence charges) and potentials obtained in the CNDO/2 calculations are not consistent with the theoretically estimated values for k but are still adequate in showing the trends.

TABLE 4.15 Calculated potential model shifts (eV) obtained from CNDO/2 calculation[a]

	ΔE_B^b		$-\Delta E_{AUG}^c$			ΔE_B^b		$-\Delta E_{AUG}^c$	
Molecule	GPM	RPM	GPM	RPM	Molecule	GPM	RPM	GPM	RPM
PH_3	0.00	0.00	0.00	0.00	H_2S	0.00	0.00	0.00	0.00
SPF_3	7.76	7.43	6.04	5.28	$(CH_3)SH$	-0.12	-1.17	-2.17	-2.91
$P(CH_3)_3$	0.26	-1.51	-3.40	-4.96	$(CH_3)_2S$	-0.13	-1.94	-3.68	-5.18
$SPCl_3$	6.74	4.75	2.12	-0.04	$(CH_3)_2SO$	2.81	0.69	-1.91	-3.78
OPF_3	7.40	7.73	7.01	6.91	$SOCl_2$	6.47	3.90	0.76	-2.26
$OPCl_3$	6.59	4.91	2.54	0.44	SOF_2	7.36	6.76	5.22	3.66
PF_5	10.14	10.07	8.78	8.06	SO_2	5.08	5.29	4.72	4.05
PCl_3	4.24	2.54	0.36	-1.81	SO_2ClF	9.88	8.22	5.21	2.95
PF_3	4.97	5.31	4.88	4.77	SO_2Cl_2	9.44	7.02	3.51	0.41
$SP(CH_3O)_2Cl$	5.98	3.85	0.90	-1.36	SO_2F_2	10.43	9.76	7.75	6.15
$(CH_3O)_3PO$	5.24	3.42	0.80	-1.29	SF_5Cl	14.95	12.75	9.12	5.86
$(CH_3O)_3PS$	5.65	3.54	0.56	-1.62	SPF_3	0.04	-1.35	-2.65	-4.27
$(CH_3O)_3P$	2.99	1.24	-1.14	-3.14	$SPCl_3$	-0.67	-2.83	-4.88	-6.95

(Cont'd.)

TABLE 4.15 (cont'd.)

$P(CH_3)Cl_2$	2.86	1.19	-0.84	-2.78	$(CH_3O)_2SO$	4.80	2.18	-1.20	-3.95
$P(C_2H_5)_3$	0.13	-2.40	-4.99	-7.31	$(CH_3O)_3PS$	-1.87	-4.15	-6.30	-8.27
$OP(CH_2Cl)Cl_2$	5.68	3.76	1.24	-0.82	SF_6	15.63	13.98	10.65	7.83
$SP(CH_3)Cl_2$	5.52	3.51	0.89	-1.14	CF_3SSCF_3	2.10	-0.65	-3.41	-5.51
$P(CH_3)_3$	3.39	0.91	-1.61	-3.82	CH_3SSCH_3	0.08	-2.35	-4.73	-6.54
					$SP(CH_3O)_2Cl$	-1.50	-3.78	-6.11	-8.10
					$(CH_3O)_2SO_2$	7.62	4.78	0.71	-2.27
					SF_4	10.78	9.42	6.90	4.32

(a) GPM = Ground Potential Model; RPM = Relaxation Potential Model.

(b) Core electron shifts are given by equation 3.3 for the GPM and equation 3.5 for the RPM.

(c) Auger shifts are given by equation 3.6. ΔE_{XRAY}, as required in equation 3.6, are shown in Table 4.12.

Table 4.16. Correlation obtained from least-squares fit on calculated versus experimental shifts (CNDO/2 calculation:potential model).

	slope	intcpt	corr. coeff.
Phosphorus series			
1s (GPM)	1.0066	1.4230	0.9527
1s (RPM)	1.2124	-0.6626	0.9914
2p (GPM)	1.1371	1.6727	0.9427
2p (RPM)	1.3767	-0.3814	0.9862
KL_2L_3 (GPM)	1.2158	1.0925	0.9593
KL_2L_3 (RPM)	1.4372	-0.5510	0.9761
Sulphur series			
1s (GPM)	1.1869	0.7235	0.9878
1s (RPM)	1.2122	-1.1111	0.9895
2p (GPM)	1.3736	0.8730	0.9876
2p (RPM)	1.4049	-0.9644	0.9908
KL_2L_3 (GPM)	1.4662	0.6209	0.9845
KL_2L_3 (RPM)	1.4080	-1.3835	0.9766

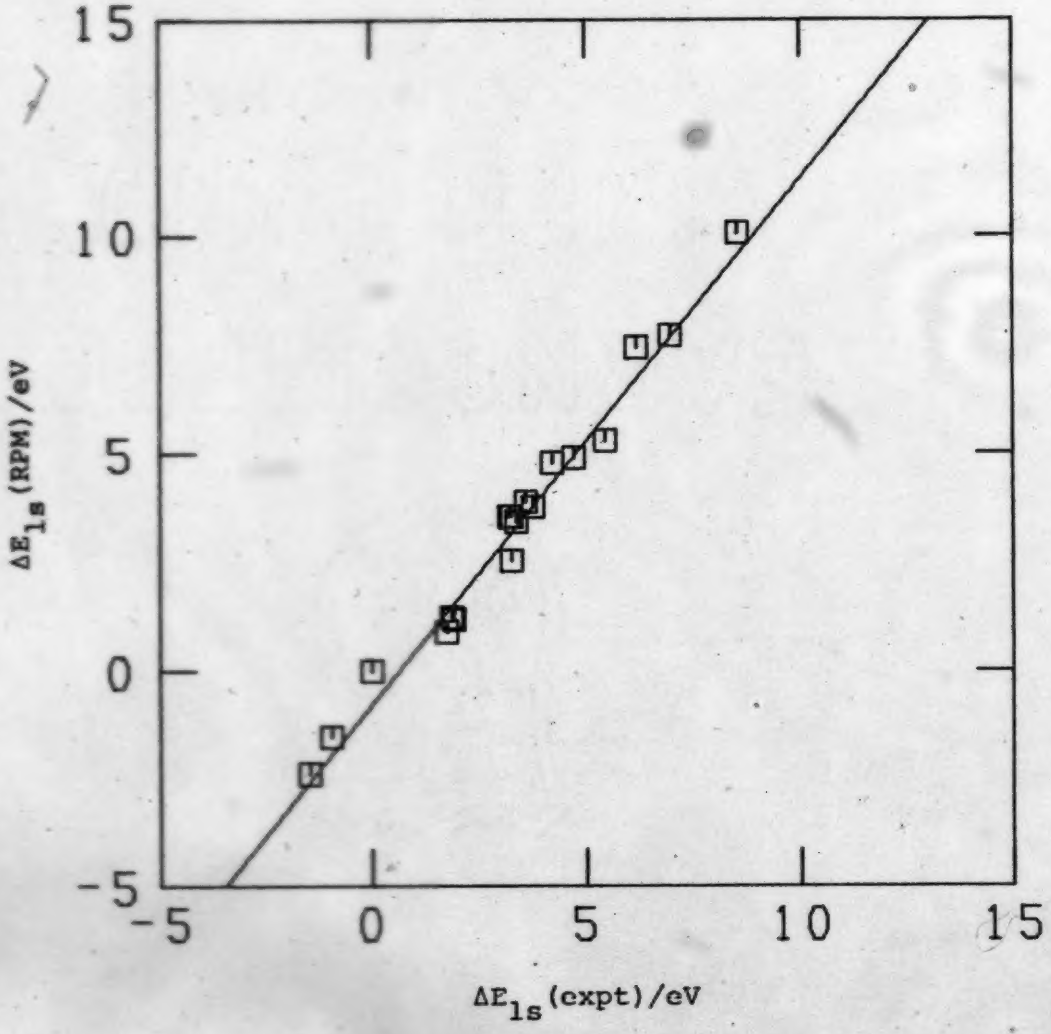

Figure 4.17 Correlation of calculated (potential model) shifts versus experimental P1s binding energy shifts. Calculated shifts are obtained using CNDO/2 RPM point charge potentials.

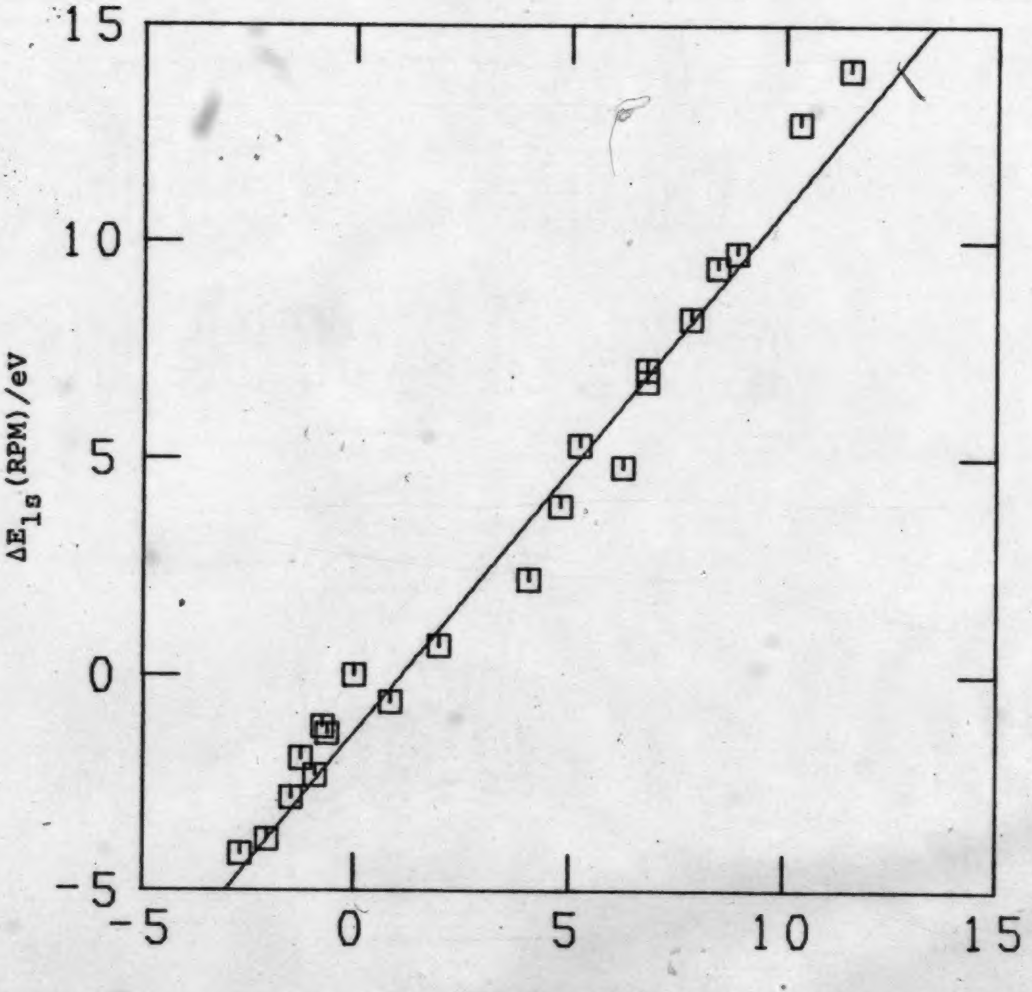

Figure 4.18 Correlation of calculated (potential model) shifts versus experimental S1s binding energy shifts. Calculated shifts are obtained using CNDO/2 RPM point charge potentials.

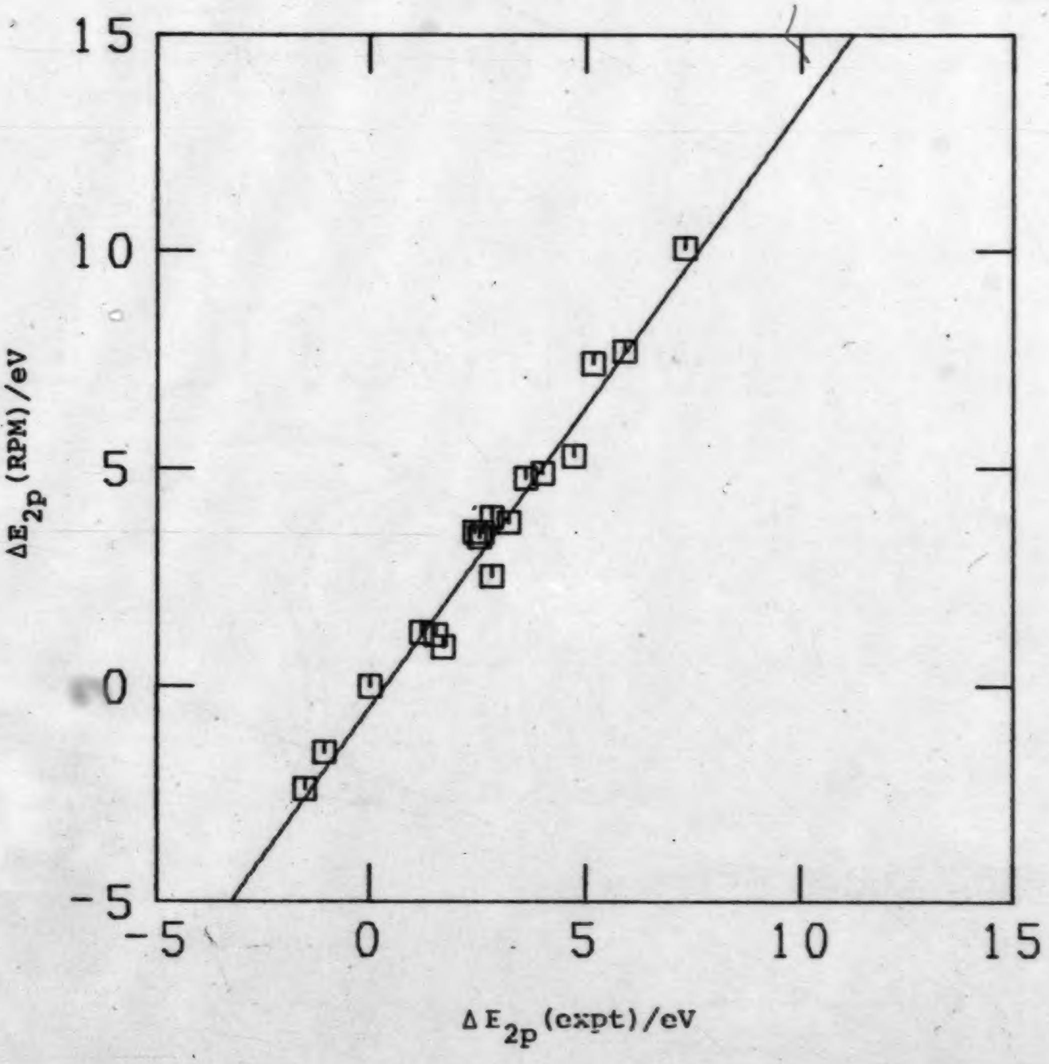

Figure 4.19 Correlation of calculated (potential model) shifts versus experimental P2p binding energy shifts. Calculated shifts are obtained using CNDO/2 RPM point charge potentials.

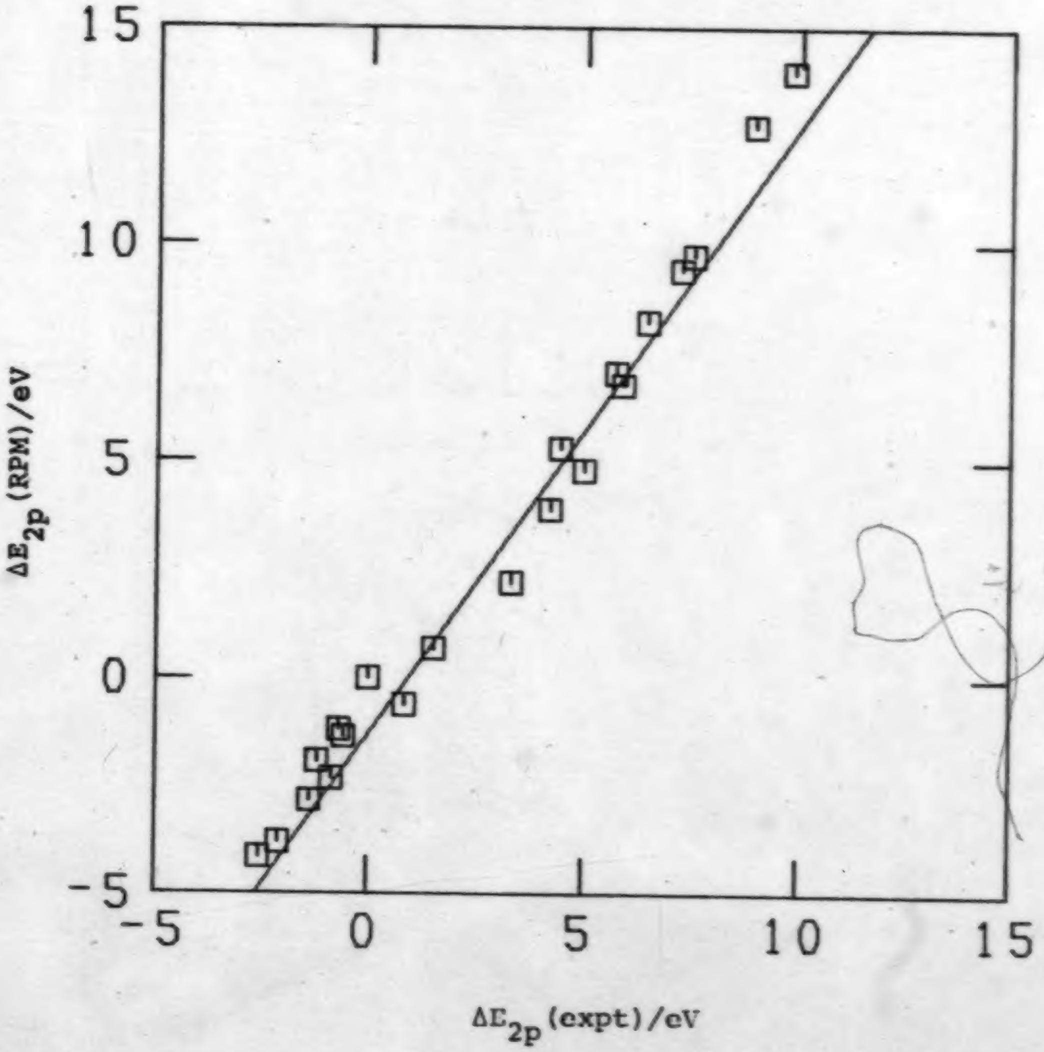

Figure 4.20 Correlation of calculated (potential model) shifts versus experimental S_{2p} binding energy shifts. Calculated shifts are obtained using CNDO/2 RPM point charge potentials.

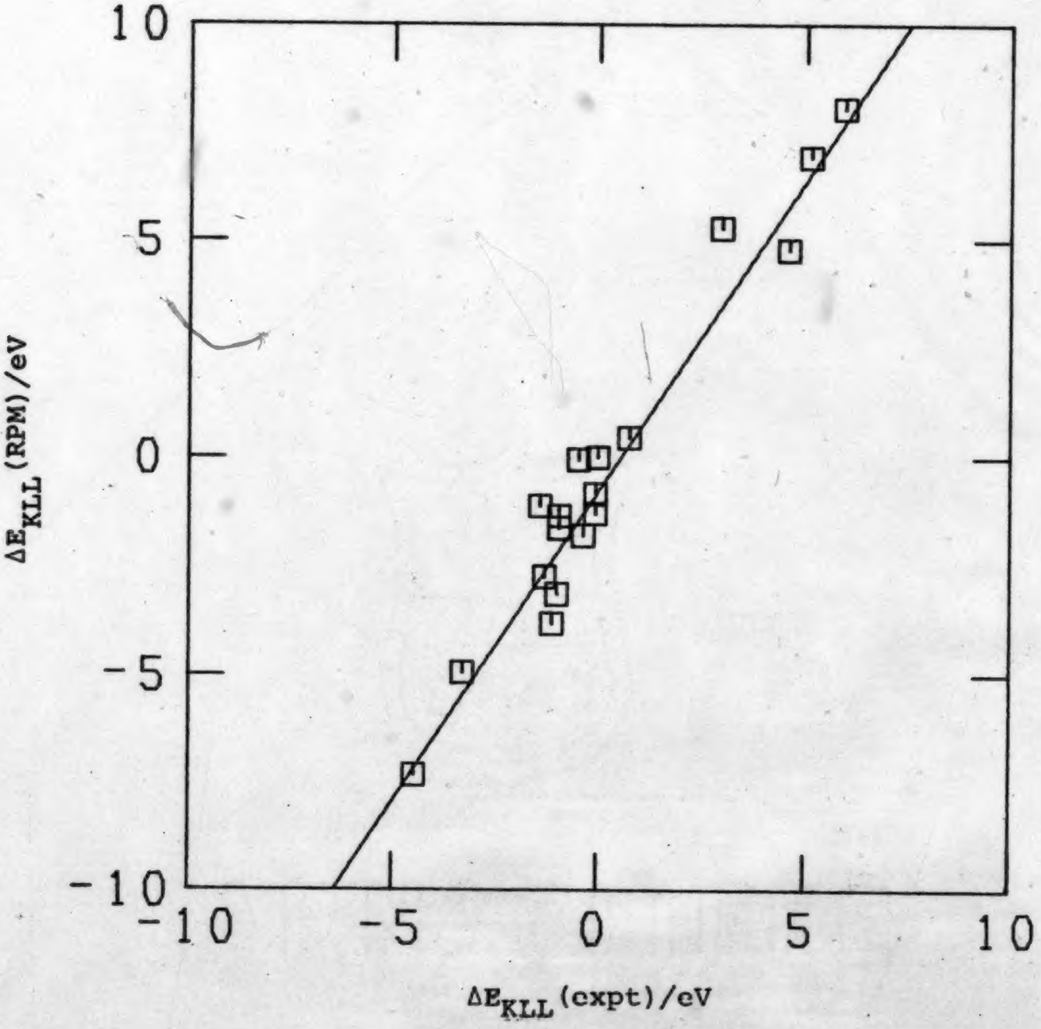

Figure 4.21 Correlation of calculated (potential model) shifts versus experimental P KL_2L_3 Auger energy shifts. Calculated shifts are obtained using CNDO/2 RPM point charge potentials.

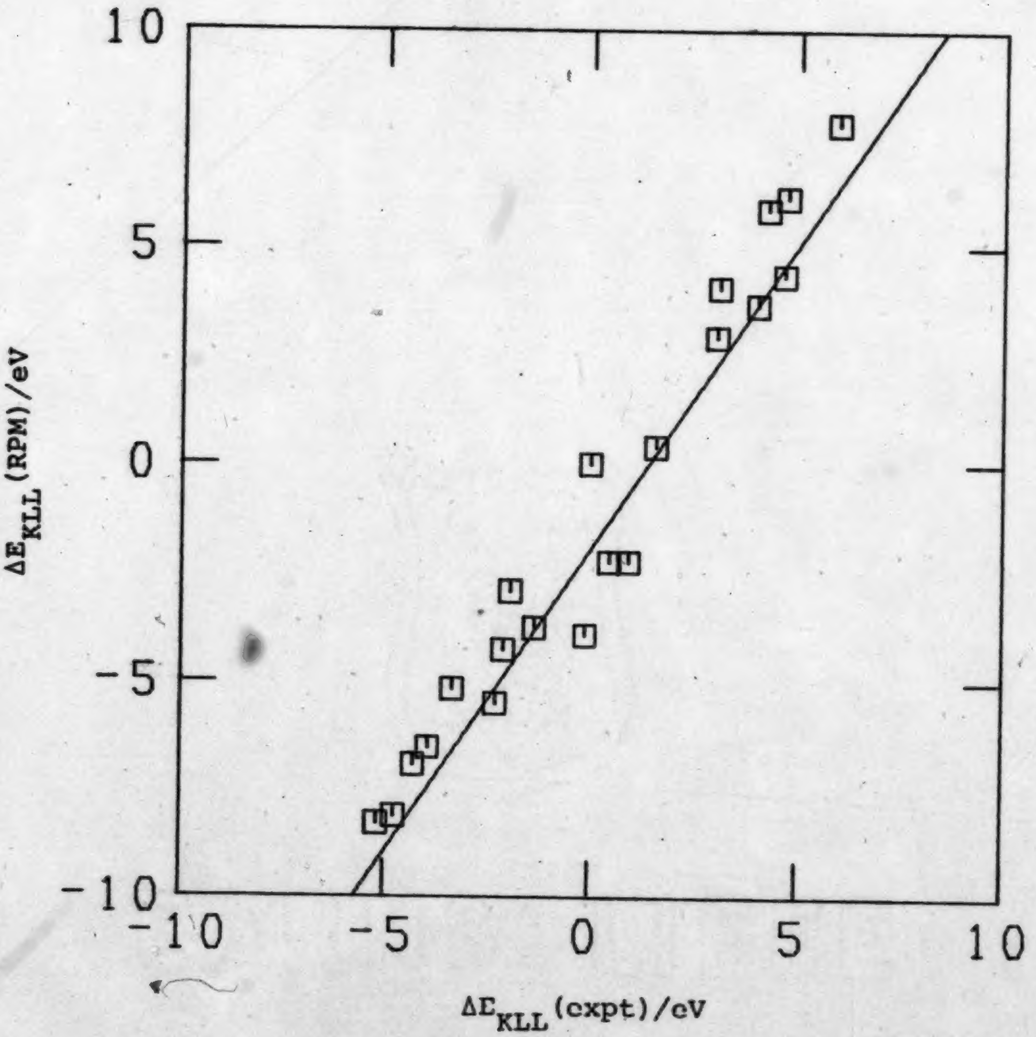

Figure 4.22 Correlation of calculated (potential model) shifts versus experimental S KL_2L_3 Auger energy shifts. Calculated shifts are obtained using CNDO/2 RPM point charge potentials.

The slope obtained for the 1s shift prediction is closer to unity than that for the equivalent 2p shift, reflecting the fact that the point-charge approximation is more appropriate for the deeper levels. The 2p electrons will have a greater interaction with the valence shell than will the 1s level because of its closer proximity.

CNDO/2 calculations with d-orbitals included in the basis set were performed for the phosphorus series. Convergence problems occurred in many cases and so only the results of a limited series are presented. Table 4.17 shows the calculated shifts along with the correlations obtained from least-squares fits on the calculated versus experimental shifts. The correlations obtained are considerably poorer than those obtained from calculations omitting d-orbitals. Furthermore, the values for k (Table 4.18), though larger than those obtained when d-orbitals were omitted, do not follow the expected theoretical trend when comparing the loss of a 2p electron from the molecule to the loss of a 2p electron from the ion. It can be concluded that the charges and potentials obtained from the CNDO/2 calculation including d-orbitals in the basis set are inadequate.

(ii) EWMO (Hückel) Calculations

Only the atom-charge model was used in conjunction with charges and potentials from the EWMO (Hückel) calculation.

TABLE 4.17 Calculated atom charge model shifts (eV) obtained from CNDO/2 charges and potentials with d-orbitals included in basis set [a,b]

	Δ1s		Δ2p		$\Delta 2p^*$			$-\Delta KL_2L_3$ [d]	
Molecule	GPM	RPM	GPM	RPM	GPM	RPM	ΔE_{XRAY} [c]	GPM	RPM
PH_3	0.00	0.00	0.00	0.00	0.00	0.00	0.00	0.0	0.0
$P(CH_3)_3$	-2.01	-3.14	-1.80	-2.94	-4.56	-5.74	0.12	-4.68	-5.86
PF_5	8.21	5.93	7.27	5.12	4.93	2.88	1.22	3.71	1.66
PCl_3	0.82	-0.37	0.82	-0.36	-1.55	-3.10	0.49	-2.04	-3.59
PF_3	4.14	4.20	3.69	3.63	4.96	3.81	0.76	4.20	3.05
$(CH_3O)_3P$	-0.18	-1.35	-0.28	-1.48	-2.36	-4.32	0.63	-2.99	-4.95
$P(CH_3)Cl_2$	-0.12	-1.28	-0.06	-1.22	-2.52	-3.95	0.36	-2.88	-4.31
$P(C_2H_5)_3$	-1.86	-3.77	-1.64	-3.50	-6.01	-7.74	0.05	-6.06	-7.79
$P(CF_3)_3$	2.18	0.06	2.40	0.35	-2.40	-3.96	0.04	-2.44	-4.00

(Cont'd.)

TABLE 4.17 (cont'd.)

Correlations	slope	intcpt	corr coeff
1s (GPM)	0.9646	-0.9319	0.9505
1s (RPM)	0.9336	-2.0725	0.9376
2p (GPM)	0.9790	-0.6535	0.9519
2p (RPM)	0.9475	-1.7958	0.9407
KL_2L_3 (GPM)	1.0132	-1.3354	0.9795
KL_2L_3 (RPM)	1.0014	-2.7393	0.9349

(a) GPM = Ground Potential Model; RPM = Relaxation Potential Model.

(b) Correlation obtained from least-squares fit on calculated versus experimental shift.

(c) $\Delta E_{XRAY} = \Delta(E(1s) - E(2p))$; experimental values have been used.

(d) $\Delta E(KL_2L_3) = \Delta E_{XRAY} - \Delta E(2p^*)$.

Table 4.18. k values obtained from least-squares fit[a] using CNDO/2 charges and potentials - d orbitals included in the basis set.

Phosphorus series	k
1s (GPM)	18.9895
1s (RPM)	17.6137
2p (GPM)	17.8466
2p (RPM)	16.4861
2p* (GPM)	17.8507
2p* (RPM)	16.1429

(a) k obtained from fit to

$$\Delta E - V = kq + \ell$$

The fitted values of k and ℓ for the GPM, RPM and TPM approaches are listed in Table 4.19. The results of calculations done with the original parameterisation[48] and with new phosphorus parameters (Appendix 2) are compared. The shifts for the phosphorus series are given in Table 4.20 for the case of the original parameterisation for P and in Table 4.21 for the new parameters. Shifts for the sulphur series are given in Tables 4.22 and 4.23 respectively. Table 4.24 summarises the correlations between the various calculated shifts and experiment, some of which are shown in Figures 4.23 to 4.30.

The correlations between the calculated and experimental shifts are very similar for both parameterisations. The original parameterisation gives a slightly better fit for the phosphorus series whereas the converse is true for the sulphur series in which a phosphorus group is present as a substituent on the sulphur. The use of fitting techniques to obtain k and ℓ values tends to obscure the effect that the new parameterisation may have on the fit. The new parameterisation clearly gives a lower value for the k associated with the initial photo-ionisation in the phosphorus series and this may indicate that the new parameterisation is more realistic, however it is difficult to draw any definite conclusions.

The correlations between experimental and calculated

Table 4.19. Parameters from least-squares fit[a] for atom-charge model (EWMO charges and potentials).

	Original Parameterisation			New Parameterisation		
	k	ℓ	corr. coeff.	k	ℓ	corr. coeff.
Phosphorus Series						
1s (GPM)	14.7377	-0.7551	0.9954	14.0566	- 1.5194	0.9948
1s (RPM)	14.4145	-6.1286	0.9959	14.0772	- 6.4272	0.9960
1s (TPM)	14.3463	-5.7885	0.9957	13.9111	- 5.9191	0.9959
2p (GPM)	14.0946	-0.8423	0.9953	13.4995	- 1.5465	0.9947
2p (RPM)	13.7688	-6.0436	0.9960	13.4779	- 6.3222	0.9960
2p (TPM)	13.7012	-5.7315	0.9958	13.3243	- 5.8592	0.9960
2p* (GPM)	14.2826	-14.0775	0.9844			
2p* (RPM)	14.2724[b]	-19.1749[b]	0.9850[b]			
2p* (TPM)	13.8873	-18.4883	0.9828			

(Cont'd.)

Table 4.19. (Cont'd.)

Sulphur Series

1s (GPM)	14.8420	-1.0040	0.9980	14.7832	- 0.9058	0.9983
1s (RPM)	14.8507	-6.3686	0.9984	14.8146	- 6.3086	0.9986
1s (TPM)	14.6803	-5.8050	0.9982	14.6565	- 5.7691	0.9984
2p (GPM)	14.1751	-1.0325	0.9980	14.1368	- 0.9647	0.9982
2p (RPM)	14.1396	-6.2193	0.9985	14.1246	- 6.1932	0.9987
2p (TPM)	13.9776	-5.7037	0.9983	13.9743	- 5.6994	0.9985
2p* (GPM)	14.1014	-13.5964	0.9973	14.1225	-13.6367	0.9975
2p* (RPM)	14.2189	-19.3294	0.9977	14.2590	-19.4146	0.9980
2p* (TPM)	14.0907	-19.0981	0.9976	14.1371	-19.1956	0.9979

(a) Data fitted to $\Delta E\text{-}V = kq + \ell$

(b) $P(C_2H_5)_3$ not included, note 2p* (GPM): $k = 14.1979$

$\ell = -13.9358$ in this case

corr. coeff. = 0.9811

Table 4.20. Calculated atom charge model shifts (ev) obtained from EHMO (original parameterisation) charges and potentials[a,b] - Phosphorus series.

MOLECULE	Δ_{1s} GPM	Δ_{1s} RPM	Δ_{1s} TPM	Δ_{2p} GPM	Δ_{2p} RPM	Δ_{2p} TPM	Δ_{2p^*} GPM	Δ_{2p^*} RPM[c]	Δ_{2p^*} TPM	$\Delta E_{X\text{-}ray}$[d]	$-\Delta_{KL_2L_3}$[e] GPM	$-\Delta_{KL_2L_3}$[e] RPM	$-\Delta_{KL_2L_3}$[e] TPM
PH_3	0.0	0.0	0.0	0.0	0.0	0.0	0.0	0.0	0.0	0.0	0.0	0.0	0.0
SPF_3	6.81	5.88	5.76	6.01	5.13	5.00	5.21	4.18	4.38	1.05	4.16	3.13	3.33
$P(CH_3)_3$	0.23	-0.97	-1.14	0.17	-0.99	-1.16	-2.14	-3.24	-3.38	0.12	-2.26	-3.36	-3.50
$SPCL_3$	5.59	4.36	4.24	5.11	3.92	3.79	3.30	1.78	1.81	0.64	2.66	1.14	1.17
OPF_3	7.66	6.81	6.70	6.69	5.87	5.76	6.26	5.51	5.06	1.05	5.21	4.46	4.01
$OPCl_3$	5.53	4.29	4.16	4.88	3.69	3.55	3.26	1.83	1.48	0.69	2.57	1.14	0.79
PF_5	8.99	8.00	7.88	7.94	6.98	6.86	7.33	6.39	5.91	1.22	6.11	5.17	4.69
PCl_3	2.59	1.34	1.21	2.38	1.19	1.05	0.19	-1.21	-1.44	0.49	-0.30	-1.70	-1.93
PF_3	5.37	4.52	4.41	4.75	3.95	3.84	3.88	3.12	2.81	0.76	3.12	2.36	2.05
$SP(CH_3O)_2Cl$	4.37	3.11	2.96	3.71	2.50	2.36	2.08	0.68	0.76	0.82	1.26	-0.14	-0.06
$(CH_3O)_3PO$	3.94	2.73	2.57	3.04	1.87	1.72	1.80	0.60	0.25	0.80	1.00	-0.12	-0.55
$(CH_3O)_3PS$	3.68	2.46	2.30	2.93	1.76	1.60	1.49	0.24	0.35	0.87	0.62	-0.63	-0.52
$(CH_3O)_3P$	1.34	0.12	-0.05	0.82	-0.34	-0.51	-0.92	-1.91	-2.18	0.63	-1.55	-2.54	-2.81
$P(CH_3)Cl_2$	1.90	0.67	0.53	1.73	0.55	0.41	-0.48	-1.80	-2.00	0.36	-0.84	-2.16	-2.36
$OP(CH_2Cl)Cl_2$	5.25	3.86	3.73	4.62	3.29	3.15	2.69	1.14	0.81	0.59	2.10	0.55	0.22
$SP(CH_3)Cl_2$	5.06	3.81	3.68	4.60	3.39	3.25	2.72	1.24	1.93	0.60	2.12	0.64	1.33
$P(C_2H_5)_3$	0.20	-1.43	-1.60	0.17	-1.40	-1.57	-3.03	-	-4.77	0.05	-3.08	-	-4.82

(a) GPM = Ground Potential Model; RPM = Relaxation Potential Model; TPM - Transition Potential Model

(b) Parameters obtained from least-squares fit on equation 4.2 are listed in Table 4.19.

(c) $P(C_2H_5)_3$ not included in fit due to convergence problems for the (Z+2) equivalent core case.

(d) $\Delta E_{X\text{-}ray} = \Delta(E(1s)-E(2p))$; experimental values have been used.

(e) $\Delta E(KL_2L_3) = \Delta E_{X\text{-}ray} - \Delta E(2p^*)$.

Table 4.21. Calculated atom charge model shifts (eV) obtained from EWMO (new P parameterisation) charges and potentials used[a].

	Δ_{1s}			Δ_{2p}		
MOLECULE	GPM	RPM	TPM	GPM	RPM	TPM
PH_3	0.0	0.0	0.0	0.0	0.0	0.0
SPF_3	7.18	6.10	5.92	6.38	5.33	5.16
$P(CH_3)_3$	0.48	-0.82	-1.05	0.43	-0.84	-1.06
$SPCl_3$	6.26	4.73	4.51	5.77	4.28	4.07
OPF_3	7.70	6.85	6.69	6.73	5.91	5.75
$OPCl_3$	6.08	4.59	4.39	5.43	3.98	3.78
PF_5	9.12	8.09	7.91	8.07	7.07	6.89
PCl_3	3.05	1.61	1.37	2.84	1.45	1.21
PF_3	5.44	4.58	4.42	4.83	4.01	3.85
$SP(CH_3O)_2Cl$	4.90	3.41	3.19	4.24	2.80	2.58
$(CH_3O)_3PO$	4.20	2.89	2.67	3.30	2.03	1.81
$(CH_3O)_3PS$	4.11	2.71	2.48	3.36	2.00	1.78
$(CH_3O)_3P$	1.50	0.24	-0.01	0.99	-0.22	-0.46
$P(CH_3)Cl_2$	2.29	0.89	0.66	2.12	0.77	0.54
$OP(CH_2Cl)Cl_2$	5.77	4.16	3.95	5.14	3.57	3.37
$SP(CH_3)Cl_2$	5.68	4.15	3.93	5.21	3.72	3.50
$P(C_2H_5)_3$	0.52	-1.24	-1.49	0.49	-1.21	-1.46

(a) 2p* and KL_2L_3 shifts are unchanged from Table 4.20.

TABLE 4.22 Calculated atom charge model shifts (eV) obtained from EWMO (original parametrisation) charges and potentials[a,b] - sulphur series

	Δ1s			Δ2p			Δ2p*				-ΔKL$_2$L$_3$		
Molecule	GPM	RPM	TPM	GPM	RPM	TPM	GPM	RPM	TPM	ΔE XRAY	GPM	RPM	TPM
H_2S	0.0	0.0	0.0	0.0	0.0	0.0	0.0	0.0	0.0	0.0	0.0	0.0	0.0
$(CH_3)SH$	-0.15	-0.74	-0.89	-0.15	-0.73	-0.87	-1.30	-1.73	-1.80	-0.04	-1.26	-1.69	-1.76
$(CH_3)_2S$	-0.17	-1.29	-1.55	-0.19	-1.27	-1.52	-2.34	-3.17	-3.30	-0.08	-2.26	-3.09	-3.22
$(CH_3)_2SO$	3.98	2.49	2.13	3.37	1.95	1.60	0.54	-0.47	-0.67	0.47	0.07	-0.94	-1.14
$SOCl_2$	5.67	3.93	3.55	4.99	3.33	2.96	1.68	0.33	0.86	0.57	1.11	-0.24	0.29
SOF_2	7.40	6.26	5.95	6.46	5.39	5.09	4.32	3.58	3.40	0.95	3.37	2.63	2.45
SO_2	5.51	4.64	4.34	4.74	3.93	3.65	3.13	2.65	2.49	0.77	2.36	1.88	1.72
SO_2ClF	9.19	7.81	7.50	7.92	6.59	6.29	5.28	4.34	4.51	1.34	3.94	3.00	3.17
SO_2Cl_2	8.54	6.91	6.59	7.36	5.80	5.49	4.25	3.05	3.53	1.09	3.16	1.96	2.44
SO_2F_2	10.06	8.94	8.65	8.69	7.62	7.33	6.56	5.91	5.71	1.35	5.21	4.56	4.36
SF_5Cl	11.87	10.11	9.78	10.47	8.78	8.47	7.11	5.80	5.95	1.44	5.67	4.36	4.51
SPF_3	2.53	0.54	0.08	2.57	0.68	0.24	-1.20	-2.43	-2.62	-0.10	-1.10	-2.33	-2.52
$SPCl_3$	-1.33	-3.15	-3.59	-1.10	-2.84	-3.27	-4.57	-5.73	-5.27	-0.10	-4.47	-5.63	-5.17

TABLE 4.22 (cont'd.)

$(CH_3O)_2SO$	4.91	3.35	2.99	4.07	2.59	2.24	1.11	-0.15	-0.26	0.76	0.35	-0.91	-1.02
$(CH_3O)_3PS$	-1.35	-3.24	-3.74	-1.16	-2.97	-3.44	-4.76	-5.87	-6.01	-0.14	-4.62	-5.73	-5.87
SF_6	12.69	11.12	10.81	11.18	9.69	9.38	8.21	7.14	6.93	1.68	6.53	5.46	5.25
CF_3SSCF_3	4.42	2.50	2.39	4.31	2.46	2.33	0.62	-0.92	-1.10	0.01	0.61	-0.93	-1.11
CH_3SSCH_3	-0.09	-1.51	-1.48	-0.11	-1.47	-1.47	-2.83	-3.95	-4.10	-0.06	-2.77	-3.89	-4.04
$SP(CH_3O)_2Cl$	-1.27	-3.16	-3.65	-1.07	-2.88	-3.35	-4.67	-5.80	-5.73	0.05	-4.72	-5.85	-5.78
$(CH_3O)_2SO_2$	7.55	6.01	5.68	6.23	4.77	4.45	3.32	2.24	2.05	1.23	2.09	1.01	0.82
SF_4	9.23	7.81	7.47	8.18	6.83	6.50	5.50	4.51	4.29	1.17	4.33	3.34	3.12

(a) GPM = Ground Potential Model; RPM = Relaxation Potential Model, TPM = Transition Potential Model.

(b) Parameters obtained from least-square fit on equation 4.2 are listed in Table 4.19.

(c) $\Delta E_{XRAY} = \Delta(E(1s)-E(2p))$; experimental values have been used.

(d) $\Delta E(KL_2L_3) = \Delta E_{XRAY} - \Delta E(2p^*)$.

Table 4.23. Calculated atom charge model shifts (eV) obtained from EHMO (new P parameterisation) charges and potentials used[a].

MOLECULE	Δ1s GPM	Δ1s RPM	Δ1s TPM	Δ2p GPM	Δ2p RPM	Δ2p TPM	Δ2p* GPM	Δ2p* RPM	Δ2p* TPM	$\Delta E_{X\text{-ray}}$	$-\Delta KL_2L_3$ GPM	$-\Delta KL_2L_3$ RPM	$-\Delta KL_2L_3$ TPM
H_2S	0.00	0.00	0.00	0.00	0.00	0.00	0.00	0.00	0.00	0.0	0.00	0.00	0.00
$(CH_3)SH$	-0.15	-0.74	-0.89	-0.15	-0.73	-0.87	-1.30	-1.74	-1.80	-0.04	-1.26	-1.70	-1.76
$(CH_3)_2S$	-0.18	-1.29	-1.55	-0.19	-1.26	-1.52	-2.34	-3.18	-3.30	-0.08	-2.26	-3.10	-3.22
$(CH_3)_2SO$	3.92	2.47	2.11	3.34	1.94	1.60	0.55	-0.45	-0.64	0.47	0.08	-0.92	-1.11
$SOCl_2$	5.61	3.90	3.53	4.95	3.31	2.96	1.69	0.35	0.88	0.57	1.12	-0.22	0.31
SOF_2	7.32	6.22	5.93	6.41	5.37	5.09	4.34	3.62	3.44	0.95	3.39	2.67	2.49
SO_2	5.44	4.60	4.32	4.69	3.91	3.65	3.14	2.68	2.52	0.77	2.37	1.91	1.75
SO_2ClF	9.08	7.74	7.46	7.85	6.57	6.29	5.31	4.40	4.57	1.34	3.97	3.06	3.23
SO_2Cl_2	8.44	6.86	6.56	7.29	5.78	5.48	4.28	3.10	3.59	1.09	3.19	2.01	2.50
SO_2F_2	9.94	8.88	8.61	8.61	7.59	7.33	6.60	5.97	5.78	1.35	5.25	4.62	4.43
SF_5Cl	11.75	10.04	9.74	10.39	8.76	8.46	7.14	5.86	6.01	1.44	5.70	4.42	4.57
SPF_3	2.05	0.23	-0.18	2.18	0.45	0.05	-1.28	-2.43	-2.60	-0.10	-1.18	-2.33	-2.50
$SPCl_3$	-1.41	-3.11	-3.51	-1.13	-2.76	-3.15	-4.39	-5.52	-5.05	-0.10	-4.29	-5.42	-4.95
$(CH_3O)_3PO$	4.84	3.31	2.96	4.02	2.57	2.24	1.13	-0.12	-0.23	0.76	0.37	-0.88	-0.99
$(CH_3O)_3PS$	-1.59	-3.35	-3.79	-1.33	-3.01	-3.44	-4.70	-5.77	-5.89	-0.14	-4.56	-5.63	-5.75
SF_6	12.55	11.05	10.76	11.10	9.66	9.37	8.25	7.21	7.00	1.68	6.57	5.53	5.32
CF_3SSCF_3	4.41	2.49	2.39	4.31	2.46	2.33	0.62	-0.93	-1.11	0.01	0.61	-0.94	-1.12
CH_3SSCH_3	-0.09	-1.51	-1.48	-0.11	-1.47	-1.47	-2.84	-3.96	-4.11	-0.06	-2.78	-3.90	-4.05
$SP(CH_3O)_2Cl$	-1.45	-3.21	-3.65	-1.19	-2.87	-3.30	-4.56	-5.65	-5.57	0.05	-4.61	-5.70	-5.62
$(CH_3O)_2SO_2$	7.43	5.95	5.64	6.16	4.74	4.44	3.35	2.29	2.11	1.23	2.12	1.06	0.88
SF_4	9.14	7.76	7.44	8.12	6.81	6.50	5.52	4.55	4.34	1.17	4.35	3.38	3.17

(a) The shifts obtained for the non-P containing compounds may be different from those given in Table 4.22 since a different k and t (Table 4.19) was obtained.

TABLE 4.24 Correlation obtained from least-squares fit on calculated versus experimental shifts (EWMO calculation)

	Original Parametrisation			New P Parametrisation		
	slope	intcpt	corr coeff	slope	intcpt	corr coeff
Phosphorus Series						
1s (GPM)	0.9649	0.7501	0.9617	0.9626	1.0972	0.9490
1s (RPM)	0.9802	-0.4154	0.9682	0.9800	-0.2174	0.9658
1s (TPM)	0.9819	-0.5537	0.9672	0.9812	-0.4222	0.9647
2p (GPM)	0.9739	0.8077	0.9554	0.9711	1.1559	0.9394
2p (RPM)	0.9941	-0.3188	0.9646	0.9936	-0.1229	0.9614
2p (TPM)	0.9964	-0.4580	0.9638	0.9958	-0.3267	0.9605
KL_2L_3 (GPM)	0.7970	1.1197	0.8878			
KL_2L_3 (RPM)	0.8247[a]	0.0164[a]	0.9051[a]			
KL_2L_3 (TPM)	0.8230	-0.1739	0.8897			
Sulphur Series						
1s (GPM)	0.9949	1.2105	0.9816	0.9956	1.1071	0.9833
1s (RPM)	0.9951	-0.2113	0.9873	0.9939	-0.2563	0.9880
1s (TPM)	0.9929	-0.5034	0.9852	0.9912	-0.5276	0.9861
2p (GPM)	0.9983	1.1953	0.9774	0.9999	1.1210	0.9795
2p (RPM)	0.9995	-0.1653	0.9854	0.9989	-0.1853	0.9865
2p (TPM)	0.9976	-0.4525	0.9835	0.9965	-0.4529	0.9848
KL_2L_3 (GPM)	0.9461	0.7002	0.9703	0.9440	0.7274	0.9714
KL_2L_3 (RPM)	0.9655	-0.2844	0.9788	0.9629	-0.2390	0.9803
KL_2L_3 (TPM)	0.9583	-0.3061	0.9776	0.9559	-0.2537	0.9788

(a) $P(C_2H_5)_3$ not included in fit, note KL_2L_3(GPM): slope = 0.7559
intcpt = 1.1210
corr coeff = 0.8609

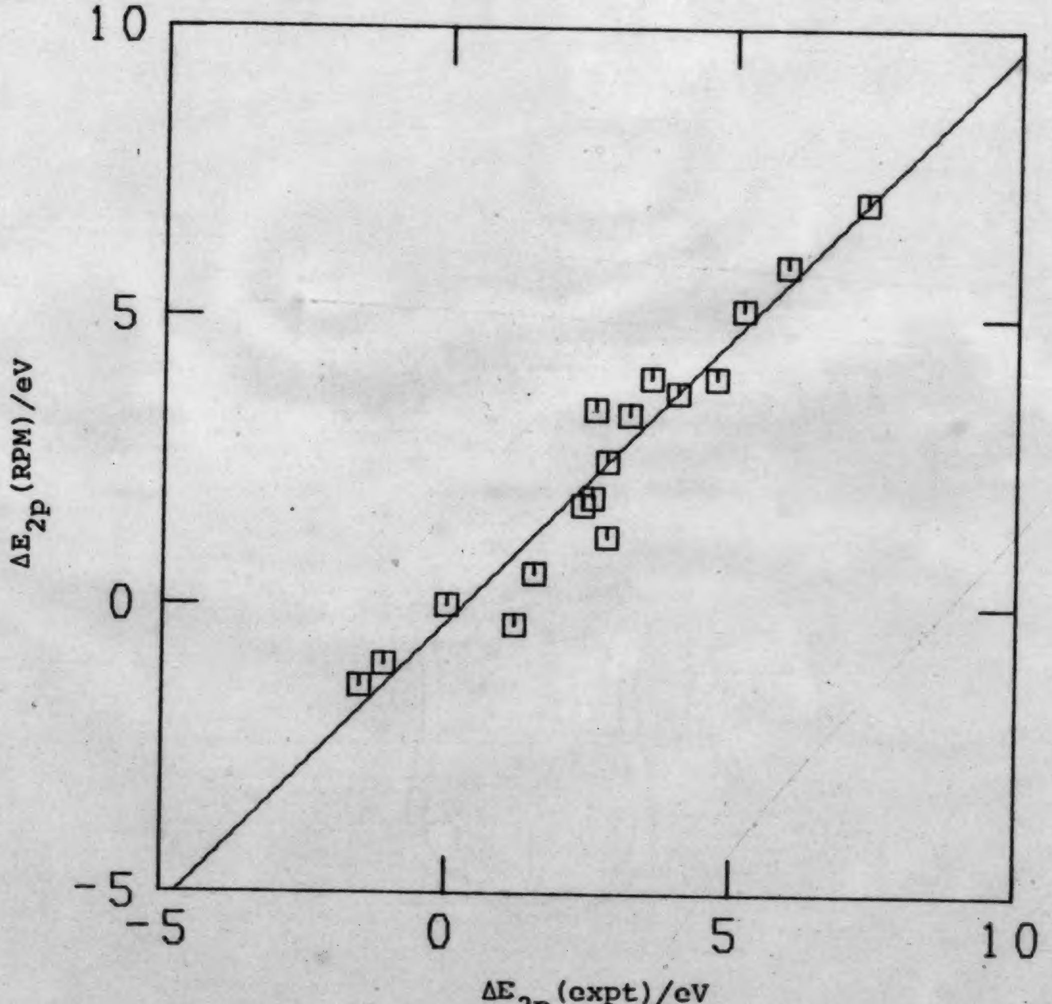

Figure 4.23 Correlation of calculated versus experimental P2p binding energy shifts. Calculated shifts are obtained from the atom charge model using EWMO RPM charges and potentials.

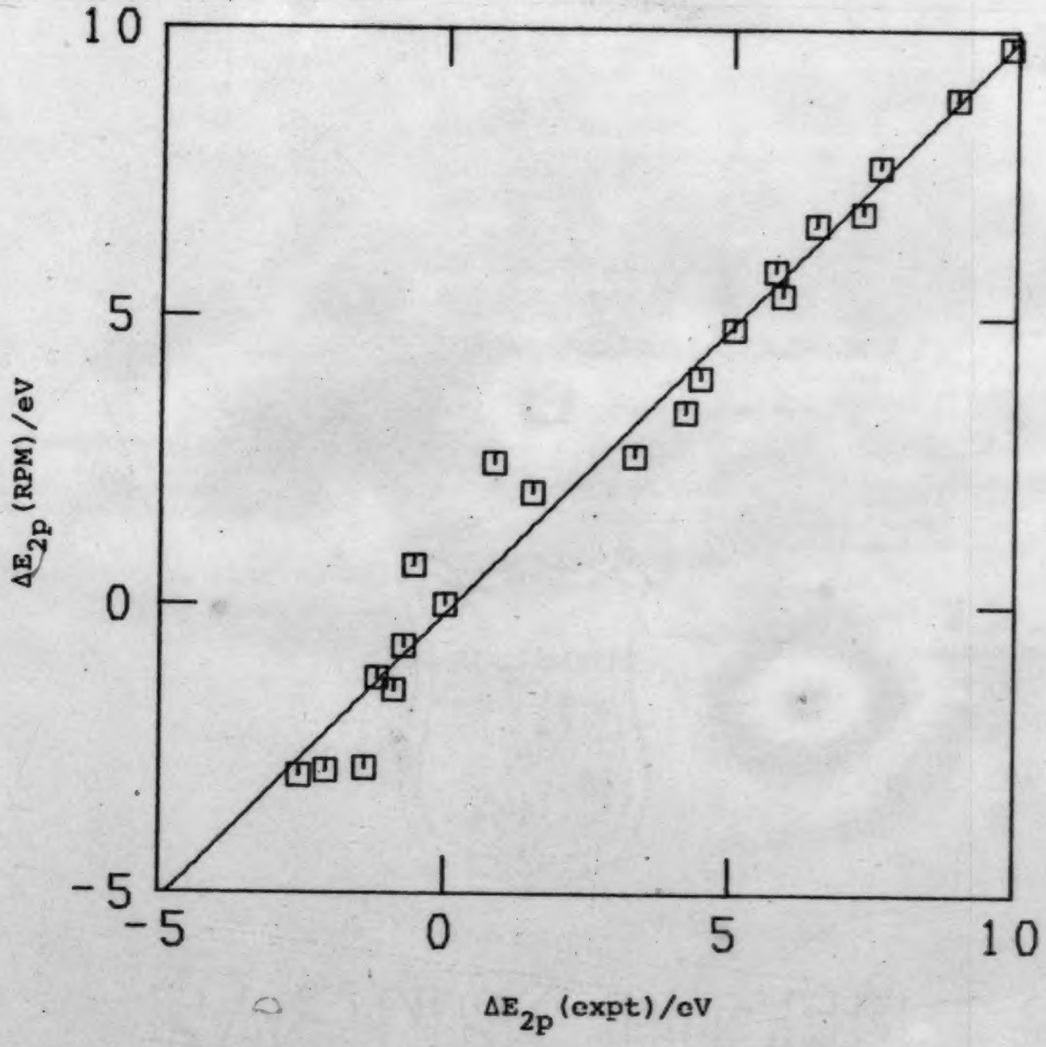

Figure 4.24 Correlation of calculated versus experimental S2p binding energy shifts. Calculated shifts are obtained from the atom charge model using EWMO RPM charges and potentials.

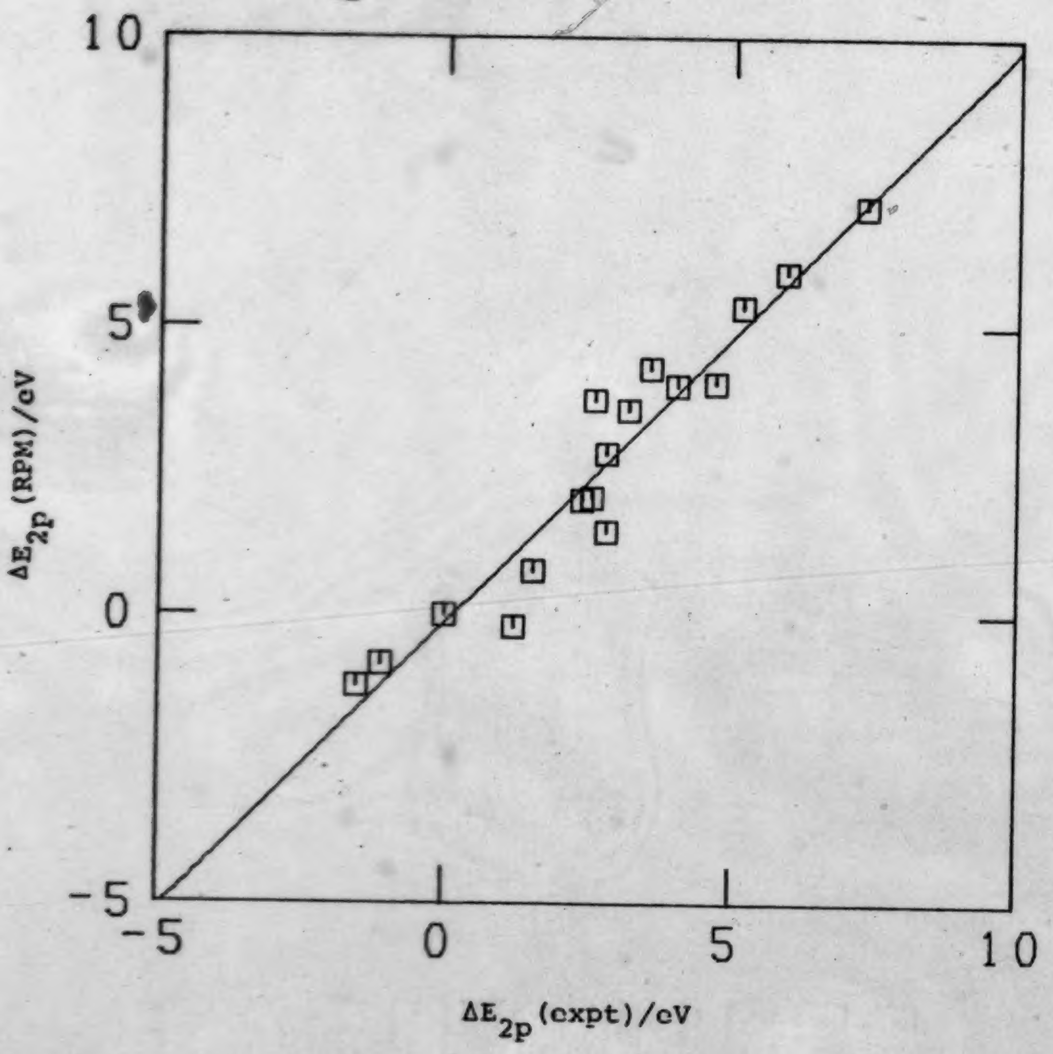

Figure 4.25 Correlation of calculated versus experimental P2p binding energy shifts. Calculated shifts are obtained from the atom charge model using EWMO (new P parameterisation) RPM charges and potentials.

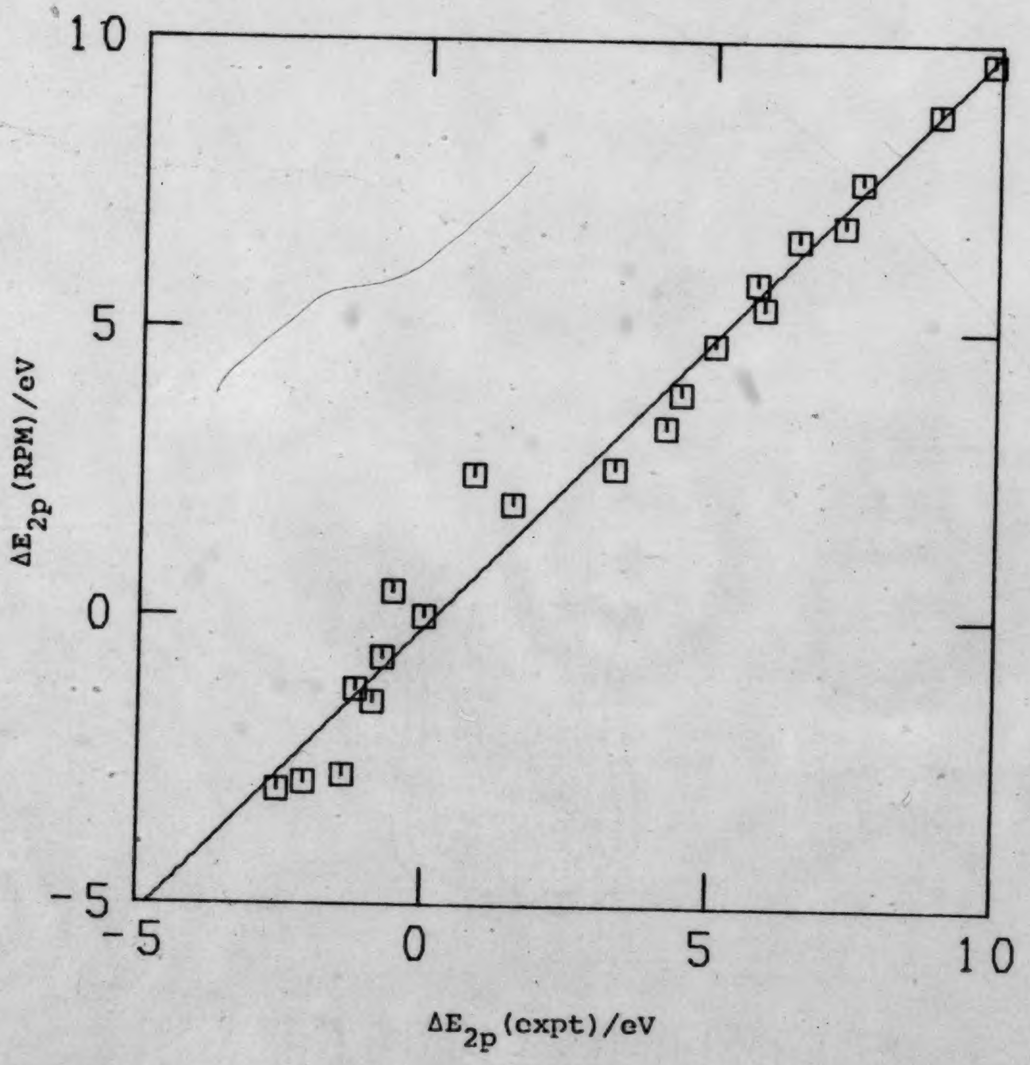

Figure 4.26 Correlation of calculated versus experimental S2p binding energy shifts. Calculated shifts are obtained from the atom charge model using EWMO (new P parameterisation) RPM charges and potentials.

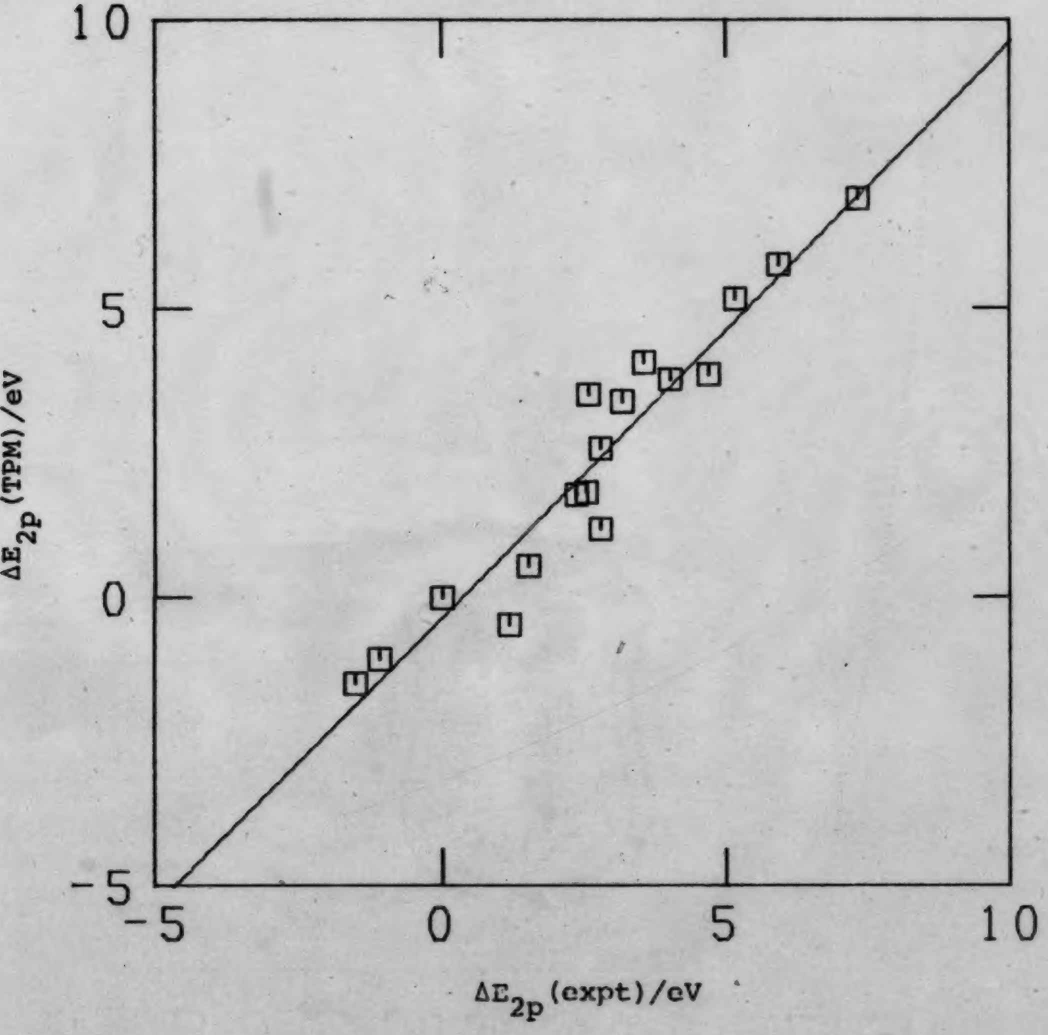

Figure 4.27 Correlation of calculated versus experimental P2p binding energy shifts. Calculated shifts are obtained from the atom charge model using EWMO (new P parameterisation) TPM charges and potentials.

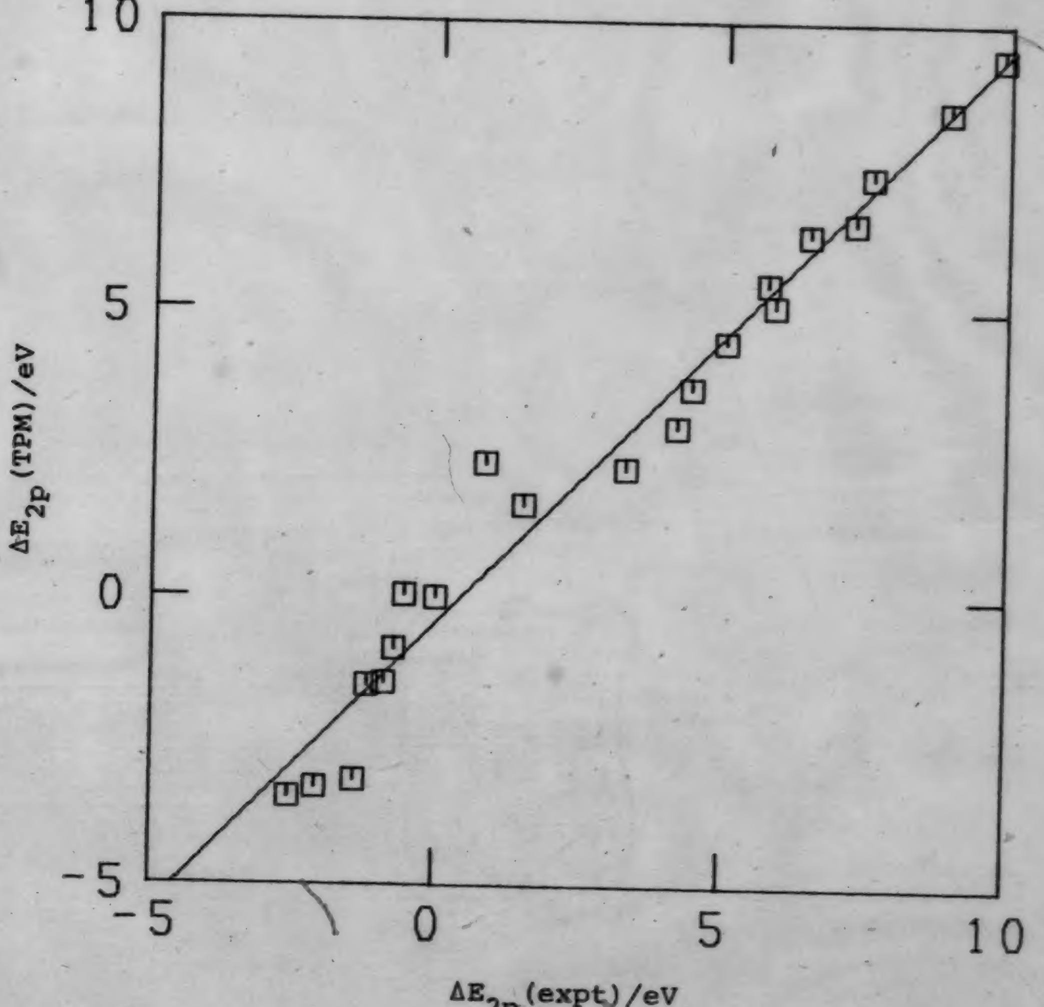

Figure 4.28 Correlation of calculated versus experimental S2p binding energy shifts. Calculated shifts are obtained from the atom charge model using EWMO (new P parameterisation) TPM charges and potentials.

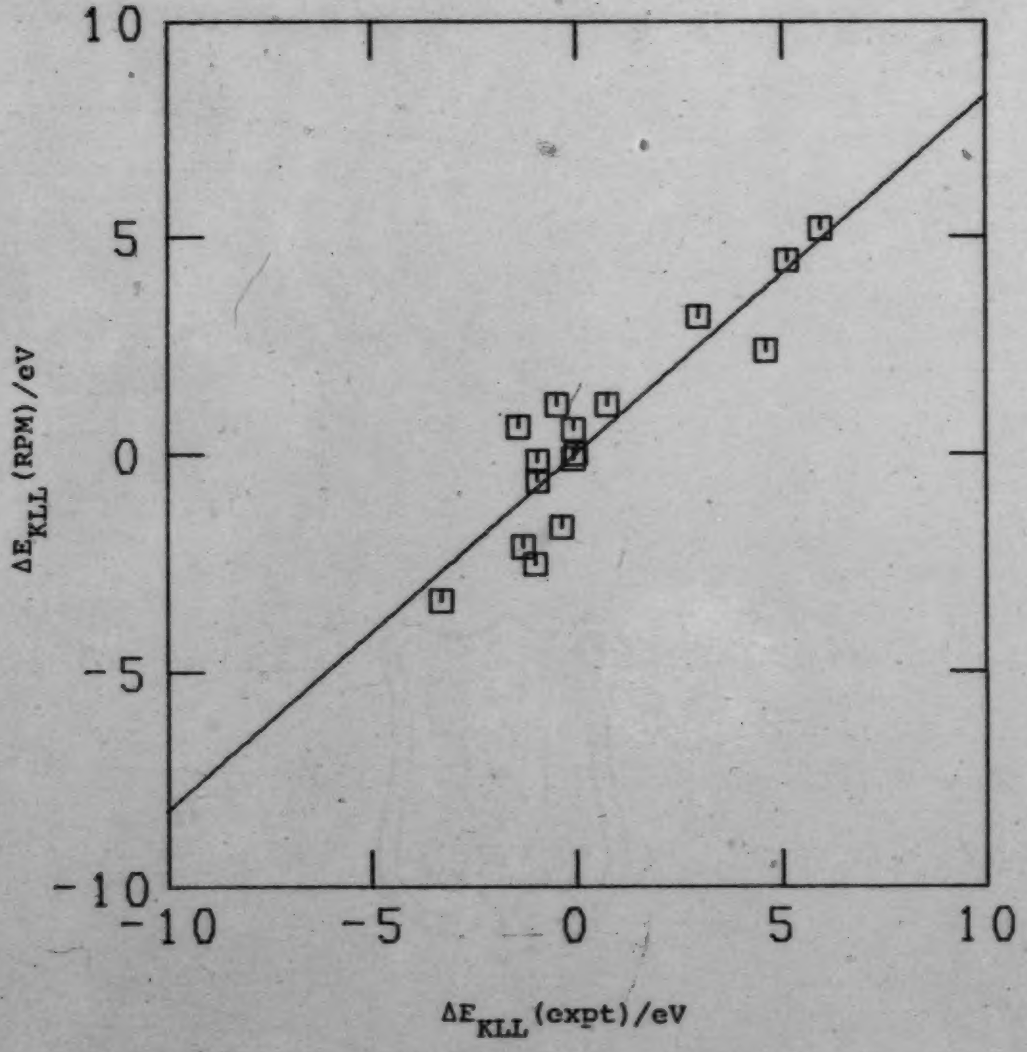

Figure 4.29 Correlation of calculated versus experimental P KL_2L_3 Auger energy shifts. Calculated shifts are obtained from the atom charge model using EWMO RPM charges and potentials.

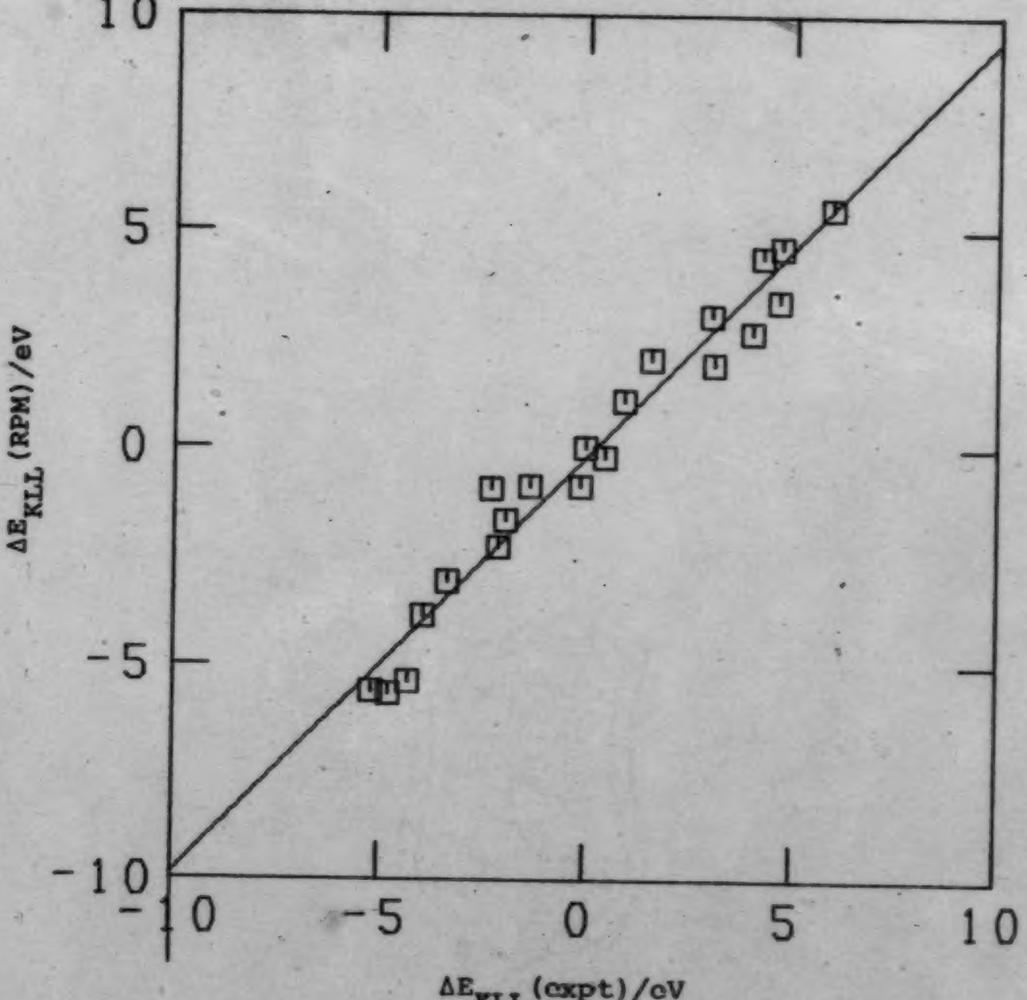

Figure 4.30 Correlation of calculated versus experimental S KL_2L_3 Auger energy shifts. Calculated shifts are obtained from the atom charge model using EWMO (new P parameterisation) RPM charges and potentials.

shifts for both the RPM and TPM approaches are equally good. The TPM approach gives a slightly lower value for k. Since the TPM approach was not used with the CNDO/2 formalisation we cannot compare the advantages of the TPM and thus we shall only consider the RPM approach. However, it seems that the TPM approach gives as reasonable an estimate of chemical shifts at this level of approximation as does the RPM approach and does so with one calculation rather than two.

The EWMO (Hückel) calculations, for the sulphur series, gave as good a correlation of experimental versus calculated shifts at all levels as the CNDO/2 calculations, however the value for k obtained on the RPM fit on the $2p^*$ data was virtually the same as that for the 2p data. In the phosphorus series the correlations derived from the EWMO (Hückel) calculations were considerably worse than those derived from the CNDO/2 calculations. While the experimental versus calculated shift correlations for the 1s and 2p electrons were reasonable, the correlation of the Auger data was poor. The model, utilising EWMO (Hückel) charges and potentials, exhibits deficiencies when dealing with the loss of the second electron and the concomitant electron reorganisation. This is demonstrated by the significantly lower correlation coefficient obtained on the fit of equation 4.2 for the $P2p^*$ shift. The poor fit here will result in a lack of correlation between the experimental and calculated shifts. Figure 4.31 shows the correlation of ($\Delta E - V$) with q for the $P2p^*$ shifts using the RPM charges and potentials appropriate to the ion. It is clear why a poor correlation was obtained. The EWMO (Hückel) calculation results for phosphorus compounds with a lone pair on the central atom are different from those without a lone pair. This difference is also illustrated by a similar plot for the $S2p^*$ shifts (Figure 4.32). The molecules can be grouped according to the number of lone pairs on the central atom. The "pivoting" is not as dramatic in the sulphur case as with the phosphorus series and hence a fit over all the groups gives a reasonable correlation, however, the pivoting results in an unreasonable value for k. Similar differences in the correlation of ($\Delta E - V$) against q are observed for the P1s shifts using the RPM charges and potentials appropriate to the molecule (Figure 4.33). The differences are not as pronounced as those associated with the $P2p^*$ shifts, and as in the sulphur case, results in a reasonable fit. Correlation of ($\Delta E - V$) with q for the $P2p^*$ shifts, using RPM charges and potentials appropriate to the ion from the CNDO/2 calculation (Figure 4.34) shows a consistent trend regardless of coordination.

Table 4.25 summarises the k and ℓ values obtained with

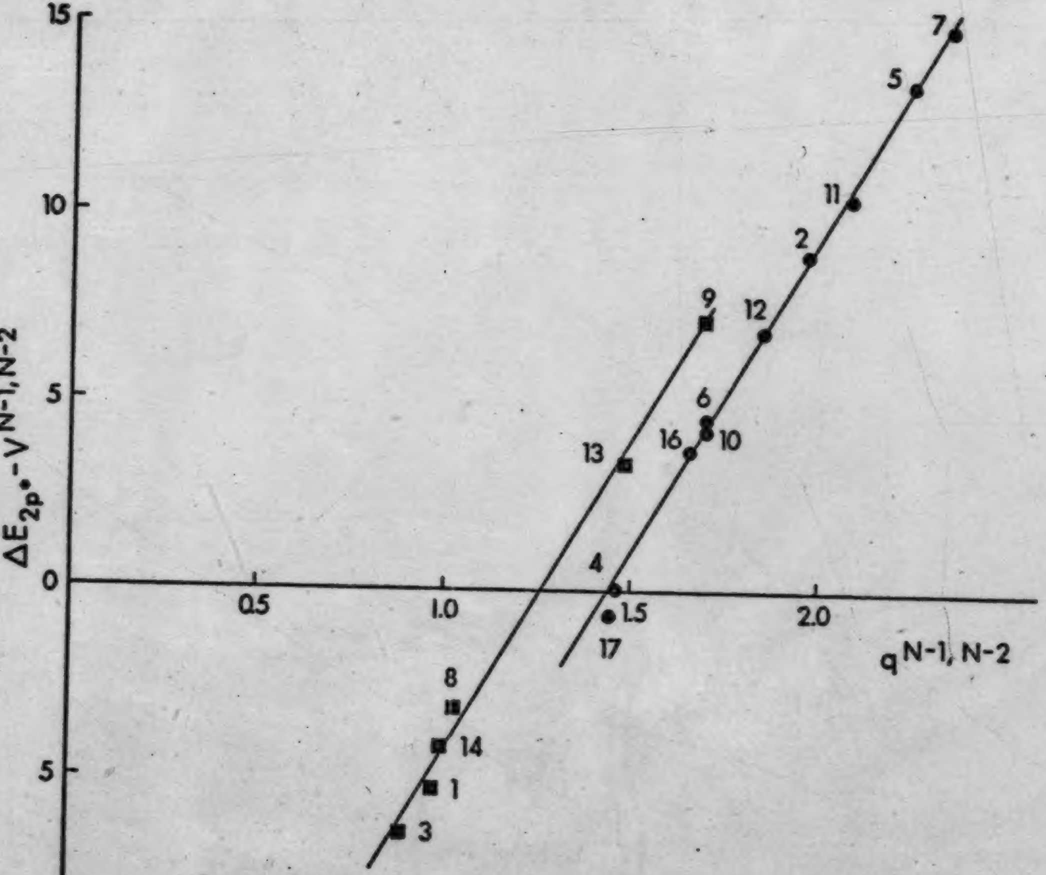

Figure 4.31 Correlation of $(\Delta E_{2p*}-V)$ with $(kq+\ell)$ using EWMO (new P parameterisation) RPM charges and potentials appropriate to the ion state - phosphorus series. Compound numbers are presented in Table 4.1. The compounds are grouped according to those with one lone pair (■) and no lone pairs (●) on the phosphorus atom.

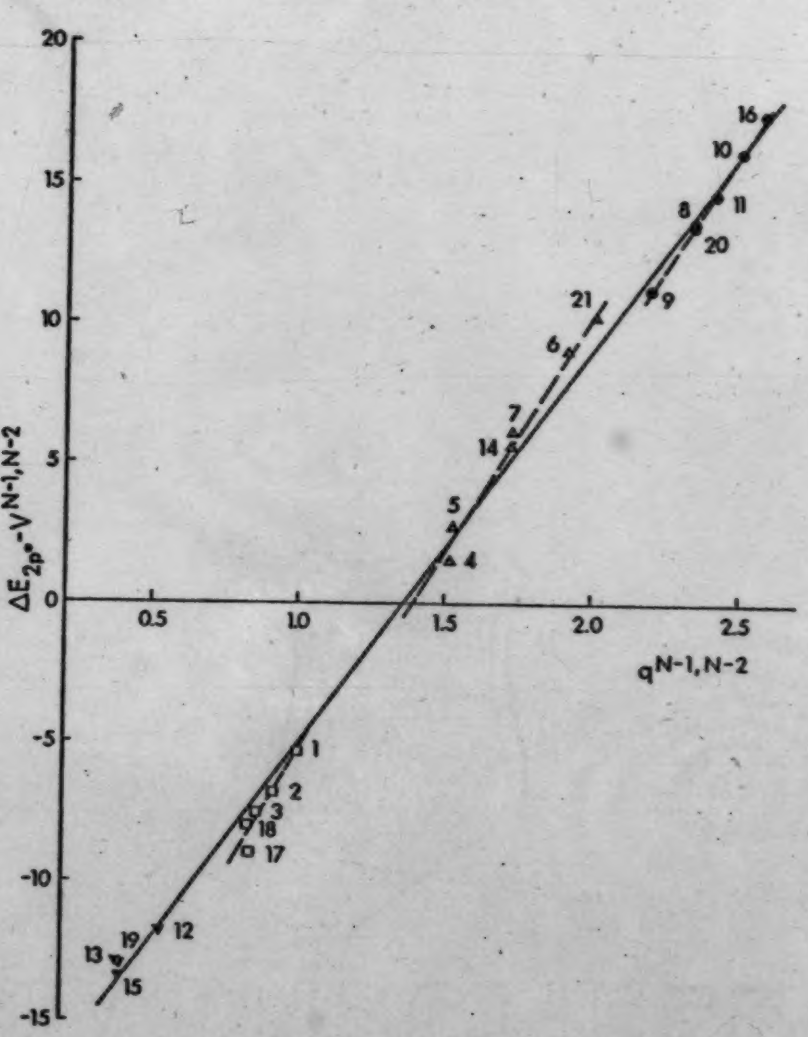

Figure 4.32 Correlation of (ΔE_{2p*}-V) with (kq+ℓ) using EWMO (new P parameterisation) RPM charges and potentials appropriate to the ion state – sulphur series. Compound numbers are presented in Table 4.2. The compounds are grouped according to those with three lone pairs (▼), two lone pairs (□), one lone pair (Δ) and no lone pairs (●) on the sulphur atom.

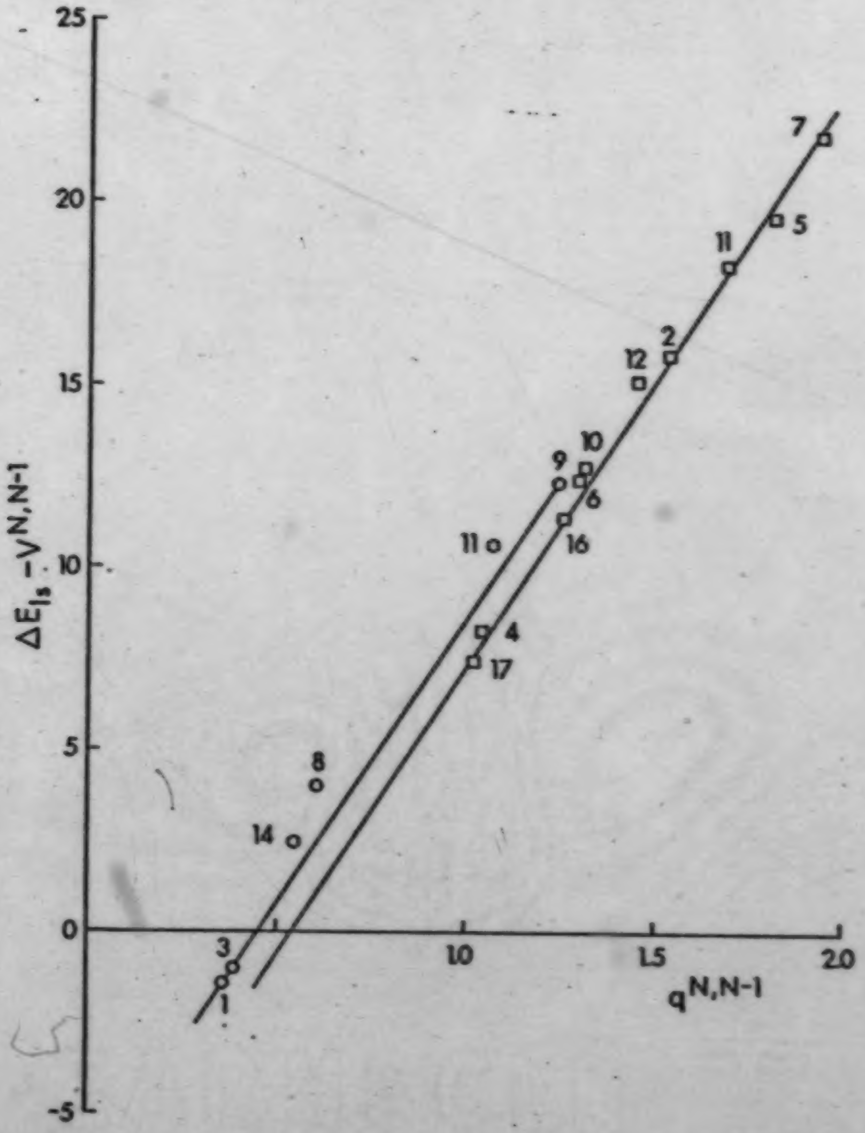

Figure 4.33 Correlation of (ΔE_{1s}-V) with (kq+ℓ) using EWMO (new P parameterisation) RPM charges and potentials appropriate to the molecule - phosphorus series. Compound numbers are presented in Table 4.1. The compounds are grouped according to those with one lone pair (○) and no lone pairs (□) on the phosphorus atom.

Table 4.25. Fits on limited P and S series where there are no lone pairs on the central atom (EWMO calculation).

	fit on $(\Delta E-V) = kq + \ell$			fit on calc vs. expt shift[a]		
	k	ℓ	corr. coeff.	slope	incpt	corr. coeff.
Phosphorus Series						
Original Parameterisation						
1s (GPM)	16.0267	-11.0956	0.9982	1.0313	-0.0513	0.9887
1s (RPM)	15.2881	-16.1683	0.9975	1.0615	0.1006	0.9874
2p (GPM)	15.4128	- 9.9893	0.9982	1.0683	-0.0212	0.9893
2p (RPM)	14.6762	-14.9038	0.9971	1.1000	0.1276	0.9862
2p* (GPM)	17.8170	-27.8660	0.9990	0.9874	-0.3405	0.9956
2p* (RPM)	17.0380	-31.9707	0.9987	0.9976	-0.1715	0.9948
Phosphorus Series						
New Parameterisation						
1s (GPM)	15.7799	-12.9462	0.9989	1.0267	-0.1017	0.9912
1s (RPM)	15.2060	-17.0363	0.9981	1.0594	0.0736	0.9892
2p (GPM)	15.2380	-11.7655	0.9989	1.0628	-0.0758	0.9919
2p (RPM)	14.6321	-15.7423	0.9977	1.0975	0.0985	0.9881
Sulphur Series						
1s (GPM)	15.8067	-.416023	0.9985	1.0240	0.0497	0.9979
1s (RPM)	15.8042	-19.9900	0.9986	1.0037	0.0736	0.9979
2p (GPM)	14.6863	-12.0797	0.9976	1.0396	0.0284	0.9968
2p (RPM)	14.6091	-17.1685	0.9983	1.0169	0.0491	0.9975

(Cont'd.)

Table 4.25. (Cont'd.)

2p* (GPM)	16.3446	-26.5354	0.9920	0.9916	-0.0322	0.9874
2p* (RPM)	16.2270	-32.0450	0.9988	0.9996	0.1086	0.9983

(a) Fit on KL_2L_3 not 2p*.

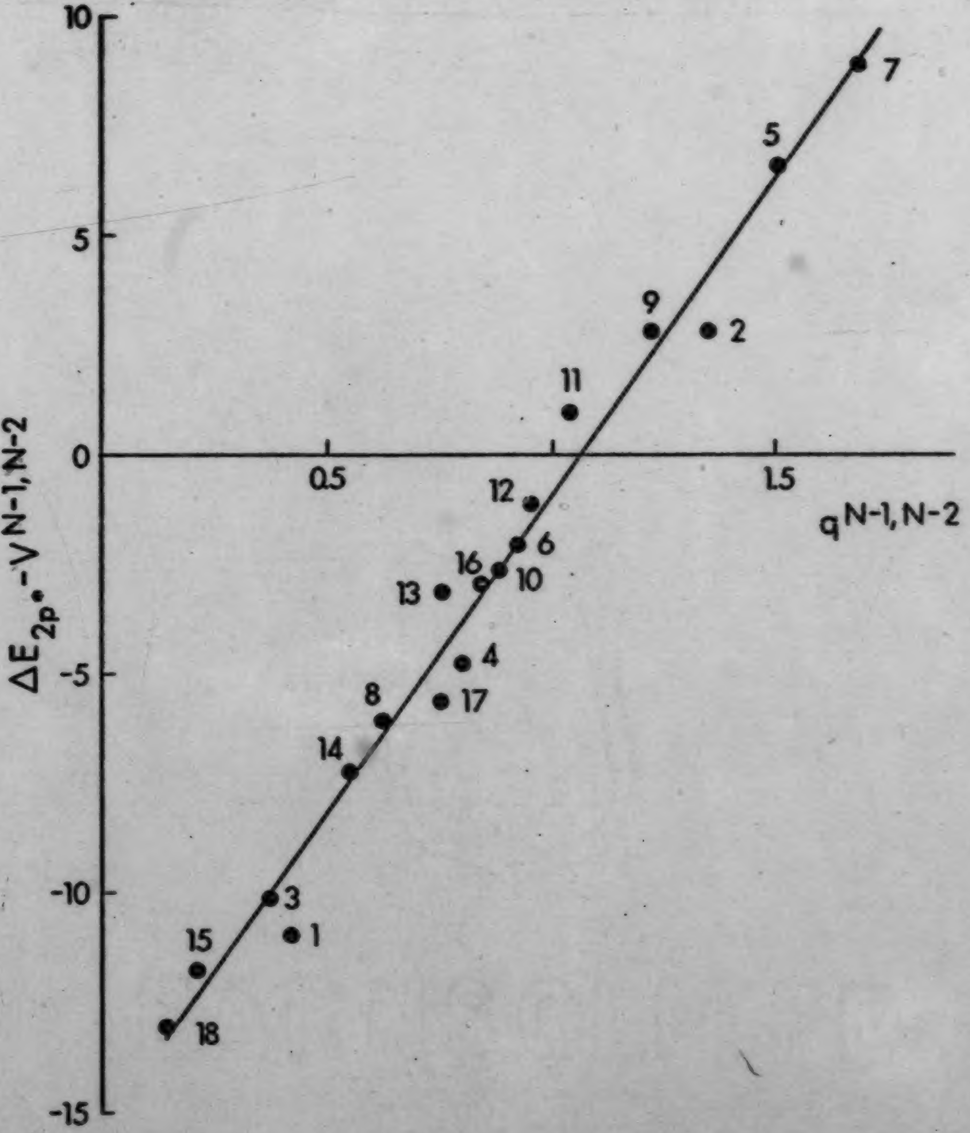

Figure 4.34 Correlation of (ΔE_{2p^*}-V) with (kq+ℓ) using CNDO/2 RPM charges and potentials appropriate to the ion state - phosphorus series. Compound numbers are presented in Table 4.1.

EWMO (Hückel) charges and potentials, as well as the correlation between the experimental and calculated shifts, for the phosphorus (original and new parameterisation) and sulphur series in which only molecules without lone pairs on the central atom have been considered. The correlation obtained is a clear improvement over that when all the molecules are considered. The k values obtained for the RPM approach now reflect the theoretical trend. The new parameterisation gives lower values for k but again the differences are too small to permit definite conclusions.

The EWMO (Hückel) calculation seems to partition charge differently when lone pairs are involved on the atom and as a result series of molecules related by equal numbers of lone pairs are established. It must be concluded that the general applicability of the EWMO (Hückel) calculation to estimate shifts is limited except in the case of a carefully selected series of compounds.

E. Relationship of the Auger Electron Shift to the Core Electron Binding Energy Shift

The Auger parameter[34] was originally defined as

$$\Delta\alpha = (\Delta E_{AUG} + \Delta E_{BE}) = 2\Delta R_{EA} \qquad (4.4)$$

The sum of the Auger chemical shift and the binding energy shift of a specified core electron equals twice the extra atomic relaxation energy associated with the photoelectron. It was shown in the introduction that a more accurate expression can be obtained. For the KLL Auger shifts the Auger parameter becomes

$$(\Delta E_{KLL} + \Delta E_{L}) = \Delta R_{L} + \Delta R_{L^*} + \Delta E^{L\rightarrow K}_{X\text{-}ray} \qquad (4.5)$$

with the specified core electron coming from the L-shell. The Auger parameter depends not only on the relaxation energy associated with the loss of the initial photoelectron but also with that of the second electron which is leaving a singly-charged ion. The X-ray term corrects for the difference in the chemical shift associated with the K-shell and that associated with the L-shell, this must be considered since the K-shell is refilled by an L-electron in the Auger process. If the specified electron is from the K shell, the Auger parameter becomes

$$(\Delta E_{KLL} + \Delta E_{K}) = \Delta R_{L} + \Delta R_{L^*} + 2\Delta E^{L\rightarrow K}_{X\text{-}ray} \qquad (4.6)$$

The relaxation terms are still associated with the L shell, the shell which provides the Auger electron which we observe.

The values for ΔR in the above equations express changes in total relaxation energies. If the atomic contribution is considered to be constant for the whole series then the values for ΔR are shifts in extra atomic relaxation.

Rearrangement of equation (4.5) gives

$$\Delta E_{KLL} = (\Delta R_L + \Delta R_{L^*}) - (\Delta E_L - \Delta E^{L\to K}_{X\text{-ray}}) \tag{4.7}$$

The Auger chemical shift depends on a reference level $(\Delta E_L - \Delta E^{L\to K}_{X\text{-ray}})$ which is modified by the relaxation contributions arising from the removal of both the initial and secondary electrons. This expression provides a convenient way of relating the Auger shift to the binding-energy shift. This is shown diagramatically in Figure 4.35 for the phosphorus series and Figure 4.36 for the sulphur series. Only experimental values have been used and hence the relaxation contribution shown is the sum of ΔR_L and ΔR_{L^*} contributions. The diagram clearly indicates where and why reversals occur between the Auger and photoelectron chemical shifts. The relaxation contribution can greatly alter the shifts--adding as much as 3.5 eV in some cases relative to the reference.

The results from the calculations have also been applied to equation 4.5. In view of the discussion in the previous section only the results from the CNDO/2 calculations will be considered for the complete series of molecules. The Auger parameter, experimental relaxation energy shifts, as well as the calculated relaxation energy shifts for both electrons obtained from the atom charge and potential models are shown in Table 4.26 for the phosphorus series

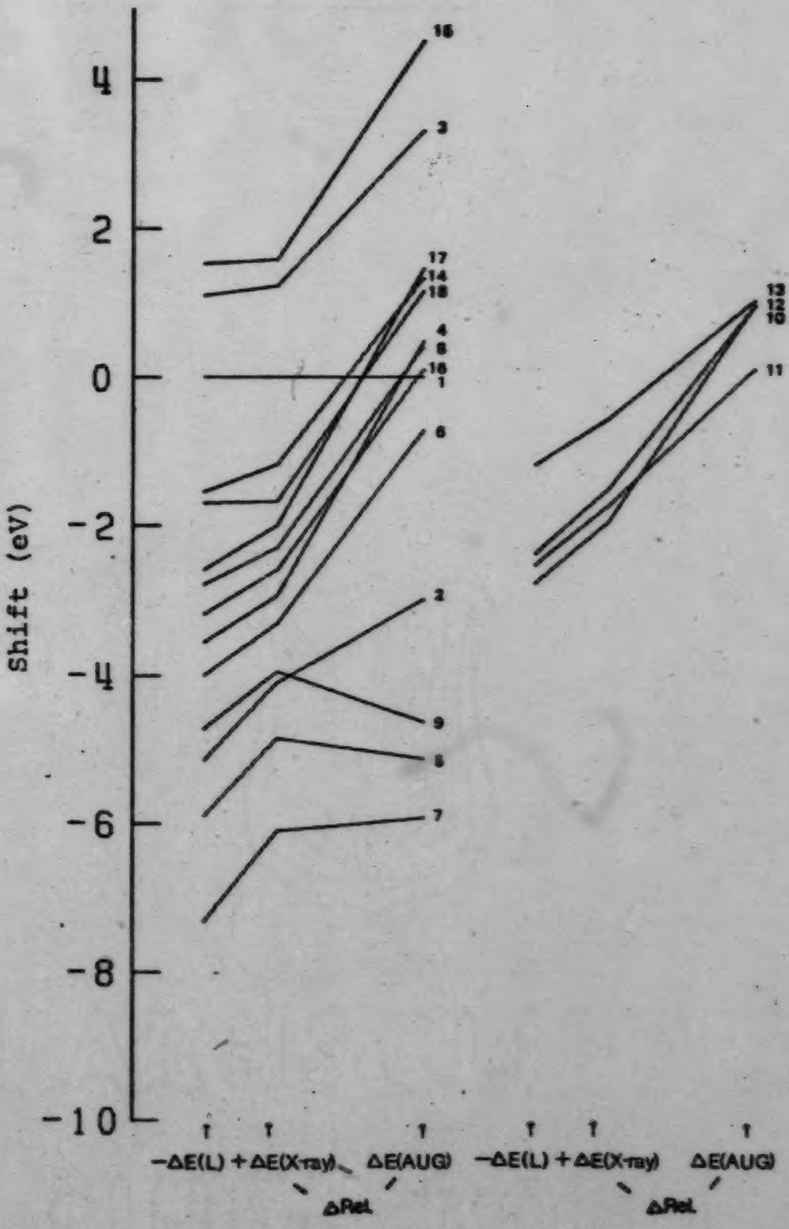

Figure 4.35 Relationship of the Auger energy shift to the photoelectron binding energy shift for the phosphorus series. Compound numbers are presented in Table 4.1.

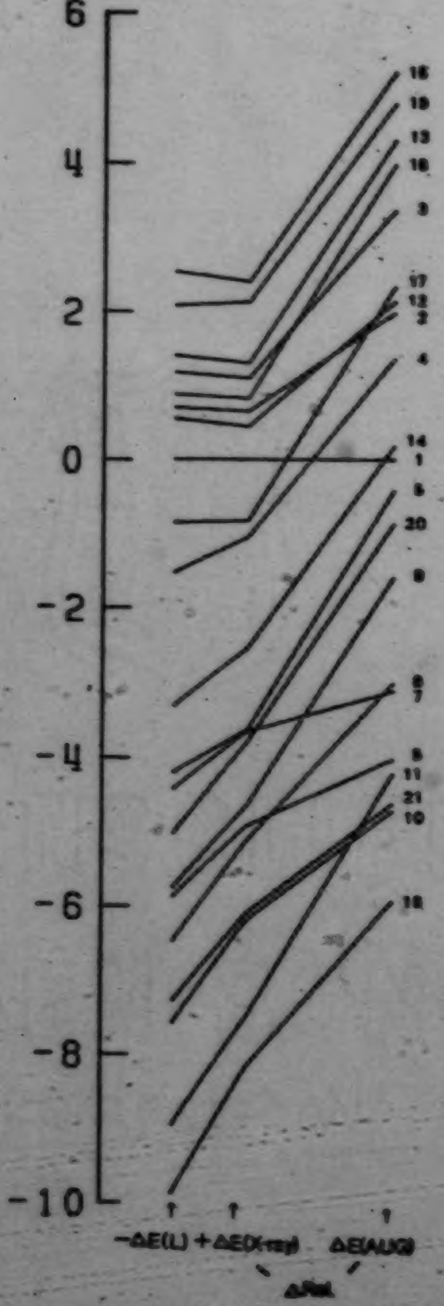

Figure 4.36 Relationship of the Auger energy shift to the photoelectron binding energy shift for the sulphur series. Compound numbers are presented in Table 4.2.

TABLE 4.26 Relaxation - experimental and from CNDO/2 calculation and the Auger parameter - P series (all shifts in eV)

Molecule	Experimental			Atom Charge Model[c]			Potential Model		
	Total Relax[a]	ΔE_{XRAY}	$\Delta\alpha$[b]	ΔR_L	$\Delta R_L'$	$\Delta R_L+\Delta R_L'$ $+\Delta E_{XRAY}$	ΔR_L	$\Delta R_L'$	$\Delta R_L+\Delta R_L'$ $+\Delta E_{XRAY}$[e]
PH_3	0.00	0	0	0	0	0	0	0	0
SPF_3	1.12	1.05	2.17	0.67	0.86	2.58	0.33	0.76	2.14
$P(CH_3)_3$	2.08	0.12	2.20	1.68	1.61	3.41	1.77	1.56	3.45
$SPCl_3$	3.40	0.64	4.04	1.95	1.99	4.58	1.99	2.16	4.79
OPF_3	-0.28	1.05	0.77	0.15	0.34	1.54	-0.33	0.10	0.82
$OPCl_3$	2.60	0.69	3.29	1.73	1.95	4.37	1.68	2.10	4.47
PF_5	0.18	1.22	1.40	0.52	0.78	2.52	0.07	0.72	2.01
PCl_3	2.69	0.49	3.18	1.68	1.98	4.15	1.70	2.17	4.36
PF_3	-0.66	0.76	0.10	0.12	0.39	1.27	-0.34	0.11	0.53
$SP(CH_3O)_2Cl$	2.91	0.82	3.73	2.10	2.09	5.01	2.13	2.26	5.21
$(CH_3O)_3PO$	1.85	0.80	2.65	1.89	1.97	4.66	1.82	2.09	4.71
$(CH_3O)_3PS$	2.47	0.87	3.34	2.11	2.04	5.02	2.11	2.18	5.16
$(CH_3O)_3P$	1.59	0.63	2.22	1.78	1.89	4.30	1.75	2.00	4.38
$P(CH_3)Cl_2$	2.50	0.36	2.86	1.65	1.84	3.85	1.67	1.94	3.97
$P(C_2H_5)_3$	2.90	0.05	2.95	2.29	2.19	4.53	2.53	2.32	4.90
$OP(CH_2Cl)Cl_2$	2.68	0.59	3.28	1.93	1.97	4.49	1.92	2.06	4.57
$SP(CH_3)Cl_2$	3.43	0.60	4.03	1.96	1.91	4.47	2.01	2.03	4.64
$P(CF_3)_3$	2.82	0.04	2.86	2.19	2.06	4.29	2.48	2.21	4.73

(a) $(\Delta R_L + \Delta R_{L'}) = \Delta\alpha - \Delta E_{XRAY}$

(b) $\Delta\alpha = \Delta E_{KLL} + \Delta E_L$

(c) k's used GPM(2p) = 13.1646 RPM(2p) = 13.5715
GPM(2p*) = 13.9785 RPM(2P*) = 14.3854

(d) Correlation with Δα (see Fig. 4.37)
slope = 1.0499 incpt = 0.8845 corr coeff = 0.9281

(e) Correlation with Δα (see Fig. 4.37)
slope = 1.2969 incpt = 0.3549 corr coeff = 0.9323

and in Table 4.27 for the sulphur series.

The ground potential values for k used in the atom-charge model were obtained from a linear extrapolation based upon the relaxation potential values for k. Figures 4.37 and 4.38 show the correlation of $(\Delta E_{KLL} + \Delta E_L)$ with $(\Delta R_L + \Delta R_{L^*} + \Delta E^{L\rightarrow K}_{X\text{-ray}})$ for the phosphorus and sulphur series respectively. The correlation is satisfactory with the sulphur series having less scatter than the phosphorus series. In both cases the potential model (utilising theoretical k's) gives the better correlation. Unit slopes are not obtained, which is not surprising in view of the correlations obtained between the experimental and calculated shifts presented previously. With the exception of the molecules containing the $(-OCH_3)$ ligand, the calculated values follow the same general trends as experiment though they are somewhat larger.

The CNDO/2 calculation used here fails with $(-OCH_3)$. Lee et al.[54] have calculated the "electron flow" (relaxation) during core-ionisation for a series of tervalent phosphorus compounds using a CNDO/2 program which was modified by Sherwood.[55] They found that upon core ionisation, the $P(OCH_3)_3$ molecule exhibited substantially less relaxation than PCl_3 and $P(CH_3)_3$.

The results from the EHMO (Hückel) calculations have been applied to select series of compounds. Each series contains molecules with the same number of lone pairs on the

Table 4.27. Relaxation (experimental and from CNDO/2 calculations) and the Auger parameter - S series (all shifts in eV).

	Experimental			Atom charge model[c]			Potential charge model		
Molecule	Total[a] Relax	$\Delta E_{X\text{-ray}}$	$\Delta\alpha$[b]	ΔR_L	ΔR_{L*}	$\Delta R_L+\Delta R_{L*}+\Delta E_{X\text{-ray}}$[d]	ΔR_L	ΔR_{L*}	$\Delta R_L+\Delta R_{L*}+\Delta E_{X\text{-ray}}$[e]
H_2S	0.00	0.00	0.00	0.00	0.00	0.00	0.00	0.00	0.00
$(CH_3)SH$	1.31	-0.04	1.27	0.96	0.75	1.69	1.05	0.74	1.75
$(CH_3)_2S$	2.26	-0.08	2.18	1.68	1.51	3.11	1.81	1.50	3.23
$(CH_3)_2SO$	2.39	0.47	2.86	1.87	1.72	4.06	2.12	1.87	4.46
$SOCl_2$	3.21	0.57	3.78	2.19	2.51	5.37	2.57	3.02	6.16
SOF_2	0.90	0.95	1.85	0.57	1.19	2.71	0.60	1.56	3.11
SO_2	0.56	0.77	1.33	-0.04	0.50	1.23	-0.21	0.67	1.23
SO_2ClF	2.13	1.34	3.47	1.39	1.76	4.49	1.66	2.26	5.26
SO_2Cl_2	3.07	1.09	4.16	2.03	2.50	5.62	2.42	3.10	6.61
SO_2F_2	1.48	1.35	2.83	0.54	1.14	3.03	0.67	1.60	3.62
SF_5Cl	3.28	1.44	4.72	1.79	2.46	5.69	2.20	3.26	6.90
SPF_3	1.67	-0.10	1.57	1.41	1.52	2.83	1.39	1.62	2.91
$SPCl_3$	2.99	-0.10	2.89	2.08	2.10	4.08	2.16	2.07	4.13

(Cont'd.)

$(CH_3O)_2SO$	2.72	0.76	3.48	2.22	2.32	5.30	2.62	2.75	6.13
$(CH_3O)_3PS$	2.81	-0.14	2.67	2.19	2.07	4.12	2.28	1.97	4.11
SF_6	2.24	1.68	3.92	1.29	2.01	4.98	1.65	2.82	6.15
CF_3SSCF_3	3.15	0.01	3.16	2.41	2.00	4.42	2.75	2.10	4.86
CH_3SSCH_3	3.15	-0.06	3.09	2.16	1.77	3.87	2.43	1.81	4.18
$SP(CH_3O)_2Cl$	2.12	0.05	2.17	2.18	2.07	4.30	2.28	1.99	4.32
$(CH_3O)_2SO_2$	2.92	1.23	4.15	2.34	2.41	5.98	2.84	2.98	7.05
SF_4	1.46	1.17	2.63	1.11	1.90	4.18	1.36	2.58	5.11

(a) $(\Delta R_L + \Delta R_{L^*}) = \Delta\alpha - \Delta E_{X\text{-ray}}$

(b) $\Delta\alpha = \Delta E_{KLL} + \Delta E_L$

(c) k's used GPM (2p) = 14.4036 RPM (2p) = 14.9901

GPM (2p*) = 15.5767 RPM (2p*) = 16.1632

(d) Correlation with $\Delta\alpha$ (see Fig. 4.38)

slope = 1.2775 incpt = 0.3207 corr coeff = 0.9465

(e) Correlation with $\Delta\alpha$ (see Fig. 4.38)

slope = 1.5843 incpt = 0.0426 corr coeff = 0.9624

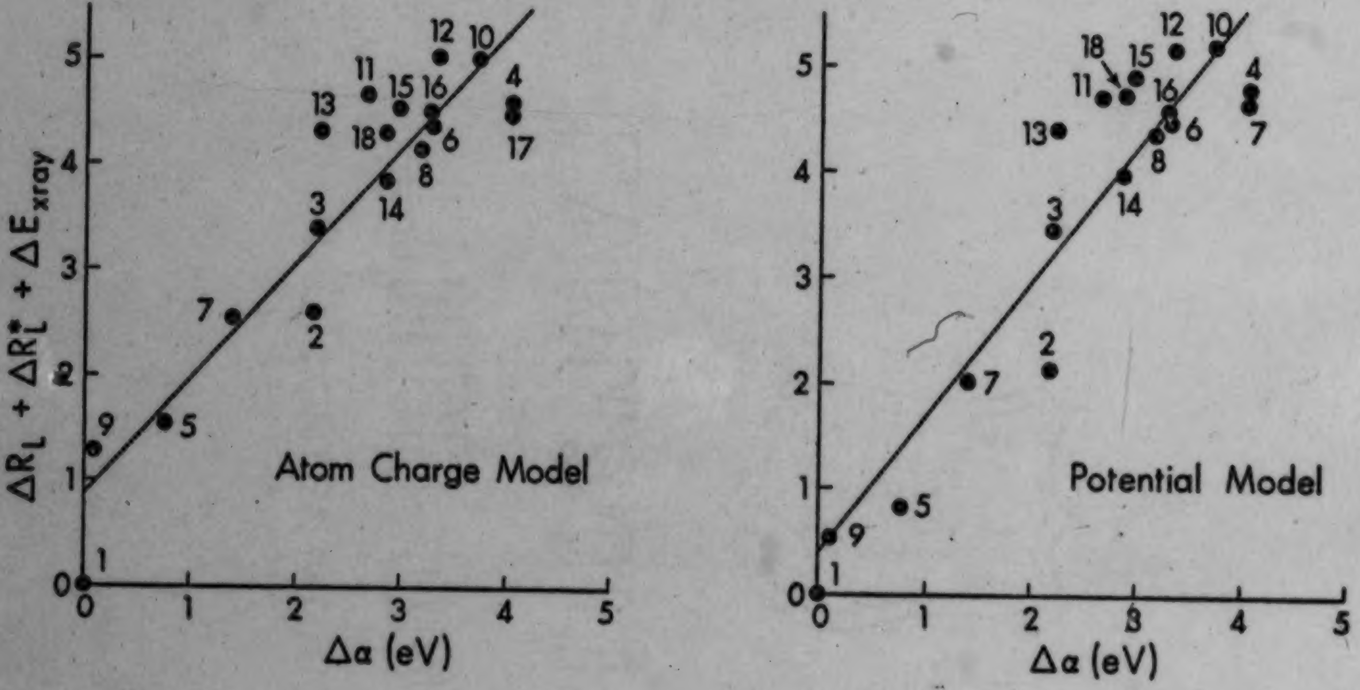

Figure 4.37 Correlation of the Auger parameter ($\Delta\alpha = \Delta E_{KLL} + \Delta E_{2p}$) and the sum of the calculated relaxation energy shifts and the K_α X-ray shift ($\Delta R_L + \Delta R_{L^*} + \Delta E_{X\text{-}ray}$) for the atom charge and potential models - phosphorus series. Compound numbers are presented in Table 4.1.

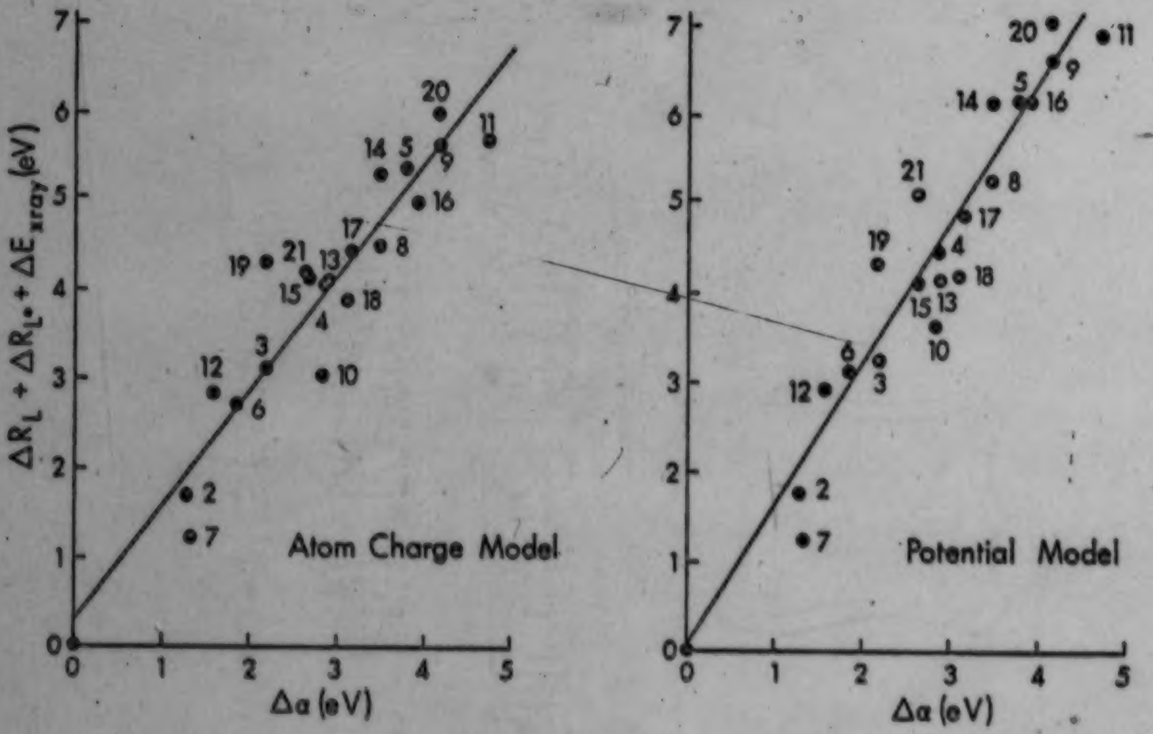

Figure 4.38 Correlation of the Auger parameter ($\Delta\alpha = \Delta E_{KLL} + \Delta E_{2p}$) and the sum of the calculated relaxation energy shifts and the K_α X-ray shift ($\Delta R_L + \Delta R_{L^*} + \Delta E_{X\text{-}ray}$) for the atom charge and potential models - sulphur series. Compound numbers are presented in Table 4.2.

central atom. The theoretical k's (Table 4.10) were used in conjunction with the atom-charge model. The results, along with the CNDO/2 relaxation energy shifts based upon the same reference values, are shown in Table 4.28 for phosphorus and Table 4.29 for sulphur. The trends in the total relaxation obtained from the EWMO (Hückel) calculations follow the experimental trends in all cases (except PF_3 compared to PH_3). The values obtained are smaller than those obtained by the CNDO/2 method and the total relaxation energy shifts are in closer agreement with experiment. In some cases the relative relaxation contributions of the first and second ionisation steps to the total relaxation have been reversed over those predicted by the CNDO/2 calculations.

In view of the difficulties and contradictions arising from the semi-empirical calculations used here, it is difficult to draw any definite conclusions about the significance of changes in relaxation energies which are associated with the first ionisation step compared to those associated with the second. However, certain observations can be made based upon the "experimental" values for total relaxation. The relaxation depends on the ability of a group to release electrons. This may be due to its electronegativity, polarisability or both. With all things being equal the more electronegative a substituent the less relaxation will occur. This is amply illustrated by the

Table 4.28. Experimental and calculated (atom charge model)[a] relaxation energy shifts (eV) - P series[b].

	Exptl.	CNDO/2		EWMO	
Molecule	$\Delta R_L+\Delta R_{L*}$	ΔR_L	ΔR_{L*}	ΔR_L	ΔR_{L*}
PH_3	0	0	0	0	0
PF_3	-0.66	-0.34	0.11	0.14	0.35
PCl_3	2.69	1.70	2.17	1.33	1.65
$P(CH_3)_3$	2.08	1.77	1.56	1.35	1.36
$P(OCH_3)_3$	1.59	1.75	2.00	0.75	0.81
$P(CH_3)Cl_2$	2.50	1.67	1.94	1.32	1.56
$P(C_2H_5)_3$	2.90	2.53	2.32	1.92	-
$P(CF_3)_3$	2.82	2.48	2.21	-	-
PF_5	0	0	0	0	0
SPF_3	0.94	0.26	0.04	0.42	0.43
$SPCl_3$	3.22	1.96	1.44	1.33	1.39
$SP(OCH_3)_3$	2.29	2.04	1.46	0.83	0.77
$SP(OCH_3)_2Cl$	2.73	2.06	1.54	1.05	1.07
$SP(CH_3)Cl_2$	3.45	1.94	1.31	1.34	1.25
OPF_3	-0.46	-0.40	-0.62	-0.08	-0.15
$OPCl_3$	2.42	1.61	1.38	1.06	1.10
$OP(CH_3O)_3$	1.67	1.75	1.37	0.53	0.44
$OP(CH_2Cl)Cl_2$	2.50	1.85	1.34	1.22	1.26

(a) Theoretical values for k used (Table 4.10).

(b) The molecules have been grouped according to the number of lone pairs on the central atom.

Table 4.29. Experimental and calculated (atom charge model)[a] relaxation energy shifts (eV) - S series[b].

Molecule	Exptl.	CNDO/2		EWMO	
	$\Delta R_L+\Delta R_{L*}$	ΔR_L	ΔR_{L*}	ΔR_L	ΔR_{L*}
H_2S	0	0	0	0	0
$(CH_3)SH$	1.31	1.05	0.74	0.69	0.63
$(CH_3)_2S$	2.26	1.81	1.50	1.28	1.17
CH_3SSCH_3	3.15	2.43	1.81	1.68	1.64
CF_3SSCF_3	3.15	2.75	2.10	2.15	2.14
SF_4	0	0	0	0	0
SOF_2	-0.56	-0.76	-1.02	-0.20	-0.33
$(CH_3)_2SO$	0.93	0.76	-0.71	0.52	0.13
$SOCl_2$	1.75	1.21	0.44	0.78	0.65
SO_2	-0.90	-1.57	-1.91	-0.27	-0.58
$(CH_3O)_2SO$	1.26	1.26	0.17	0.41	0.48
SF_6	0	0	0	0	0
SO_2ClF	-0.11	0.01	-0.56	0.05	-0.12
SO_2Cl_2	0.83	0.77	0.28	0.45	0.28
SO_2F_2	-0.76	-0.98	-1.22	-0.38	-0.58
SF_5Cl	1.04	0.55	0.44	0.36	0.40
$(CH_3O)_2SO_2$	0.71	1.19	0.16	0.21	0.13

(a) Theoretical values for k used (Table 4.10).

(b) The molecules have been grouped according to the number of lone pairs on the central atom.

comparison of similar molecules containing F and Cl substituents, or comparison of molecules with a terminal sulphur with those containing the more electronegative terminal O in the phosphorus series or comparison of the $-PF_3$ ligand with the $-PCl_3$ in the sulphur series.

Other factors, however, appear to be equally important. Based upon the simple electronegativity arguments it might be expected that $-C_2H_5$ and $-CH_3$ would behave similarly and that PF_3 would have substantially less relaxation than PH_3, as would molecules with a $-CF_3$ group when compared to similar molecules containing a $-CH_3$ group This is not the case, the $-C_2H_5$ group exhibits more relaxation than the $-CH_3$ group, and in the latter two examples the reverse is observed. These can be attributed to an increase in the polarisability of the group due to the presence of a larger number of electrons thereby contributing a larger total "electron flow".

Replacement of a lone pair by two F groups (e.g. comparing, respectively, PF_3 SF_4, SO_2 with PF_5, SF_6, SO_2F_2) increases the number of electrons able to "flow" onto the ionised centre and hence increases the relaxation in spite of the high electronegativity of the F groups. This is also the case when replacing the lone pair with a terminal S group, however, substitution of a terminal O group for the lone pair produces little net effect; presumably the electronegativity of O cancels out the increase in relaxation due to the presence of more electrons.

Obviously relaxation is the sum of many complex contributions. The above examples have been discussed in terms of "number of electrons" and electronegativity. Such factors as "single" and "double" bonds allowing more or less electron flow could also contribute to the total amount of relaxation.

One final interesting point to note is the reversal of relaxation effects between $-OCH_3$ and $-CH_3$ in the comparison of the phosphorus and sulphur series of compounds. The EWMO (Hückel) calculation correctly predicts this. The calculation shows that in $P(OCH_3)_3$ and $P(CH_3)_3$ the difference in relaxation between them is approximately the same for both ionisation steps whereas in $(CH_3O)_2SO$ there is an increase in the relaxation for the second ionisation compared to that for $(CH_3)_2SO$.

Chapter 5. Summary and Conclusions

The KL_2L_3 Auger line, 1s and 2p core electron lines were collected in a series of phosphorus and sulphur compounds and their chemical shifts were compared. The potential model was used to attempt to explain the shifts.

The correlation between the 1s photoelectron shift and the 2p photoelectron shift was very good. The 1s photoelectron shift was larger. There was no such correlation when comparing the Auger electron shift to the core electron shifts. The Auger parameter,[34] when defined properly, related the Auger electron shift to the core electron shift in a convenient way and the variations in shift could be rationalised by consideration of the shifts in relaxation due to the loss of two electrons. It was found that the relaxation depends upon the ability of a group attached to the central atom to release electrons. Many factors can contribute to this and it is necessary to keep all of them in mind. For instance, the results showed that an increase in the polarisability of a group due to the presence of a large number of electrons can reverse the expected relaxation trends based solely upon electronegativity.

The lack of success of the group shift concept when related to a large series of molecules indicated that the groups are affected by the other substituents on the central atom and that they cannot be ignored.

The models were tested with the aid of two types of semi-empirical methods. The CNDO/2 calculation gave reasonable correlation when using fitted parameters though the values obtained for k (the coulombic repulsion integral) did not match the expected theoretical trends too well. It was thus difficult to relate the relaxation associated with the loss of the second electron to that associated with the initial photoionisation. The EWMO (Huckel) calculation was found to partion charge differently depending upon the number of lone pairs present on the ionised atom and thus the general applicability of this method is limited.

It is apparent that more work is required in formulating semi-empirical approaches to give "correct" charge distributions, especially if one wants to relate the relaxation processes involved with the ions of the Auger electron to the relaxation processes involved with the loss of initial core electron.

REFERENCES

1. S.B.M. Hagstrom, C. Nordling and K. Siegbahn, Z. Physik, 178, 433 (1964); ibid p. 439.
2. See for example:
   T.A. Carlson, "Photoelectron and Auger Spectroscopy". Plenum Press, New York (1975).
3. P. Auger, J. Phys. Radium, 6, 205 (1925).
4. J. Wayne Rabalais, "Principles of Ultraviolet Spectroscopy", p. 50, Wiley-Interscience, New York (1977)
5. For a brief description of UPS, the reader is referred to Chapter 1 of reference 4.
6. M.O. Krause, J. Phys. Chem. Ref. Data, 8, 307 (1979).
7. D.A. Shirley in "Advances in Chemical Physics", (eds. I. Prigogine and S.A. Rice), Vol. 23, pp 85-159, Wiley-Interscience, New York (1973).
8. R.G. Cavell and R. Sodhi, J. Electron. Spectrosc. Relat. Phen., 15, 145 (1979).
9. D.A. Shirley, Phys. Rev. A, 7, 1520 (1973).
10. Kenneth D. Sevier, "Low Energy Electron Spectroscopy", Wiley-Interscience, New York (1972).
11. W.E. Moddeman, Doctoral Thesis, Oak Ridge Nat. Lab., ORNL-TM-3012 (1970).
12. K. Faegri, Jr. and O. Keski-Rahkonen, J. Electron Spectrosc. Relat. Phenom., 11, 275 (1977).

13. L. Asplund, P. Kelfve, B. Blomster, H. Siegbahn and K. Siegbahn, Phys. Scripta, 16, 268 (1977).

14. L. Asplund, P. Kelfve, B. Blomster, H. Siegbahn, K. Siegbahn, R.L. Lozes and U.I. Wahlgren, Phys. Scripta, 16, 273 (1977).

15. A.C. Hurley, "Introduction to the Electron Theory of Small Molecules", Chap. 7, Academic Press, London (1976).

16. M.E. Schwartz in "Modern Theoretical Chem. 4", Chap. 9 (ed. H.F. Schaeffer), Plenum Press, New York (1977).

17. T. Koopman, Physica, 1, 104 (1934).

18. L. Hedin and A. Johannson, J. Phys. B (Ser. 2), 2, 1336 (1969).

19. Harold Basch, Chem. Phys. Lett., 5, 337 (1970).

20. Maurice E. Schwartz, Chem. Phys. Lett., 6, 631 (1970).

21. John A. Pople and David L. Beveridge, "Introduction to Approximate Molecular Orbital Theory", McGraw Hill, New York (1970).

22. U. Gelius, Physica Scripta, 9, 133 (1974).

23. (a) D.W. Davis and D.A. Shirley, J. Electron Spectrosc. Relat. Phenom., 3, 137 (1974).
    (b) D.W. Davis, M.S. Banna and D.A. Shirley, J. Chem. Phys., 60, 237 (1974).
    (c) D.W. Davis and D.A. Shirley, Chem. Phys. Lett., 15, 325 (1972).

24. P. Kelfve, B. Blomster, H. Siegbahn, K. Siegbahn, E. Sanhueza and O. Goscinski, Physica Scripta, 21, 75 (1980).

25. D. Liberman, Bull. Am. Phys. Soc., 9, 731 (1964).

26. W.L. Jolly and D.N. Hendrickson, J. Am. Chem. Soc., 92, 1863 (1970).

27. A.H. Compton and S.K. Allison, "X-rays in Theory and Experiment", Van Nostrand, Princeton, N.J. (1935).
see also
W.L. Jolly in "Electron Spectroscopy: Theory, Techniques and Applications", (eds. C.R. Brundle and A.D. Baker), Vol. 1, pp 119-149, Academic Press, London (1977).

28. G. Howat and O. Goscinski, Chem. Phys. Lett., 50, 87 (1975).

29. O. Goscinski, B.T. Pickup and G. Purvis, Chem. Phys. Lett., 22, 167 (1973).

30. O. Goscinski, M. Hehenberger, B. Roos and P. Siegbahn, Chem. Phys. Lett., 33, 427 (1975).

31. D.B. Adams, J. Electron Spectrosc. Relat. Phenom., 10, 247 (1977).

32. J.B. Mann, Atomic Structure Calculations, LA-3690, Los Alamos (1968).

33. H. Siegbahn and O. Goscinski, Physica Scripta, 13, 225 (1976).

34. C.D. Wagner, Faraday Disc. Chem. Soc., 60, 291 (1975).

35. O. Keski-Rahkonen and M.O. Krause, J. Electron Spectrosc. Relat. Phenom., 9, 391 (1976).

36. L.A. Asplund, P. Kelfve, H. Siegbahn, O. Goscinski, H. Fellner-Feldegg, K. Hamrin, B. Blomster and K. Siegbahn, Chem. Phys. Lett., 40, 353 (1976).

37. D.B. Adams, J. Chem. Soc. Far. Trans. 2, 73, 991 (1977).

38. CNDO/2 QCPE prog. 141; D.P. Santry and C.A. Segal, J. Chem. Phys., 47, 158 (1967). This program has been modified for use on potential calculations pertinant to ESCA.

39. EWMO - Energy Weighted Maximum Overlap. This is a modified version of the iterative extended Hückel method. The program used in QCPE 246 modified to include transition calculations.

40. G. Johansson, J. Hedman, A. Berndtsson, M. Klasson and R. Nilsson, J. Electron Spectrosc. Relat. Phenom. 2, 295 (1973).

41. T.D. Thomas and R.W. Shaw, Jr., J. Electron Spectrosc. Relat. Phenom., 5, 108 (1974).

42. The program is based upon SUNDER by C.S. Fadley and C. Lederer, Lawrence Berkeley Laboratory and is described in C.S. Fadley, Thesis (Univ. Calif., 1970), UCRL 19535.

43. R.G. Cavell, Spectrochimica Acta, 23A, 249 (1967).

44. F.W. Bennett,H.J. Emeleus and R.N. Haszeldine, J. Chem. Soc., 1565 (1953).

45. N. Bartlett and P.L. Robinson, J. Chem. Soc., 3417 (1961).

46. H. Siegbahn, R. Medeiros and O. Goscinski, J. Electron Spectrosc. Relat. Phenom., 8, 149 (1976).

47. A. Støgård and R. Manne, Chem. Phys., 8, 348 (1975).

48. Jens Spanget-Larsen, J. Electron Spectrosc. Relat. Phenom., 2, 33 (1973).

49. J.M. Sichel and M.A. Whitehead, Theor. Chim. Acta (Berl.), 7, 32 (1967).

50. A.J. Ashe, III, M.K. Bahl, K.D. Bomben, W.-T Chan, J.K. Gimzewski, P.G. Sitton and T.D. Thomas, J. Am. Chem. Soc., 101, 1764 (1979).

51. B.E. Mills, R.L. Martin and D.A. Shirley, J. Am. Chem. Soc., 98, 2380 (1976).

52. W.L. Jolly and W.B. Perry, Inorg. Chem., 13, 2686 (1974).

53. E. Clementi and D.L. Raimondi, J. Chem. Phys., 38, 2864 (1963).

54. T.H. Lee, W.L. Jolly, A.A. Bakke, R. Weiss and J.G. Verkade, J. Am. Chem. Soc., 102, 2631 (1980).

55. P.M.A. Sherwood, J. Chem. Soc. Far. Trans. 2, 72, 1791 (1976).

56. J. Hinze and H.H. Jaffé, J. Am. Chem. Soc., 84, 540 (1962); J. Phys. Chem., 67, 1501 (1963).

57. L. Oleari, L. Di Sipio and G. De Michelis, Mol. Phys., 10, 97 (1966).

APPENDIX 1

Molecular Geometries Used in the Calculations

Where experimental geometries were available only the reference is given. These are presented in Table A1.1. Where the bond lengths and angles had to be estimated, the assumptions made are also presented (Table A1.2).

Table A1.1. References from which experimental geometries were obtained.

Reference[a]	Compound
A1.1	PH_3, PF_3, PF_5, OPF_3, $OPCl_3$, $SPCl_3$, $(CH_3O)_3PO$, SCl_2, SF_4, $SiCl_4$
A1.2	SF_6, SF_5Cl, $SOCl_2$, SO_2Cl_2
A1.3	H_2S, $(CH_3)SH$, $(CH_3)_2S$, $(CH_3)_2SO$, $(CH_3)SS(CH_3)$ SOF_2, SO_2F_2, SO_2ClF
A1.4	$P(CH_3)_3$
A1.5	$P(CF_3)_3$
A1.6	SPF_3, PCl_3, $(CF_3)SS(CF_3)$
A1.7	SO_2

[a] References are:

A1.1 Landolt-Bornstein (New Series) Group II, Vol. 7, Springer-Verlag, Berlin (1976).

A1.2 P.H. Laur in "Sulphur in Organic and Inorganic Chemistry", (ed. A. Senning), Vol. 3, Chap. 24, Marcel Dekker, New York (1972).

A1.3 M.D. Harmony, V.W. Laurie, R.L. Kuczkowski, R.H. Schwendeman, D.A. Ramsay, F.J. Lovas, W.J. Lafferty and A.G. Maki, J. Phys. Chem. Ref. Data, 8, 619 (1979).

Cont'd.

Table Al.1. Cont'd.

Al.4 I.M. Hillier and V.R. Saunders, Trans. Far. Soc., 66, 2401 (1970).

Al.5 C.J. Marsden and L.S. Bartlett, Inorg. Chem., 15, 2713 (1976).

Al.6 "Tables of Interatomic Distances and Configuration in Molecules and Ions", (ed. L.E. Sutton), Chem. Soc. Spec. Publ. #11 (1958).

Al.7 L. Asplund, P. Kelfve, B. Blomster, H. Siegbahn, K. Siegbahn, R.L. Lozes and U.I. Wahlgren, Physica Spectra, 16, 273 (1977).

Table A1.2. Basis for assumed geometries of compounds.

Compound	Model Compound geometry based upon	Assumed bond lengths (Å) and angles	Source of assumptions
$P(OCH_3)$	$OP(OCH_3)_3$		
$SP(OCH_3)_3$	$OP(OCH_3)_3$	P=S = 1.90	$SP(OCH_3)_3$[a] (crystallographic data)
$SP(OCH_3)_2Cl$	$OP(OCH_3)_3$	P=S = 1.885	$\overline{S(CH_2)_2SP}(S)Cl$[b]
		P-Cl = 2.066	
		<SPCl = 113.2°	
$P(C_2H_5)_3$	$H_2P(C_2H_5)_2$[c]	<CPC = 98.9°	$P(CH_3)_3$
$P(CH_3)Cl_2$	PCl_3 and $P(CH_3)_3$		
$SP(CH_3)Cl_2$	$P(CH_3)Cl_2$	P=S = 1.885	$SPCl_3$
$(CH_2Cl)P(O)Cl_2$	$OPCl_3$	P-C = 1.843	$P(CH_3)_3$
		C-H = 1.091	
		C-Cl = 1.772	CH_2Cl_2[d]
$(CH_3O)_2SO$		S-O = 1.629	$\overline{O(CH_2)_2OS}O$[e]
		C-O = 1.438	
		<O=SO = 104.5	

Cont'd.

Table A1.2. Cont'd.

Compound	Model Compound geometry based upon	Assumed bond lengths (Å) and angles	Source of assumptions
		<OSO = 102°	
		<COS = 108.8°	
		S=O = 1.485	$(CH_3)_2SO$
		HC = 1.10	$OP(OCH_3)_3$
		<HCH = 110.0°	
$(CH_3O)_2SO_2$	$(CH_3O)_2SO$	S=O = 1.431	$(CH_3)_2SO_2$ [d]
		<O=S=O = 121.0°	
		<OSO = 103.5°	as <CSC in $(CH_3)_2SO_2$

(a) Per Andersen and K.E. Hjortaas, Acta Chem. Scand. 14, 829 (1960).

(b) V.A. Naumov, V.N. Semashoko, A.P. Zav'yalov, R.A. Cherkasov and L.N. Crishina, Zh. Str. Khim., 14, 739 (1973).

(c) J.R. Durig and A.W. Cox Jr., J. Chem. Phys., 64, 1930 (1976).

(d) Table A1.1 reference A1.1.

(e) B.A. Arbuzov, V.A. Naumov, N.M. Zaripov and J.D. Pronicheva, Doil. Akad. Nauk. SSSR, 195, 933 (1970).

APPENDIX 2

Reparameterisation of the EWMO (Hückel) Program

The program was a modified iterative extended Hückel program (EWMO).[39] The major features of this program have been adequately described[24,48] and will not be dealt with here with the exception of the parameterisation.

The core-energy parameters and the values for the electron repulsion integrals were taken from Sichel and Whitehead.[49] These atom parameters are based upon valence state energies for the atom given by Hinze and Jaffé.[56] Figure A2.1 shows a plot of the core-integrals, U_{ss} and U_{pp}, against the second-row elements. The manner in which the argon values were obtained has already been described in chapter 3.

The graph shows a smooth trend of values with the exception of those pertaining to phosphorus. A similar plot for the values obtained by Oleari et al.[57] is shown in Figure A2.2. In this case a smooth curve through all the points is obtained.

As mentioned previously in chapter 3, the electron repulsion integrals, g_{ss}, in the CNDO formalism become proportional to the Slater exponent, ζ_s, and so a plot of g_{ss} versus ζ for the second row should be linear. Sichel and Whitehead,[49] in their parameterisation, obtained values for an average electron repulsion integral, g_{AA}, for the

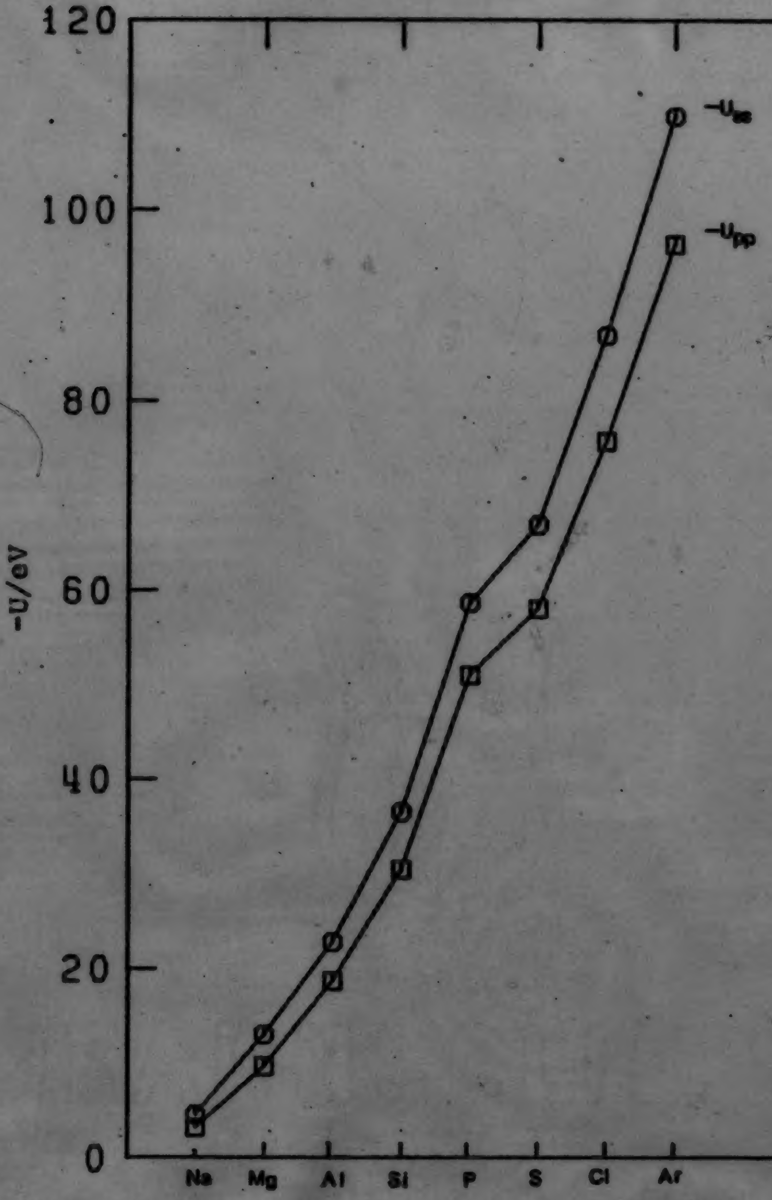

Figure A2.1 Core integrals ($-U_{ss}$ and $-U_{pp}$) taken from Sichel and Whitehead[49] versus the second row elements.

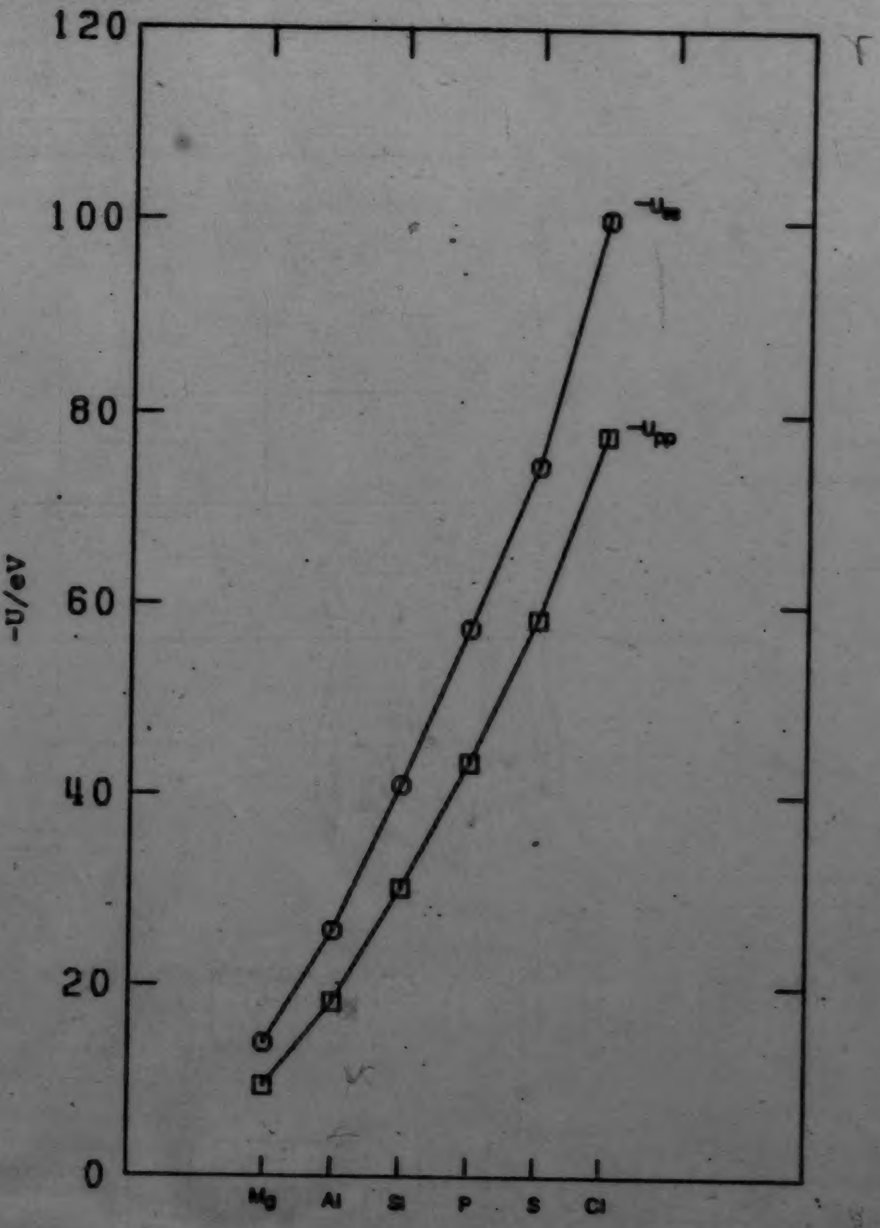

Figure A2.2 Core integrals ($-U_{ss}$ and $-U_{pp}$) taken from Oleari et al.[57] versus the second row elements.

one-centre term and g_{AA}^{*} for the two-centre term. These values are defined as

$$g_{AA} = \frac{1}{28}(g_{ss} + 12g_{sp} + 3g_{pp} + 12g_{pp'})$$

$$g_{AA}^{*} = \frac{1}{16}(g_{ss} + 6g_{sp} + 3g_{pp} + 6g_{pp'})$$

where g_{ij} are the appropriate electron-repulsion integrals between the s and p electrons. It is not unreasonable to assume, to the level of the semi-empirical approximation used here, that the average electron repulsion terms are also proportional to the Slater exponent. A plot of g_{AA} versus ζ_s is shown in Figure A2.3 for both sets of parameters. The parameter values given by Oleari et al.[57] are approximately linear for all elements in the row whereas in the values given by Sichel and Whitehead[49] the value assigned to phosphorus deviates substantially from the linearity of the parameters assigned to the remaining elements. This deviation of the phosphorus parameter in the latter case seems to reflect the stability of the half-filled shell in atomic phosphorus. However, when dealing with changes in the *molecular* environment the concept of the stability of the half-filled shell is no longer relevant because all systems are based on filled valence shells. Thus for the series from Si through to Cl a smooth, gradual increase in parameter values would be expected. In this context the trends exhibited by the parameterisation of Oleari

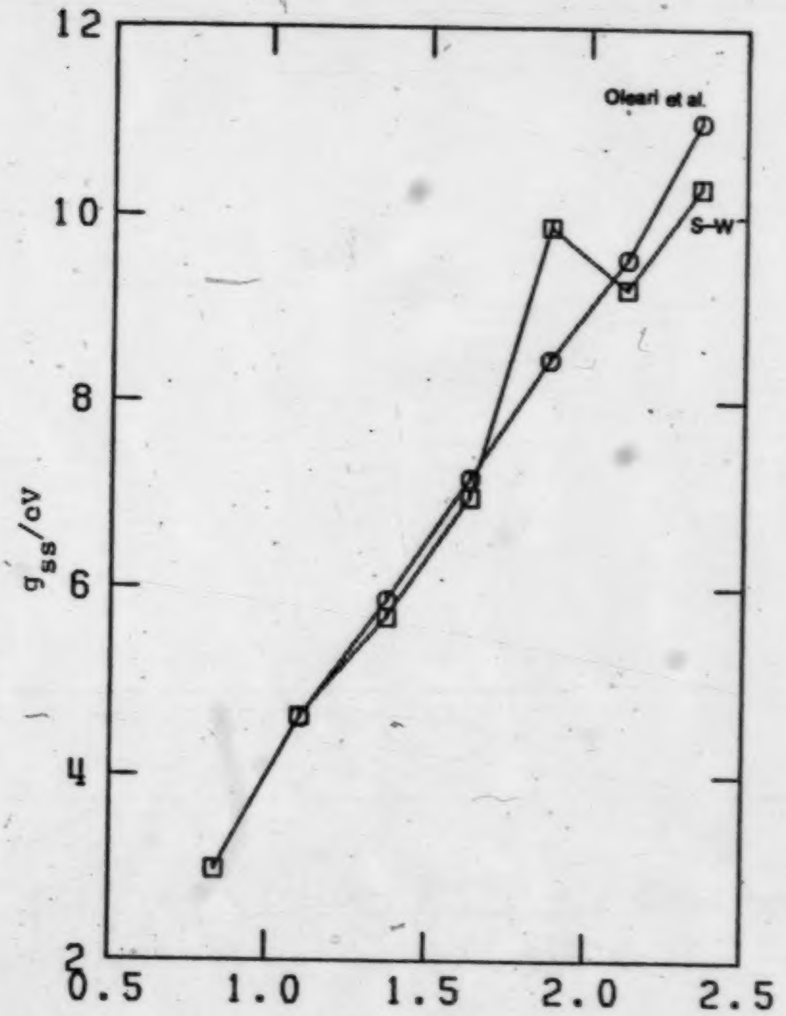

Slater Exponent (ζ_{3s})

Figure A2.3 Average one-centre repulsion integral (g_{ss}) versus the Slater orbital exponent (ζ_{3s}) of the second row elements.

et al.[57] seems more reasonable.

Rather than attempt to reparameterise the entire program using the values given by Oleari et al.,[57] we thought that it would be more efficient and equally justified to interpolate new values for the phosphorus parameters, in effect obtaining new parameters for phosphorus which would be related to the other atomic parameters given by Sichel and Whitehead.[49] This set in general would parallel those of Oleari et al.[57] The one-centre electron repulsion integral was estimated from a least-squares fit of atomic parameters for the second row (with the exception of P) as shown in Figure A2.3. A similar procedure was used to estimate the two-centre electron repulsion integral. A correlation of the core integrals from both works is shown in Figure A2.4. The phosphorus parameter value given by Oleari et al. was then converted to an interpolated "Sichel and Whitehead" core integral value for phosphorus using the least-squares correlation function defined by the data in Figure A2.4.

The final values for the new phosphorus parameters are presented in Table A2.1. Figure A2.5 shows the new relationship of the core integrals for the second row elements.

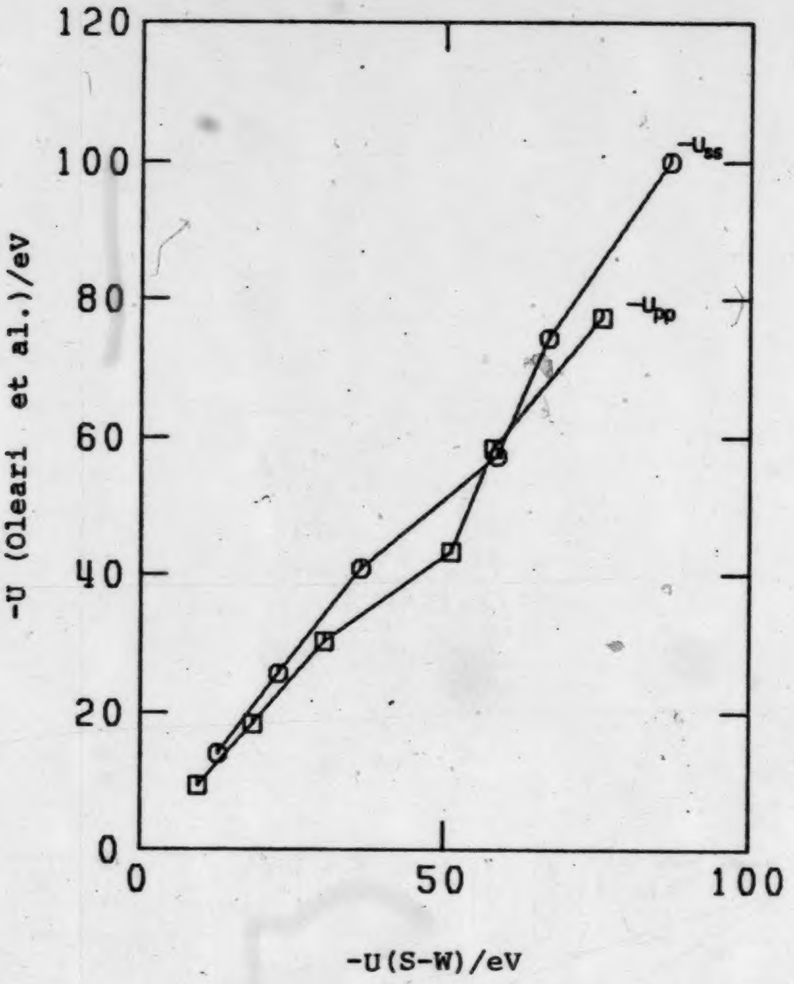

Figure A2.4 Core integrals ($-U_{ss}$ and $-U_{pp}$) of Oleari et al.[57] versus those of Sichel and Whitehead.[49]

Table A2.1

New Parameters for P (in eV)

	$-U_{ss}$	$-U_{pp}$	g_{AA}	$\bar{g}^*_{AA}$
P	50.648	42.949	8.079	8.124

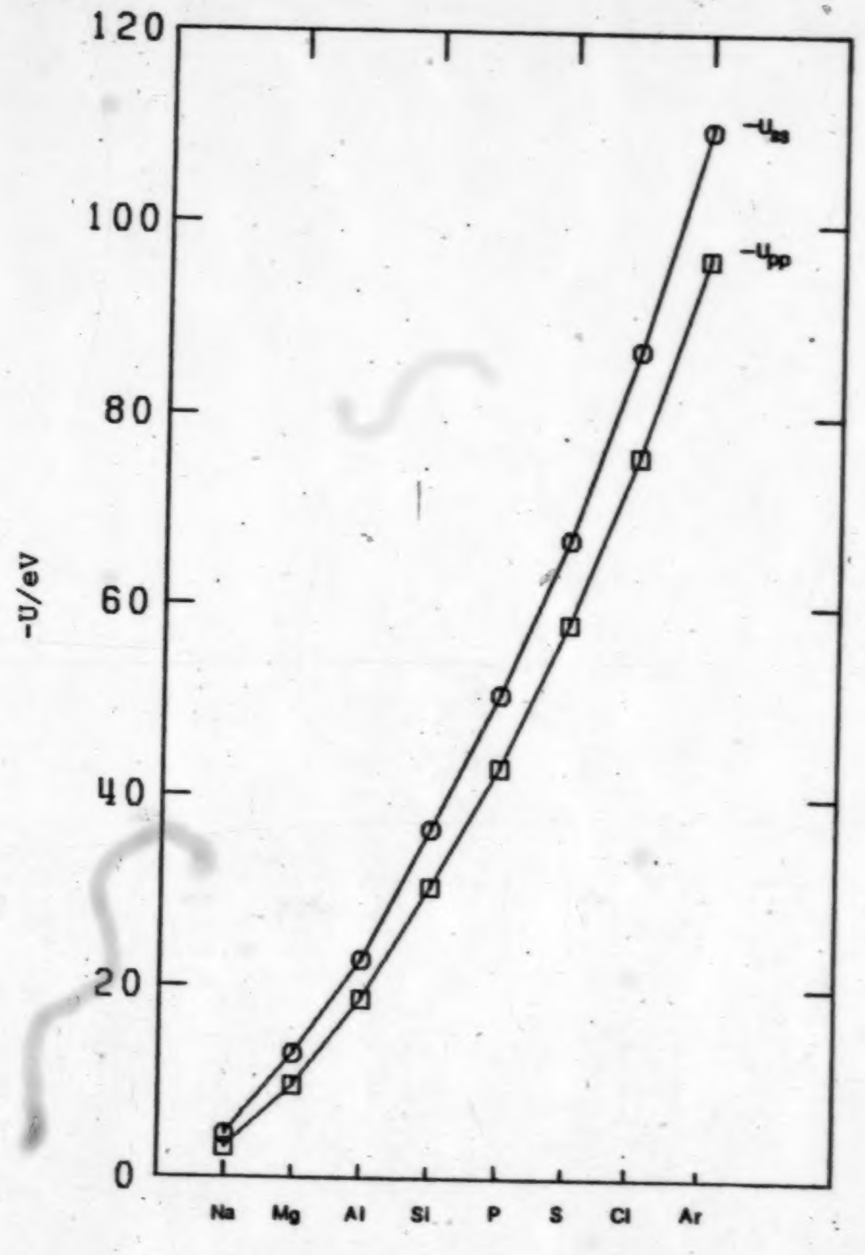

Figure A2.5 Core integrals ($-U_{ss}$ and $-U_{pp}$) taken from Sichel and Whitehead[49] with the new P parameterisation versus the second row elements.

APPENDIX 3

Corrected values for the calculated Auger shifts as presented in Table 1, ref. 8.

	Auger	
	2 step eqn. 5	3 step eqn. 6
PH_3	0	0
PCl_3	-1.78	-1.32
PF_3	5.08	5.53
$SPCl_3$	0.43	0.60
SPF_3	5.90	6.33
$OPCl_3$	0.72	1.13
OPF_3	7.54	7.96
PF_5	8.64	9.28